Aus dem Helmholtz Zentrum München
Institut für Stammzellforschung
Direktorin: Prof. Dr. Magdalena Götz

An organotypic assay for the quantification and characterization of regenerative primary human mammary epithelial cells

Dissertation
zum Erwerb des Doktorgrades der Naturwissenschaften
an der Medizinischen Fakultät
der Ludwig-Maximilians-Universität München

vorgelegt von
Jelena Linnemann

aus
Bielefeld

2017

Gedruckt mit Genehmigung der Medizinischen Fakultät
der Ludwig-Maximilians-Universität München

Betreuerin: Prof. Dr. Magdalena Götz

Zweitgutachter: Prof. Andreas Ladurner, Ph.D.

Dekan: Prof. Dr. med. dent. Reinhard Hickel

Tag der mündlichen Prüfung: 19.12.2017

Within the scope of the present PhD thesis, the following original article has been published in an international peer reviewed journal:

Linnemann, J.R., Miura, H., Meixner, L.K., Irmler, M., Kloos, U.J., Hirschi, B., Bartsch, H.S., Sass, S., Beckers, J., Theis, F.J., Gabka C., Sotlar K. and Scheel C.H. (2015). Quantification of regenerative potential in primary human mammary epithelial cells. Development, DOI:10.1242/dev.123554.

Abstract

Breast cancer is a heterogeneous disease with a high degree of intra- and intertumoral diversity, which impedes accurate patient stratification, prognosis and optimal treatment. The mammary gland consists of a complex network of epithelial ducts which end in clusters of alveoli, called terminal ductal lobular units (TDLUs) which are the functional units of the mammary gland. Postnatal mammary gland development and homeostasis require an enormous regenerative output, suggesting the existence of tissue stem/progenitor cells and a high degree of cellular plasticity to ensure functional robustness, i.e. the production and secretion of milk during lactation. Therefore, the observed heterogeneity in breast cancer is likely the result of normal mammary gland architecture and functionality.

Unfortunately, the identification and characterization of human stem/progenitor cells and the analysis of cellular plasticity are hampered by the limited applicability of currently used murine *in vivo* assays and the failure of 2D and 3D *in vitro* assays to recapitulate the histological architecture and functionality of the human mammary gland. Organoid assays span the bridge between standard *in vitro* culture and *in vivo* studies by mimicking the stem cell niche during self-renewal or repair in 3D culture. Thereby, organoid assays support the formation of organoids which recapitulate the architecture and functionality of the original tissue.

In this study, a novel organotypic assay was developed for the human mammary gland, in which single, freshly isolated human mammary epithelial cells from healthy donors cultured in floating collagen gels generate spheres and branched ductal structures that resemble TDLUs. The TDLU-like organoids were shown to form alveolar buds, express lineage markers at correct positions, and display functionality by contraction. In line with recent literature from transplantation studies, it was found that TDLU-like structure formation is enriched in a $CD49f^{hi}/EpCAM^{-}$ population, commonly referred to as basal, while $CD49f^{+}/EpCAM^{+}$ LP cells predominantly formed spheres. In addition, by performing limiting dilution analysis, the metalloendopeptidase CD10 was revealed as marker to enrich for TDLU-like structure forming cells within the $CD49f^{hi}/EpCAM^{-}$ population. The use of CD10 further led to identification of stromal cells present within the $CD49f^{hi}/EpCAM^{-}$ population. As expression of CD10 was not restricted to the $CD49f^{hi}/EpCAM^{-}$ cell population, it was shown that a combination of all three markers is required to optimally enrich for TDLU-like structure forming cells.

Importantly, the formation of TDLU-like structures was observed only in floating/compliant, but not in attached/rigid collagen gels and required actin-myosin-based cellular contraction.

Structures generated in attached collagen gels exhibited aberrant marker expression and invasive phenotype, emphasizing the importance of physical parameters in directing differentiation of the mammary gland and suggesting a role in tumorigenesis. In summary this study describes a defined *in vitro* assay system to quantify mammary epithelial cells with regenerative potential by limiting dilution, to analyze cellular plasticity, differentiation potential and functionality and to systematically investigate interactions with the physical environment at distinct steps of morphogenesis and the effect on cell fate decisions.

Zusammenfassung

Brustkrebs ist durch eine hohe intra- und intertumorale Heterogenität gekennzeichnet, wodurch Stratifizierung sowie optimale Prognose und Behandlung von Patienten erschwert werden. Die adulte humane Brustdrüse besteht aus komplex verzweigten Milchgängen, welche in traubenartigen Strukturen, den so genannten Drüsenlappen (Terminal ductal lobular units, TDLUs), den funktionellen Einheiten der normalen Brustdrüse, enden. Die Entwicklung und Homöostase der Brustdrüse finden hauptsächlich postnatal statt und erfordern eine enorme regenerative Leistung, welche die Existenz von Stamm- oder Progenitorzellen sowie zelluläre Plastizität suggerieren, wodurch auch die Funktion der Brustdrüse, insbesondere die Produktion und Sekretion von Milch während der Laktation, sichergestellt werden kann.

Die komplexe Architektur sowie der hohe regenerative Druck, dem die normale Brustdrüse unterliegt, spielen eine wichtige Rolle in der Heterogenität von Brustkrebs. Die heutzutage genutzten *in vivo* sowie 2D- und 3D-*in vitro* Modelle scheitern jedoch darin, die Architektur und Funktion der normalen humanen Brustdrüse korrekt nachzubilden, wodurch die Identifizierung und Charakterisierung von humanen Brust Stamm-/Progenitorzellen und die Analyse zellulärer Plastizität erschwert werden. Organoid-Ansätze bilden eine Brücke zwischen standard *in vitro* und *in vivo* Modellen, indem sie die Stammzellnische während der Gewebserneuerung/-reparatur nachbilden. Hierdurch fördern Organoid-Modelle die Bildung von Organoiden, die die normale Gewebearchitektur und -funktion widerspiegeln.

In dieser Studie wurde ein neuer, organotypischer Assay für die humane Brustdrüse entwickelt, in dem einzelne, frisch isolierte humane Brustepithelzellen verzweigte Strukturen bilden, die den TDLUs ähneln. Die TDLU-ähnlichen Strukturen bilden Alveolen, exprimieren Zelltypmarker an den korrekten Positionen und zeigen Funktionalität, indem sie kontrahieren. In Übereinstimmung mit der aktuellen Literatur, basierend auf murinen Transplantationsstudien, konnten die TDLU-ähnliche Struktur bildenden Zellen einer $CD49f^{hi}/EpCAM^{-}$ Population zugeordnet werden, welche als basal gilt, wohingegen gezeigt wurde, dass $CD49f^{+}/EpCAM^{+}$ luminale Vorläuferzellen vornehmlich Sphären bilden. Durch die Verwendung von „Limiting Dilution“ konnte zudem gezeigt werden, dass die Expression der Metalloendopeptidase CD10 die TDLU-ähnliche Struktur bildenden Zellen innerhalb der $CD49f^{hi}/EpCAM^{-}$ Population weiter anreichert. Die Verwendung von CD10 führte außerdem zu der Entdeckung, dass die $CD49f^{hi}/EpCAM^{-}$ Population Stromazellen enthält. Da die Expression von CD10 sich nicht auf die $CD49f^{hi}/EpCAM^{-}$ Population beschränkt, wurde

bestimmt, dass die Kombination der drei Marker CD49f, EpCAM und CD10 nötig ist, um TDLU-ähnliche Struktur bildende Zellen sauber anzureichern.

Es ist beachtenswert, dass die Bildung von TDLU-ähnlichen Strukturen nur in schwimmenden/weichen Collagen-Gelen, jedoch nicht in festen/rigiden Collagen-Gelen beobachtet wurde, sowie Aktin-Myosin-basierte zelluläre Kontraktilität benötigte. So zeigten Strukturen in festen Collagen Gelen abnormale Zellmarker Expression und invasives Wachstum. Die physikalischen Matrixeigenschaften spielen somit eine wichtige Rolle in der Differenzierung der Brustdrüse und der Krebsentwicklung und können in dem hier präsentierten Assay nachgebildet werden.

Zusammenfassend beschreibt diese Arbeit einen neuen organotypischen *in vitro* Assay, der die Quantifizierung von humanen Brustepithelzellen mit regenerativem Potential, die Erforschung von zellulärer Plastizität, Differenzierung und Funktionalität ermöglicht, sowie die Erforschung des Einflusses physikalischer Parameter während verschiedener Schritte der Morphogenese und der Differenzierung von Zellen erlaubt.

Contents

Abbreviations

%	Percent
°C	Degrees Celsius
2D	Two-dimensional
3D	Three-dimensional
7-AAD	7-Aminoactinomycin D
ADP	Adenosine diphosphate
ATP	Adenosine triphosphate
B−	$CD10^{-}/CD49f^{hi}/EpCAM^{-}$
B+	$CD10^{+}/CD49f^{hi}/EpCAM^{-}$
BRCA1	Breast cancer 1
BSA	Bovine serum albumin
B-SFU	Branched-structure forming unit
cAMP	Cyclic adenosine monophosphate
CD	Cluster of differentiation
CDM3	Chemically defined medium, 3 components
cDNA	Complementary DNA
CI	Confidence interval
CO_2	Carbon dioxide
DAPI	4’,6-diamidino-2-phenylindole
DMEM	Dulbecco's Modified Eagle's Medium
DMSO	Dimethyl sulfoxide
ECM	Extracellular matrix
ELDA	Extreme limiting dilution analysis
Elf5	E74 like ETS transcription factor 5
EMT	Epithelial-mesenchymal transition
EPAC1	Exchange factor directly activated by cAMP 1
EpCAM	Epithelial cell adhesion molecule
ER	Estrogen receptor
ERK, MAPK	Mitogen-activated protein kinase
FACS	Fluorescence-activated cell sorting
FAK	Focal adhesion kinase
FITC	Fluorescein isothiocyanate
FRZM	Freezing medium
FSC	Forward scatter
FZD	Frizzled
g	Gravitational Acceleration
g	Gram(s)
GATA3	Trans-acting T-cell-specific transcription factor
GFP	Green fluorescent protein
GO	Gene ontology

GPR30/GPER	G protein-coupled receptor 30
h	Hour(s)
HBSS	Hanks' Balanced Salt Solution
HEPES	4-(2-hydroxyethyl)-1-piperazineethanesulfonic acid
HER2	Human epidermal growth factor receptor 2
HF	HBSS with HEPES and FCS
HMEC	Human mammary epithelial cell
HR	Hormone receptor
IgG	Immunoglobulin G
K, KRT	Keratin
l	Liter(s)
Lgr5	Leucine-rich repeat-containing G-protein coupled receptor 5
LIMK	LIM domain kinase 1
Lin	Lineage
LP	Luminal progenitor
m	Meter
M	Molar
MaSC	Mammary stem cell
MEC	Mammary epithelial cell
MECGM	Mammary epithelial cell growth medium
MEK, MAPKK	Mitogen-activated protein kinase kinase
MET	Mesenchymal-epithelial transition
MG	Mammary gland
min	Minute(s)
MLC	Myosin light chain
MME	Membrane metalloendopeptidase, CD10
mRNA	Messenger RNA
n	Nano
n.a.	Not applicable
n.d.	Not detectable
n.s.	Not significant
PB	Pacific blue
PBS	Phosphate-buffered saline
PCA	Principal component analysis
PCB	Primary cell buffer
PE	Phytoerythrin
PFA	Paraformaldehyde
PI3K	Phosphatidylinositol-4,5-Bisphosphate 3-Kinase
PI3KCA	Phosphatidylinositol-4,5-Bisphosphate 3-Kinase Catalytic Subunit Alpha
Popdc	Popeye domain-containing protein
PR	Progesterone receptor

Prl	Prolactin
Procr	Protein C Receptor
PVDF	Polyvinylidene fluoride
qPCR	Quantitative real-time polymerase chain reaction
rBM	Reconstituted basement membrane, Matrigel
Rho	Ras homolog gene family, member A
ROCK	Rho-associated protein kinase
RT	Room temperature
RT-PCR	Quantitative real-time polymerase chain reaction
s	Second(s)
SC	Stem cell
s.d.	Standard deviation
SSC	Side scatter
S-SFU	Sphere-structure forming unit
TAZ	Tafazzin
TDB	Tissue digestion buffer
TDLU	Terminal ductal lobular unit
TEB	Terminal end bud
TGF-β1	Transforming growth factor beta 1
TM	Transport medium
TNBC	Triple-negative breast cancer
TNS	Trypsin neutralizing solution
U	Enzyme unit
YAP	Yes-associated protein 1
ZO	Zonula occludens
αSMA	Alpha smooth muscle actin
µ	Micro

Aims of the study

The complex architecture and functionality of the normal mammary gland (MG) and the possible existence of tissue stem/progenitor cells and high cellular plasticity likely underlie the heterogeneity of breast cancer, which impairs accurate patient stratification, prognosis and optimal treatment. However, investigation of MG architecture and functionality during normal tissue homeostasis and disease is hampered by the fact that currently used murine *in vivo* assays and 2D and 3D *in vitro* assays fail to recapitulate the architecture and functionality of the human MG. The rationale of three-dimensional organotypic assays is to mimic the normal tissue environment and thereby permit formation of organoids reflecting normal MG architecture and function [Clevers, 2016]. Thus, the major aim of this study has been the development of an organotypic 3D culture model for primary human mammary epithelial cells, in which morphological and physiological characteristics of the human MG *in situ* are recapitulated. Collagen I is the major component of the human MG extracellular matrix *in situ* and it has previously been shown that primary human mammary organoids cultured within floating collagen gels generate branched structures [Foster et al., 1983]. Indeed, using floating collagen I gels as substrate for 3D culture allowed primary human mammary epithelial cells to build structures that resembled terminal ductal lobular units, the functional units of the human MG *in situ*. After improvement of culture conditions to optimally promote TDLU-like structure formation in floating collagen gels, the further aims of this study have been the development of a protocol for quantification of TDLU-like structure formation as readout for regenerative potential, followed by enrichment of regenerative cells and their classification into the basal and luminal mammary epithelial cell lineages. Furthermore, the degree of cellular differentiation and polarization of TDLU-like structures should be revealed by analysis of marker expression and assessment of cellular functionality. Finally, the interplay of flotation of collagen gels, i.e. matrix compliance, and medium supplements for promotion of TDLU-like structure formation and cellular differentiation and plasticity were supposed to be assessed.

1 Introduction

1.1 Breast cancer

1.1.1 Breast cancer incidence and mortality

Breast cancer is the most commonly diagnosed cancer among women worldwide, accounting for approximately 1.7 million new cases in 2012. Breast cancer also represents the second most common cancer related death of women in more developed countries, after lung cancer [Ferlay et al., 2013]. In Germany, the current lifetime risk for women to develop breast cancer is approximately one in 8, while more than 25% of them (one in 29 women) will die from the disease [RKI, 2015]. Notably, survival rates have increased since the mid-90s due to improvements in therapy and widespread introduction of mammographic screening in the 80s, improving early detection of breast cancer [Althuis et al., 2005].

However, while 5-year relative survival rates for stage 0 or I breast cancers are almost 100%, those for late stage IV or metastasized cancers remain low at approximately 22% [ACS, 2014] and treatment options for certain types of cancer like the aggressive triple negative breast cancer are limited [Podo et al., 2010]. In addition, patients are frequently under- or overtreated due to lack of information for patient stratification [Shieh et al., 2016]. Thus, a better understanding of breast cancer progression and subtypes is needed in order to improve treatment and develop more targeted therapies.

1.1.2 Breast cancer classification and considerations for treatment

In the clinic, classification of breast cancer, prognostic predictions and treatment decisions are usually based on the clinical parameters age, node status, tumor size and histological grade and expression of the pathological markers estrogen receptor (ER), progesterone receptor (PR) and human epidermal growth factor receptor 2 (HER2/neu) [Prat et al., 2011]. This classification yields three main types of breast cancer: hormone receptor (HR) positive breast cancer (HR+, positive for ER, PR or both), HER2-amplified breast cancer and triple negative breast cancer (TNBC), signified by its lack of HR expression and HER2-amplification. Approximately two thirds of breast tumors are HR+. Patients with HR+ tumors benefit from treatment with hormone therapy, including treatment with Tamoxifen and aromatase inhibitors [ACS, 2014]. HER2+ cancers exhibit increased HER2 protein expression or contain extra copies of the HER2 gene. Patients with HER2 positive tumors can be treated with Herceptin, an antibody which binds to the HER2 receptor, thereby causing reduction in tumor

cell proliferation. TNBCs account for approximately 15% of invasive breast cancers, i.e. cancers that break through the basement membrane and invade the surrounding tissue. TNBC have an increased incidence in BRCA1 mutation carriers and women of African ancestry [Carey et al., 2006, Foulkes et al., 2010]. These tumors usually occur at a lower age and are more aggressive than non-TNBCs [Dent et al., 2007]. Due to lack of HR and HER2 overexpression, chemotherapy is often the only treatment option which results in a complete pathological response in approximately 22% of patients and a 3-year overall survival of 94%. However, the remaining 80% of TNBC patients do not show a complete pathological response to chemotherapy, resulting in a poor 3-year overall survival of only 68% [Foulkes et al., 2010]. Thus, the heterogeneous response to chemotherapy of TNBCs leads to poor prognosis and shows the need for better characterization of this tumor type and development of targeted therapies.

Within the described clinical/pathological treatment groups, there is still great biological heterogeneity concerning molecular alterations, cellular composition and response to therapy. In order to better understand biological heterogeneity and improve patient stratification, global gene expression analyses have been performed on human breast cancer samples. Thereby, five main molecular subtypes (luminal A, luminal B, HER2-enriched, basal-like and normal-like) have been identified [Perou et al., 2000, Sorlie et al., 2001]. In addition, another molecular subtype (claudin-low) has been identified more recently [Herschkowitz et al., 2007]. Notably, tumors in the luminal A/B subgroup are characterized by high expression of genes like ER, KRT18, GATA3 and FOXA1 which are associated with normal mammary luminal cells. In contrast, expression of ER and its associated genes is low in tumors classified as basal-like or HER2-enriched. Instead, basal-like tumors were characterized by high expression of genes like KRT5, KRT17 and FZD7 which are associated with normal basal mammary epithelial cells [Perou et al., 2000]. The different molecular subtypes are signified by differences in incidence, survival and response to therapy. For instance, luminal A tumors present with a much better prognosis than luminal B tumors, even though clinically speaking, both belong to the HR+ subset of breast cancers [Prat et al., 2011, Sorlie et al., 2001].

Classification of breast cancers is further complicated by the finding that molecular subtypes do not perfectly overlap with pathological markers used in the clinic. For example, up to 29% of basal-like tumors are ER+ and up to 13% of these tumors are HER2+. These tumors might therefore be classified as HR+ or HER2+ tumors in the clinic, while preliminary data suggest that their prognosis and response to therapy may have been better predicted by the basal-like

subtype [Prat et al., 2011, Sorlie et al., 2001]. Thus, there seems to be high heterogeneity even in the single molecular subtypes.

In summary, limited treatment options for certain types of breast cancer, and the high biological heterogeneity of breast tumors together with the lack of accurate markers complicate patient stratification and prevent accurate prognosis and optimal treatment.

1.1.3 The cell-of-origin and plasticity in human breast cancer

An important consideration to better understand initiation, progression and maintenance of different tumor types is the identification of the cell-of-origin which is relevant for breast cancer characterization, development of targeted therapy and prevention efforts. The definitions of the molecular breast cancer subtypes luminal A/B and basal-like suggest that the cell-of-origin of these tumors can be found in the luminal and basal cell lineage of the normal human mammary gland (MG), respectively. However, this assumption has been challenged recently [Lim et al., 2009, Molyneux et al., 2010]. Most cancers with underlying BRCA1 mutation are clinically classified as TNBC and are molecularly defined as basal-like. However, the luminal progenitor and not the basal population was shown to be expanded in tumor-free breast tissue of BRCA1 mutation carriers. Cells of this expanded luminal progenitor population exhibited increased clonogenic activity in 3D *in vitro* culture and were relatively insensitive to the lack of growth factors, indicating aberrant growth potential [Lim et al., 2009]. In addition, a second study reported that targeted deletion of BRCA1 in luminal ER− progenitors in the mouse MG caused the formation of tumors which were pathologically similar to tumors found in human BRCA1 mutation carriers, while targeted deletion of BRCA1 in basal cells led to the generation of tumors classified as malignant adenomyoepitheliomas, a tumor type that rarely occurs in the human breast [Molyneux et al., 2010].

Together, these results strongly suggest that basal-like tumors of BRCA1 mutation carriers are derived from cells of the luminal progenitor rather than from the basal population. Furthermore, these results indicate high plasticity of mammary epithelial cell lineages which seems to be triggered during the process of tumor development and progression and obscure tumor characterization. Efforts to elucidate cellular plasticity and its involvement in generation of specific tumor types will play an important role for the development of personalized medicine for breast cancer.

1.2 The normal mammary gland

Cellular plasticity and heterogeneity of breast cancer are likely a result of normal MG architecture and function. MG development is initiated in the embryo, but it is not until puberty that the MG develops into a complex network of epithelial ducts ending in clusters of alveoli called terminal ductal lobular units (TDLUs). During reproductive life, specifically every menstrual cycle, pregnancy and lactation, the MG undergoes proliferation, differentiation and remodeling. This enormous regenerative potential suggests the existence of tissue stem/progenitor cells and a high degree of cellular plasticity to ensure functional robustness, i.e. the production of milk. Therefore, understanding of MG architecture, development and differentiation processes as well as investigation of plasticity of normal mammary epithelial cells are the foundation to understanding breast cancer heterogeneity.

1.2.1 Human mammary gland development and differentiation

The MG develops after the three germ layers have formed and segmentation has taken place. It is made up of an epithelial compartment with ectodermal origin, embedded in a stromal compartment derived from the mesoderm. One of the first signs of MG development is a mammary ridge developing on each side of the trunk, going from groin to axilla, which has been reported in 15 mm human embryos. Subsequently, the mammary epithelium proliferates to first form a nodule and then further develops into a mammary bud, which starts pushing into the underlying mesenchyme. Notably, primordial cells at this stage are negative for the basal cell markers K14 and αSMA.

Eventually, the mammary bud starts to invade into the underlying mesenchyme and branches, and the developing ducts become canalized leading to formation of the MG anlage, also called rudimentary ductal tree, which is present at birth (Figure 1.1). At this stage, basal cells become positive for K14 and αSMA [Howard et al., 2000, Russo et al., 2004]. Until puberty, the MG remains mainly quiescent and grows isometrically with the rest of the body as short ductal structures in fibroblast rich stroma.

At puberty, sexual dimorphism occurs: while the MG in males remains quiescent, in females the production of reproductive hormones triggers further development (Figure 1.1). The first change is an increase in the amount of fibrous and fatty tissue, followed by the growth and division of primary and secondary ducts. Furthermore, previously blunt-ended ductal termini change to terminal end buds, which subsequently form new branches, twigs and small ductules/alveolar buds, until the MG has become a complex branched network of ducts, ending in collections of ductules/alveoli, the TDLUs [Howard et al., 2000, Russo et al., 2004].

Rescue experiments in hormone deprived mice and rats revealed that pubertal MG development is mediated by five major hormones; 17-β-estradiol, progesterone and prolactin together with growth hormone and cortisol [Brisken et al., 2010]. Later, transplantation of ERα-/- and PR-/- mammary epithelial cells into cleared fat pads of wild type mice showed that epithelial estrogen signaling is required for ductal elongation, while epithelial progesterone signaling mediates subsequent side-branching and alveologenesis [Brisken et al., 2010, Brisken et al., 1998, Mallepell et al., 2006]. In addition, engraftment of Prl-/- epithelium revealed that prolactin signaling is required at rather late stages of development, namely alveologenesis and lactogenic differentiation of mammary epithelial cells during late pregnancy [Brisken et al., 1999, Brisken et al., 2010, Gallego et al., 2001].

In the adult female, the MG undergoes cyclical changes of cell proliferation in synchronization with the menstrual cycle, but only fully differentiates during pregnancy and lactation (Figure 1.1). During pregnancy, the number of lobules increases, cells within lobules increase in size to prepare for secretory activity and secretory material accumulates within cells and in the ductules. Upon birth, the drop of placental lactogen and sex steroids, most importantly progesterone, trigger the onset of lactation. After weaning, the accumulation of milk within the ductoacinar lamina and within the cytoplasm of secretory cells inhibits the production of milk and induces involution. Specifically, secretory cells are removed by apoptosis and phagocytosis and the periductal and perilobular connective tissue is remodeled. Morphologically, the involuted gland of a parous woman resembles the MG of an adult virgin woman with more differentiated lobules [Howard et al., 2000, McManaman et al., 2003, Russo et al., 2004].

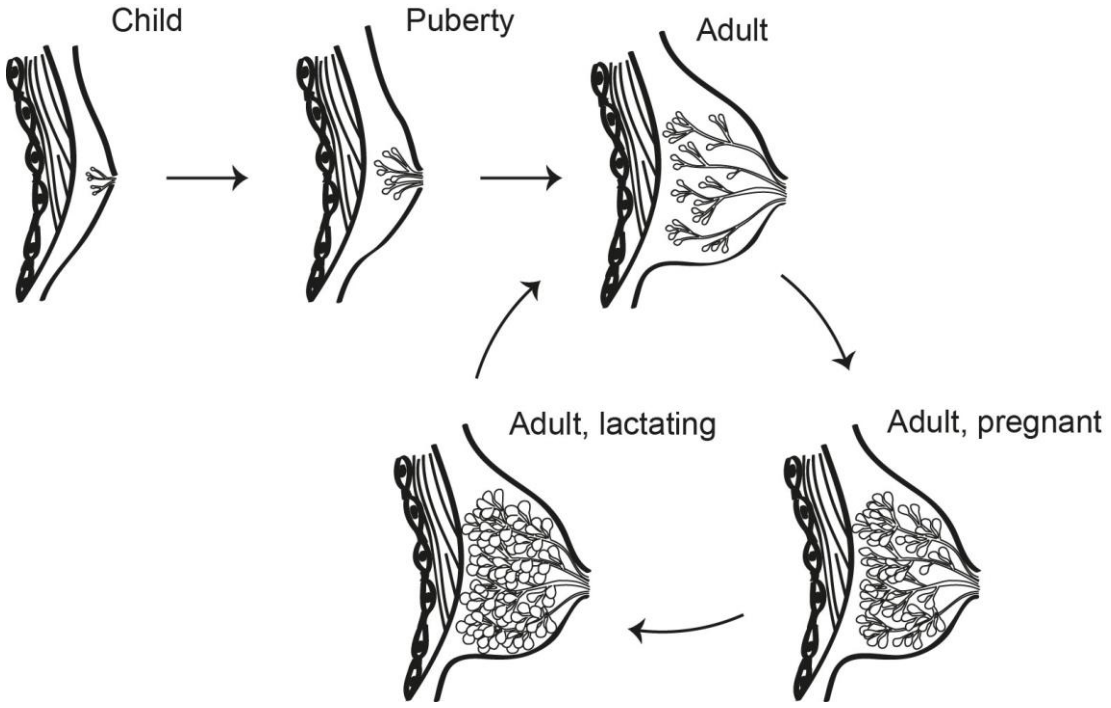

Figure 1.1 Schematic overview of postnatal human mammary gland development.
The rudimentary mammary epithelial ductal tree present after birth starts to grow and branch during puberty, until it reaches the state of the adult non-pregnant gland. The mammary epithelium further grows, branches and fully differentiates during pregnancy and lactation. The circle indicates a developmental cycle from the mature non-pregnant adult gland through pregnancy, lactation and involution back to the mature non-pregnant state.

1.2.2 Human mammary gland architecture

The adult MG consists of a complex branched network of epithelial ducts. In humans, about 10-15 lactiferous ducts arise at the nipple, invade the mammary fad pad, branch off into segmental ducts and terminate in clusters of alveoli, the terminal ductal lobular units (TDLUs) (Figure 1.1). TDLUs are the functional units of the MG and the place where milk is produced [Parmar et al., 2004]. Notably, most breast cancers arise within the luminal compartment of TDLUs [Sainsbury et al., 2000].

The mammary ducts are composed of two main cell-types, luminal and basal epithelial cells (Figure 1.2). Luminal cells are located at an inner position, surrounding a central lumen, and secrete milk into the lumen during lactation. At the outer positions, they are surrounded by a single layer of contractile basal or myoepithelial cells which facilitate the transport of milk towards the nipple. The term basal cell was partly invented to refer to myoepithelial cells lining ducts, which are more cuboidal shaped than myoepithelial cells residing in alveoli which acquire a rather elongated/flattened morphology. However, myoepithelial cells of both ducts and alveoli are functionally alike, having contractile ability, high concentrations of actin microfilaments and staining positive for alpha smooth muscle actin (αSMA) [Howard et al.,

2000]. Thus, the term myoepithelial or basal cell provides no functional differentiation and can be used interchangeably.

Basal and luminal cells of the human MG can be distinguished by differential lineage marker expression. Commonly used markers for basal/myoepithelial cells include the transcription factors p63 and Slug, αSMA, the intermediate filament vimentin, endopeptidase CD10 and cytokeratin K14 [Guo et al., 2012, Lim et al., 2010, Santagata et al., 2014]. p63 serves as a functional marker as its expression is required for maintenance of the basal cell fate in human mammary epithelial cells [Yalcin-Ozuysal et al., 2010]. In addition, αSMA was shown to mediate the contractile function of basal/myoepithelial cells [Haaksma et al., 2011, Weymouth et al., 2012]. Commonly used markers for luminal cells include the transcriptional regulators GATA3 and Elf-5, tight junction proteins ZO-1 and claudin-4, as well as cytokeratin K8/18 and the glycoprotein Mucin-1 [Asselin-Labat et al., 2007, Ewald et al., 2008, Kouros-Mehr et al., 2006, Lee et al., 2011, Oakes et al., 2008, Santagata et al., 2014, Stingl et al., 2001].

The mammary ductal epithelial network is ensheathed by a basement membrane, an approximately 100 nm thick sheet of extracellular matrix. The basement membrane provides a barrier between the epithelium and the surrounding stroma (Figure 1.2). It is composed of laminin polymers, crosslinked collagen IV fibrils, glycoproteins and proteoglycans like perlecan [Muschler et al., 2010]. Myoepithelial cells are in direct contact with the basement membrane by binding of their integrin-α6 receptors to laminin of the basement membrane. Most of the inner luminal cell population is separated from the basement membrane by myoepithelial cells. However, predominantly in acini, luminal cells with extended processes were found to contact the basement membrane in between two elongated myoepithelial cells [Howard et al., 2000]. In humans, mammary epithelial ducts and their associated basement membrane are surrounded by stroma consisting of connective tissue proteins, most abundantly collagen I, which lend structural support to the epithelial structure [Howard et al., 2000]. Stromal cells include fibroblasts and adipocytes which are interspersed with endothelial cells and a variety of innate and adaptive immune cells [Muschler et al., 2010, Plaks et al., 2015]. The various stromal cell types ensure the supply of blood and nutrients and are involved in the immune defense. Furthermore, they are involved in signaling events such as the proliferative response of mammary epithelial cells to estrogen and progesterone [Brisken et al., 2010].

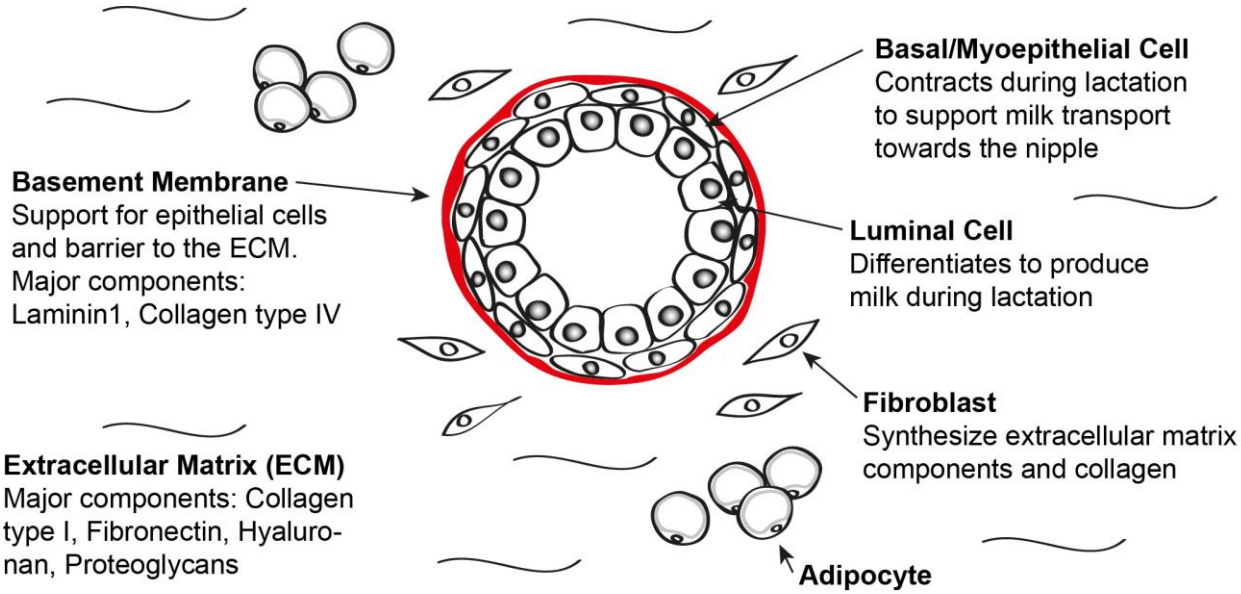

Figure 1.2 Illustration of a cross-section of a human mammary epithelial duct surrounded by extracellular matrix and stromal cells.
Luminal HMECs which secrete milk into the lumen during lactation are surrounded by a layer of contractile basal/myoepithelial cells which support the release of milk towards the nipple. The epithelial cells are surrounded by a basement membrane and are embedded in an extracellular matrix containing various cell types including fibroblasts, adipocytes, immune and endothelial cells.

1.2.3 Differences between human and mouse mammary gland architecture, development and differentiation

Detailed analysis of human MG architecture, development and cellular hierarchy is complicated by the low availability of tissue sections and interindividual differences. Mouse models do not only relieve these shortcomings, but also allow for genetic and non-genetic manipulations and have therefore become the major model organism for MG research. However, the embryonic and postnatal development of the murine MG, as well as its architecture and cellular composition are slightly different from the human MG [Sternlicht, 2006].

Like in humans, MG development in mice starts with formation of a bilateral mammary ridge which develops into placodes, leading to the formation of the rudimentary ductal tree present at birth. However, while human MG development in males and females is the same until puberty, androgen hormones induce condensation of the mesenchyme around the mammary bud in mice, resulting in its destruction already at embryonic day 14 [Sternlicht, 2006]. After birth, human mammary epithelial ducts range from blunt-ended tubular structures to well-developed acinar structures, which terminate in TDLUs [Howard et al., 2000]. In contrast, mammary epithelial ducts of mice are blunt-ended, and it is only at puberty that terminal end

buds (TEBs), club shaped structures with multiple layers of inner body cells and an outer layer of cap cells, form and invade the fat pad. In the adult mouse, TEBs regress again and mammary epithelial ducts remain largely blunt-ended until the generation of alveolar buds during pregnancy. In the murine MG, these lobular-alveolar structures are located at the ends of tertiary side branches like leaves on a branch, which is in contrast to the grape-like architecture of TDLUs in the human MG [Sternlicht, 2006].

Importantly, murine and human mammary epithelial ducts are embedded in a stroma which exhibits dramatic histological differences (Figure 1.3). In the human MG, epithelial ducts are closely associated with fibrous connective tissue and are separated from large areas of adipose tissue. In contrast, in the murine MG, the epithelium is in close contact with adipose tissue which is interspersed with only small amounts of connective tissue [Parmar et al., 2004].

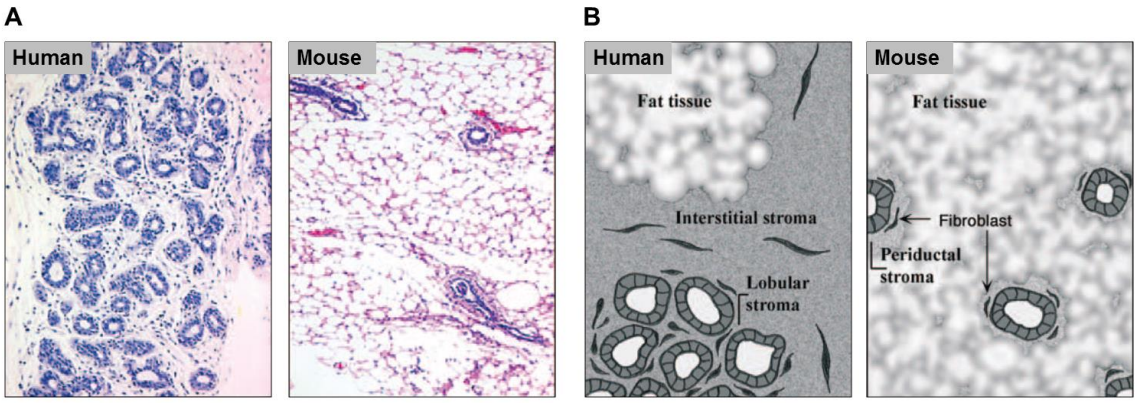

Figure 1.3 Comparison of human and mouse mammary glands.
(A) Hematoxylin & eosin (H&E) stained section of normal human and mouse breast tissue, showing a terminal ductal lobular unit embedded in a fibrous connective tissue stroma (left, human) and ducts embedded in adipose rich stroma (right, mouse).
(B) Schematic representation of a human TDLU (left), emphasizing the distance of the adipose tissue in contrast to the close association of epithelial structures with interstitial fibrous connective tissue stroma, and of the mouse MG (right), displaying ducts in intimate contact with fibroblasts and adipocytes. Adapted from [Parmar et al., 2004].

Most lineage markers can be used to identify basal and luminal mammary epithelial cells of both human and mouse. However, there are exceptions: Mouse basal cells are usually identified by use of keratins K5 and K14, αSMA and Lgr5 [Mikaelian et al., 2006, Plaks et al., 2013], while immunohistochemical and proteomic analysis of human mammary epithelial cells revealed expression of K5 and K14 in both basal and luminal cells [Gusterson et al., 2005, Santagata et al., 2014]. In addition, the expression of Lgr5 which was described as basal/stem cell marker of mouse mammary cells has not been assessed in human mammary epithelial cells yet [Plaks et al., 2013]. Importantly, the differences between human and mouse MG architecture, development and differentiation should be taken into account when comparing both systems.

1.2.4 Cellular hierarchy in the mammary gland

The high regenerative potential of the MG suggests the existence of tissue stem/progenitor cells and cellular plasticity. Indeed, the presence of mammary stem cells (MaSCs) or bipotent progenitors has been suggested by a multitude of studies, most importantly transplantation studies. Already in 1959, de Ome et al. showed that fragments of mouse mammary tissue transplanted into a murine mammary fat pad cleared of endogenous epithelium could regenerate an entire ductal network containing both epithelial cell lineages [Deome et al., 1959]. Subsequent transplantation studies showed that successful engraftment could be obtained from any tissue fragment irrespective of the temporal and spatial origin [Daniel et al., 1968, Hoshino, 1962, Smith et al., 1988, Young et al., 1971], indicating that a candidate stem cell population was located along the entire epithelial tree and persisted throughout the lifespan of a mouse. Moreover, it was shown that serial transplantation of mammary tissue fragments consistently led to regeneration of a cleared mammary fat pad at least 5-8 times [Daniel et al., 1971, Young et al., 1971], demonstrating the cell's capacity to self-renew, which is a major hallmark of stem cells (SCs). The existence of bipotent stem/progenitor cells in murine MGs was further supported by formation of a functional MG mammary fat pad. The resulting gland contained both luminal and basal cells and showed self-renewal capacity in serial transplantation [Kordon et al., 1998]. These results suggested the existence of adult murine MaSCs/bipotent progenitors, but their identity remained elusive. However, in 2006, two independent research groups shed light on the identity of the regenerative cells. Using the cell surface markers integrin-β1 (CD29) or integrin-α6 (CD49f) in combination with heat stable antigen (CD24), the authors could separate luminal, basal, and stromal subpopulations and published a protocol for the enrichment of MaSCs/bipotent progenitors. By injecting the sorted luminal and basal cells into cleared mammary fat pads of recipient mice, the authors confirmed that single murine mammary epithelial cells were able to repopulate an entire MG. More importantly, they showed that the repopulating ability was contained almost exclusively in a $CD24^{med}/CD49f^{hi}$ [Stingl et al., 2006] or $CD29^{hi}/CD24^{+}$ [Shackleton et al., 2006] population and therewith in the basal cell compartment. The stem cell frequency within the basal population was estimated to be ~1/60 to ~1/90 cells, depending on the mouse strain [Shackleton et al., 2006, Stingl et al., 2006]. By transplantation into humanized murine mammary fat pads [Kuperwasser et al., 2004] or transplantation under the kidney capsule of immune compromised mice [Eirew et al., 2008], it was shown that also human MECs contained regenerative capacity, which was found to be enriched in basal $CD49f^{+}/EpCAM^{neg-low}$ cells, suggesting that regenerative capacity is contained within the basal cell population in

both mouse and human (Figure 1.4A). More recently, an alternative approach for assessing stem cell identity and function, lineage tracing, has evolved. It allows tracking cell fate dynamics of stem and progenitor cells in the physiological context of development and homeostasis *in situ*. The first inducible cell fate mapping study tracked stem cell and progenitor activity at different stages of mammary development using fluorescent protein expression under tamoxifen or doxycycline inducible lineage specific keratin promoters. In this manner, MaSCs/ bipotent progenitors giving rise to both luminal and basal cells were only identified during embryogenesis, but not during puberty and homeostasis. It was shown that instead of MaSCs/bipotent progenitors, two types of lineage restricted progenitor cells, basal and luminal, contribute to the maintenance of their own lineage. This led to the conclusion that unipotent progenitors rather than rare MaSCs/bipotent progenitors drive development and homeostasis in the postnatal MG [Van Keymeulen et al., 2011]. In contrast, another tracing study suggested that both unipotent and bipotent progenitors contribute to postnatal MG development, depending on the developmental stage. Labeling and tracing of Wnt/β-catenin responsive Axin2+ cells revealed the presence of unipotent progenitors during puberty and adulthood and bipotent progenitors during pregnancy [Van Amerongen et al., 2012]. Strikingly, both studies demonstrated that cells that were restricted to a basal fate *in situ* gave rise to both lineages upon transplantation, suggesting that transplantation assays do not reflect the physiological behavior of mammary stem/progenitor cells [Van Amerongen et al., 2012, Van Keymeulen et al., 2011].

Further evidence for the existence of multipotent progenitors *in vivo* was provided by two recent fate-mapping studies. Using an inducible multicolor reporter under lineage specific Elf-5 and K5 promoters, Rios et al. imaged large parts of the ductal tree and found that K5+ basal cells give rise to both basal and luminal cells during puberty and adulthood, thereby representing MaSCs/bipotent progenitors [Rios et al., 2014]. It should be noted, however, that a very high fraction (30%) of the mammary epithelium was labeled in this study, thereby confounding interpretation. In the second study, labeling and tracing of cells expressing the Wnt target protein C receptor (Procr) provided evidence that Procr labels a subpopulation of basal cells with multipotent features *in vivo* and high regenerative capacity in transplantation assays [Wang et al., 2015].

The contradictory results concerning the existence of MaSCs/bipotent progenitor cells *in vivo* likely resulted from the use of transgenic and knock-in cre drivers for lineage tracing which are dynamically, temporally and heterogeneously expressed. Therefore, lineage tracing data are difficult to interpret. In the latest fate mapping study, this problem was approached by

thorough statistical analysis of multicolor lineage tracing and lineage tracing at saturation, again using fluorescent protein expression under inducible lineage specific K14 and K8 promoters. Using this approach, it was statistically confirmed with a high level of certainty that unipotent rather than bipotent stem/progenitor cells mediate pubertal development, adult tissue homeostasis as well as pregnancy and lactation in the murine MG (Figure 1.4B) [Wuidart et al., 2016].

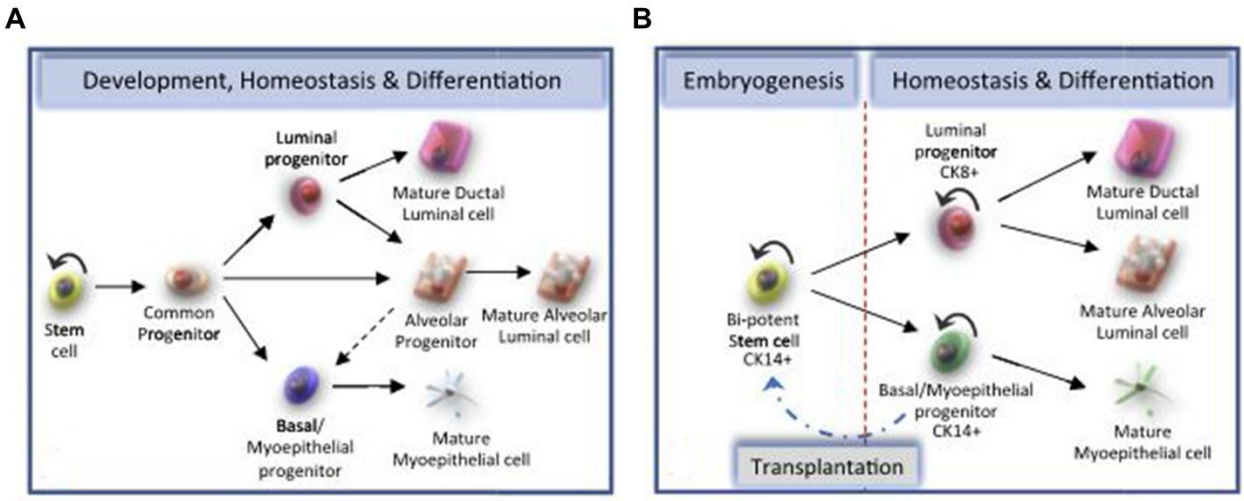

Figure 1.4 Models of mammary differentiation.
(A) Traditional model: Common bipotent progenitors maintain both luminal and basal lineages in the adult murine MG.
(B) Revised model: Common bipotent progenitors only exist during embryonic MG development, while unipotent progenitors maintain luminal and basal lineages postnatally. Notably, bipotent progenitors can be re-activated from postnatal basal/myoepithelial cells by transplantation. Adapted from [Keller et al., 2011].

Recently, the concept of a rare population exhibiting MaSC/bipotent progenitor features in transplantation assays has been challenged altogether. The authors of a paper published in 2014 showed that approximately 50% of basal mammary epithelial cells can acquire *de novo* mammary repopulating potential when cultured *in vitro* in the presence of a ROCK inhibitor [Prater et al., 2014]. In addition, repopulating potential of murine MECs can be increased by culture in the presence of fibroblast-derived factors [Makarem et al., 2013]. Together, these observations implicate high cellular plasticity and suggest a model in which MaSCs/progenitors can be generated by almost any myoepithelial cell on demand. High lineage plasticity has also been suggested by two independent research groups who found that expression of constitutively active PI3K ($PIK3CA^{H1047R}$) in lineage committed K5+ and Lgr5+ basal cells of the adult murine MG causes reprogramming into a luminal cell fate. Vice versa, expression in K8+ luminal cells lead to reprogramming to a basal cell fate [Koren et al.,

2015, Van Keymeulen et al., 2015]. Considering that PIK3CA^{H1047R} is among the most common mutations occurring in breast cancer [Cancer Genome Atlas Network, 2012], the observation that it impacts cell fate reveals a mechanism potentially underlying breast cancer plasticity and heterogeneity.

Together, MaSCs/bipotent progenitors have been found in the basal cell compartment of both human and mouse MG by transplantation, while lineage tracing studies imply that the MG is maintained by unipotent progenitors after birth. However, it is not yet solved unequivocally whether rare MaSCs/bipotent progenitors exist *in vivo* and which might be the stimuli activating them. In addition, the fact that plasticity can be triggered by 2D culture in the presence of ROCK inhibitors or fibroblast-derived factors, or by overexpression of PIK3CA^{H1047R}, suggests that regenerative cells can be generated *de novo*, which might play a role in tumor development/progression. More research is needed to investigate MaSC/bipotent progenitor features and unravel mechanisms triggering cellular plasticity and investigate their role in cancer development and progression. While up to date most studies are performed in mice, future studies should aim to confer the gained insight to the human MG. To facilitate the identification and characterization of human mammary stem/progenitor cells and the analysis of plasticity, *in vitro* culture models are needed in which HMECs recapitulate morphological and physiological characteristics of the human MG *in situ*.

1.3 The need for *in vitro* systems for the assessment of human MaSC identity and lineage plasticity

As described above, transplantation assays and lineage tracing approaches are the most commonly used methods for the identification and characterization of murine MaSCs. However, these approaches are scarcely suited for the identification and characterization of human MaSCs: Lineage tracing approaches cannot be performed in human due to obvious ethical reasons. In addition, transplantation of primary HMECs into cleared murine mammary fat pads does not lead to regeneration, potentially due to differences in the mouse host stroma, which contains more adipose tissue than the collagen rich human stroma [Parmar et al., 2004]. Although the growth of HMECs in murine transplantation can be improved by introduction of collagen and fibroblasts, these approaches still depend on the use of organoids, small tissue fragments containing all mammary cell types in unknown quantities, non-human fibroblasts and are of very low-throughput [Eirew et al., 2008, Kuperwasser et al., 2004]. Therefore, human MaSC research requires *in vitro* assays in which HMECs recapitulate morphological and physiological characteristics of the human MG *in situ*. Unfortunately, these requirements are not met by currently used *in vitro* assays. Up to date, 2D culture on stiff polystyrene cell culture plates is the most commonly used culture system. In this system, cells acquire a flattened shape and the area and plane of cell-matrix and cell-cell contacts are different from *in vivo*. Thereby, multiple cellular processes including differentiation, migration, proliferation and survival are aberrantly regulated by 2D culture [Ashe et al., 2006, Tibbitt et al., 2009, Zhang et al., 2005]. In addition, most used culture models rely on the use of cell-lines which do not represent the behavior of cells *in vivo*, as immortalization and prolonged culture introduce genetic and phenotypic changes and usually lead to the selection of a subpopulation of cells [Birgersdotter et al., 2005, Petersen et al., 1992, Prat et al., 2013]. The biological relevance is also often comprised by the use of non-MG derived stromal cells. Due to the artificial environment the histological architecture and function of the human MG *in situ* is not recapitulated by commonly used in vitro assays [Dontu et al., 2003, Eirew et al., 2008, Gudjonsson et al., 2002, Stingl et al., 2005]. Therefore, new biologically relevant culture models are needed which allow for the identification and characterization of HMECs *in vitro*.

2 Material

2.1 Reagents and chemicals

Product	Supplier (Catalog No.)
1,7-Dichloro-octamethyltetrasiloxane	Santa Cruz (sc-229834)
Aluminum potassium sulfate	Sigma (A-7167)
A83-01	Miltenyi Biotec (130-095-565)
Aqua-Poly/Mount	Polysciences (18606)
β-Mercaptoethanol	Sigma (63689)
Blebbistatin	Sigma (B0560)
Bovine serum albumin, fraction V (BSA)	Roth (CP84.2)
Carmine	Sigma (C-1022)
Collagen type I rat tail	Corning (354236)
Dimethyl sulfoxide (DMSO)	Sigma (D8418)
Forskolin	Biomol (AG-CN2_0089)
Glycine	Roth (3790.3)
Hanks' Balanced Salt Solution (HBSS)	Thermo Fisher Scientific (14175)
4-(2-hydroxyethyl)-1-piperazineethanesulfonic acid, 1M (HEPES)	Life Technologies (15630)
Growth factor reduced Matrigel	Corning (FALC354230)
n-heptane	Applichem (1948)
Normal donor donkey serum	GeneTex (GTX73205)
Normal donor goat serum	GeneTex (GTX73206)
Paraformaldehyde 16% (w/v) (PFA)	VWR International (043368-9M)
Phosphate-buffered saline (PBS), pH 7.4	Life Technologies (10010056)
Polyetyleneimine (PEI), linear	Alfa Aesar (43896)
Thiazovivin	Selleckchem (S1459)
Triton X-100	Sigma (T8787)
Y-27632	Biomol (AG-CR1_3564)

2.2 Enzymes and growth factors

Product	Supplier (Catalog No.)
Collagenase type I	Sigma Aldrich (C0130)
Dispase	Stem Cell Technologies (07913)
Hyaluronidase type I	Sigma Aldrich (H3506)
Insulin	Sigma (I6634)
TGF-β1	R&D Systems (240-B)

2.3 Cell culture media and solutions

Product	Supplier (Catalog No.)
Dulbecco's Modified Eagle Medium (DMEM)	Thermo Fisher Scientific
Fetal calf serum (FCS), PANSera ES	PAN Biotech (30-2602)
Mammary Epithelial Cell Growth Medium (MECGM) including supplements: 0.004 ml/ml Bovine Pituitary Extract 10 ng/ml Epidermal Growth Factor (recombinant human) 5 µg/ml Insulin (recombinant human) 0.5 µg/ml Hydrocortisone	PromoCell (C-21010)
Penicillin/Streptomycin (10,000 U/ml)	Invitrogen (15140122)
Trypsin-EDTA 0.05%, 0.25%	Thermo Fisher Scientific (25300, 25200)
Trypsin Neutralizing Solution (TNS)	PromoCell (C-41120)

2.4 Composition of media, buffers and solutions

2.4.1 Composition of media

Media	Composition
Freezing medium for freshly isolated cells (FRZM1)	50% (v/v) FCS 40% (v/v) PCB 10% (v/v) DMSO
Freezing medium for cultured primary cells (FRZM2)	70% (v/v) MECGM 20% (v/v) FCS 10% (v/v) DMSO
Transport medium (TM)	PCB 5% (v/v) FCS
Tissue digestion buffer (TDB)	PCB 1.5% (w/v) BSA, fraction B
HBSS with HEPES and FCS (HF)	HBSS 10 mM HEPES 2% (v/v) FCS
Seeding medium	MECGM 100 U/ml Penicillin/Streptomycin 0.5% FCS 10 µM Forskolin 3 µM Y-27632
Maintenance medium	MECGM 100 U/ml Penicillin/Streptomycin 10 µM Forskolin
Basic medium	MECGM 100 U/ml Penicillin/Streptomycin

2.4.2 Composition of buffers and solutions

Buffer/Solution	Composition
Carmine alum solution	Distilled water 0.2% (w/v) Carmine 0.5% (w/v) Aluminum Potassium Sulfate
Siloxane coating solution	n-heptane 25 g/l 1,7-Dichloro-octamethyltetrasiloxane
10+1 Neutralizing solution	11x PBS 550 mM HEPES
Primary cell buffer (PCB)	DMEM:F12 (Ratio 1:1) 10 mM HEPES 100 U/ml Penicillin/streptomycin
FACS buffer	PBS 0.1% (w/v) BSA

2.5 Kits and arrays

Product	Supplier (Catalog No.)
Easy Script Plus cDNA Synthesis Kit	Abm (G236)
FITC BrdU Flow Kit	Beckton Dickinson (559619)
GeneChip® Human Gene 2.0 ST Array	Affymetrix (902112)
Ovation Pico WTA System V2	Nugen (3302)
Power SYBR Green PCR Master Mix	Applied Biosystems (4367659)
QIAshredder	Qiagen (79656)
RNase-free DNase Set	Qiagen (79254)
RNeasy Mini Kit	Qiagen (74104)
UltraView Universal DAB Detection Kit	Ventana (760-500)

2.6 Antibodies and fluorescent stains

2.6.1 Primary antibodies and fluorescent stains

Epitope [Clone]	Conjugation	Host	Supplier (Catalog No.)	Dilution
4’,6-diamidino-2-phenylindole (DAPI)	-	-	Sigma-Aldrich (D9542)	167 ng/ml
CK18 [Ks18.04]	-	Mouse	Progen (61028)	1:100
E-cadherin [24E10]	Alexa 488	Rabbit	New England Biolabs (3199)	1:50
E-cadherin [EP700Y]	-	Rabbit	GeneTex (GTX61329)	1:250
GATA3 [L50-823]	-	Mouse	Biocare Medical (CM 405 C)	1:250
Integrin-α6 [GOH3]	-	Rat	Santa Cruz (sc-19622)	1:100
K8/18 [5D3]	-	Mouse	Dianova (DLN-10750)	1:100
Laminin	-	Rabbit	Sigma-Aldrich (L9393)	1:100
p63 [BC4A4]	-	Mouse	Abcam (ab735)	1:100
p63 [H-137]	-	Rabbit	Santa Cruz (sc-8343)	1:100
p63 [Y289]	-	Rabbit	Abcam (ab32353)	1:100

Epitope [Clone]	Conjugation	Host	Supplier (Catalog No.)	Dilution
Phalloidin	Atto 647N	-	Sigma-Aldrich (65906)	1:250
Vimentin [D21H3]	-	Rabbit	Biozol (5741)	1:100
Vimentin [V9]	-	Mouse	Abnova (MAB3578)	1:100
ZO-1 [1A12]	Alexa 594	Mouse	Thermo Fischer Scientific (339194)	1:100
ZO-1 [1A12]	-	Mouse	Thermo Fischer Scientific (339100)	1:100

2.6.2 Secondary antibodies

Host	Epitope	Conjugation	Supplier (Catalog No.)	Dilution
Goat	Mouse IgG	Alexa 594	Life Technologies (A11032)	1:250
Goat	Rabbit IgG	Alexa 488	Life Technologies (A11034)	1:250
Goat	Rat IgG	Alexa 594	Life Technologies (A11007)	1:250
Donkey	Mouse IgG	Alexa 488	Life Technologies (A21202)	1:250
Donkey	Rabbit IgG	Alexa 546	Life Technologies (A10040)	1:250
Donkey	Rabbit IgG	Alexa 594	Life Technologies (A21207)	1:250
Donkey	Rat IgG	Cy3	Dianova	1:250
Donkey	Rat IgG	Alexa 488	Life Technologies (A21208)	1:250

2.6.3 Antibodies and fluorescent stains for flow cytometry

Epitope [Clone]	Conjugation	Host	Supplier (Cat. No.)	Volume (µl) *
7-Aminoactinomycin D (7-AAD)	-	-	BD (559925)	2
CD10 [HIC10a]	APC	Mouse	Biozol (312210)	2.5
CD31 [WM59]	PB	Mouse	Biozol (303114)	0.5
CD326/EpCAM [VU-1D9]	FITC	Mouse	Biozol (GTX79849)	5
CD45 (HI30]	V450	Mouse	BD (560367)	0.5
CD49f [GoH3]	PE	Rat	BD (5557369	2.5

* used to stain $1x10^6$ cells

2.7 Consumables

Product	Supplier
6-, 24-, 48-well polystyrene cell culture plates	BD
10 cm polystyrene cell culture dishes	BD
Cell strainer (40 µm nylon)	Corning
15-, 50-ml tubes	Corning
Cyrotubes	Thermo Fisher Scientific
Filter system for sterile filtration	Sigma
0.45 µm PVDF filter	Merck Millipore
KOVA Glasstic slide 10 with counting grids	VWR International
Microscopy slides, cut edges, matt strip	Thermo Fisher Scientific
Cover glasses, 13 mm, round	VWR International

Product	Supplier
Micro cover glasses 22 mm x 40 mm	VWR International
Optical 384-well reaction plate	Life Technologies
Pipette tips filtered	Starlab
Pipette tips unfiltered	Starlab
Reaction tube 1.5 ml	Eppendorf
5-, 10-, 30- ml Stripettes	Greiner Bio-One
12x75 mm Tube with cell strainer cap (FACS tube)	BD Falcon

2.8 Technical devices

Product	Manufacturer
Axio Imager.M2m	Zeiss
Axioplan 2 Imaging Microscope	Zeiss
FACSAria™ III and IIIU	BD
FLUOVIEW FV1000 Inverted Confocal Laser Scanning Microscope	Olympus
Heracell 240i CO_2-Incubator	Thermo Fisher Scientific
Heraeus Fresco 21 Microcentrifuge	Thermo Fisher Scientific
Heraeus Megafuge 40R Centrifuge	Thermo Fisher Scientific
Leica DM IL LED	Leica
Mastercycler nexus gradient	Eppendorf
Nano-Drop ND-1000	NanoDrop Technologies
QuantStudio 12K Flex qPCR System	Life Technologies
SteREO Lumar.V12	Zeiss

2.9 Software

Product	Manufacturer
Axiovision Rel 4.7	Zeiss
FACS Diva™ v6.1.3	BD
FlowJo V10	FlowJo
FluoView FV10-ASV 1.7 Viewer	Olympus
FluoView FV10-ASW	Olympus
Gimp 2.8.2	GIM Team
GraphPad Prism 6	GraphPad Software
ImageJ 1.48	NIH
MS Office	Microsoft
Photoshop, Illustrator CS5	Adobe
QuantStudio 12K Flex Software	Life Technologies
ZEN 2 pro	Zeiss

2.10 Synthetic oligonucleotides (primers)

Target	Sequence (Forward, Reverse)
CDH1	TGCCCAGAAAATGAAAAAGG, GTGTATGTGGCAATGCGTTC
ELF5	TAGGGAACAAGGAATTTTTCGGG, GTACACTAACCTTCGGTCAACC
FN1	CAGTGGGAGACCTCGAGAAG, TCCCTCGGAACATCAGAAAC
GATA3	GCCCCTCATTAAGCCCAAG, TTGTGGTGGTCTGACAGTTCG
KRT8	TCCTCAGGCAGCTATATGAAGAG, GGTTGGCAATATCCTCGTACTGT
RPL32	CAGGGTTCGTAGAAGATTCAAGGG, CTTGGAGGAAACATTGTGAGCGATC
MME	TGGATCTTGTAAGCAGCCTCA, GCACAACGTCTCCAAGTTGC
CDH2	ACAGTGGCCACCTACAAAGG, CCGAGATGGGGTTGATAATG
OVOL2	ACAGGCATTCGTCCCTACAAA, CGCTGCTTATAGGCATACTGC
TP63	AGAGAGAGGGACTTGAGTTCT, TGGTCGATGCTGTTCAGGAGC
SNAI2	GGGGAGAAGCCTTTTTCTTG, TCCTCATGTTTGTGCAGGAG
VIM	GAGAACTTTGCCGTTGAAGC, GCTTCCTGTAGGTGGCAATC
ZEB1	GCACAAGAAGAGCCACAAGTAG, GCAAGACAAGTTCAAGGGTTC
TJP1	CTTACCACACTGTGCGTCCAT, AGGAGTCGGATGATTTTAGAGCA

2.11 Plasmids and cell lines

2.11.1 Plasmids

Plasmid	Description	Resistance	Source
pRRL.SIN.cPPT.CMV-GFP.WPRE	Lentiviral expression vector coding for eGFP	Ampicillin	Gift from Timm Schröder, ETH Basel, Switzerland
pMD2.G	VSV-G envelope expressing	Ampicillin	Addgene plasmid 12259
psPAX2	2ng generation lentiviral packaging plasmid	Ampicillin	Addgene plasmid 12260

2.11.2 Cell lines

Cell line	Description	Source
HEK 293T/17 High perfor-mance cells	Derivative of the 293 cell line into which the temperature sensitive gene for SV40 T-antigen was inserted. Highly trans-fectable and capable of producing high titers of infectious virus.	ATCC (CRL-11268)

2.12 Primary cells

Donor	Age (years)	Parity (# Offspring)
M1	44	1
M2	68	1
M3	71	2
M4	68	2
M6	69	1
M7	35	2
M8	53	2
M9	17	0
M10	42	1
M12	54	0
M16	18	0

3 Methods

3.1 Cell biological methods

All cells were maintained in sterile conditions and handled under a clean hood with laminar air flow. Cells were grown in an incubator at 37 °C, 95% humidity and 5% CO_2. In the case of primary cells, oxygen levels were maintained at 3% to reduce oxidative stress. Cell lines were cultured at ambient oxygen of around 21%. All centrifugation steps were performed at ~490 × *g*, at 4 °C for 5 min, if not specified otherwise.

3.1.1 Isolation of primary HMECs

Breast tissue was obtained from healthy women undergoing reduction mammoplasty for aesthetic purposes at the "Nymphenburger Praxis für Plastische und Ästhetische Chirurgie" (Böcklinstraße 1, 80638 München). Tissue was collected in accordance with the regulations of the ethics committee of the Ludwig-Maximilian University, Munich, Germany (proposal 397-12).

Freshly obtained tissue was transported on ice and processed immediately. The mammary epithelial ductal tree was cleaned from adipose tissue using scalpels and then minced into pieces of about 1 mm^3. These were enzymatically digested in tissue digestion buffer (TDB), supplemented with 1 µg/ml insulin, 300 U/ml collagenase, 100 U/ml hyaluronidase at 37 °C for approximately 16-20 h while slowly rotating (6 rpm). Next, cells were pelleted and the fatty supernatant was removed by aspiration after which the pellet was resuspended in primary cell buffer (PCB), transferred to a fresh tube and pelleted and resuspended in PCB again to get rid of residual fat. At this point, an optional differential centrifugation (~200 × *g*, 4 °C, 3 min) allowed for enrichment of fibroblasts in the supernatant and enrichment of epithelial cells in the pellet. Fibroblasts in the supernatant were pelleted by centrifugation and cyropreserved in freezing medium (FRZM1). The pellet enriched for epithelial cells was dissociated in 0.15% pre-warmed trypsin-EDTA while mixing by gently pipetting for 2-3 min. After addition of cold HBSS with HEPES and FCS (HF), cells were pelleted and further dissociated in 5 mg/ml pre-warmed dispase (37 °C) by gently pipetting for 1 min. Cells were pelleted, cryopreserved in freezing medium (FRZM1) and aliquots were stored in liquid nitrogen.

3.1.2 Thawing of primary HMECs

Vials containing primary human mammary epithelial cells in FRZM1 were placed in a water bath set to 37 °C. Once thawed, cells were immediately resuspended in Epithelial Cell Growth Medium (MECGM) and filtered through a 40 µm strainer to remove any residual tissue fragments and cell aggregates. Next, cells were centrifuged and the pellet was plated in seeding medium. With the first medium change after 5 days, medium was changed to maintenance medium, unless otherwise stated. After the establishment period of 5 days, medium was replaced every 2-4 days.

3.1.3 Cell counting

For cell counting, a 10 µl aliquot of cell suspension was injected into a chamber of a KOVA Glasstic Slide and live cells, identified by morphology and intracellular granularity, were counted using a light microscope (Leica DM IL LED, 10x objective). The total number of live cells was calculated using the following formula:

n (total # cells/sample) = mean of two squares x total volume (ml) x 10^4

3.1.4 2D culture of HMECs

Single cell suspensions containing the desired amount of fresh HMECs in establishment medium were seeded into polystyrene cell culture plates (12-well plate, 6-well plate or 10 cm dish). After an establishment period of 5 days, cells were cultured in maintenance medium. Once cells reached about 80-90% confluency, they were split at a ratio of 1:2 to 1:8, depending on the experiment and cell type. Generally, LP cells were split at a lower ratio than bulk, B and B+ cells. For splitting, medium was removed and cells were washed with PBS. Next, 0.15% trypsin-EDTA was added and cells were incubated at 37 °C until they detached, which usually took 2-10 min, depending on the cell type. To neutralize trypsin, three times the volume of trypsin neutralizing solution (TNS) was added and cells were separated mechanically by pipetting up and down. Optionally, 10 µl of cell suspension was taken to count cells before the desired amount was transferred to a 15 or 50 ml conical and centrifuged. The pellet was resuspended in the desired medium and seeded into a fresh 2D culture plate or collagen gel.

3.1.5 3D culture of HMECs in collagen gels

For the generation of floating collagen gels, cell culture plastics were siloxane-coated to facilitate detachment of gels. Briefly, polystyrene cell culture plates were incubated with

siloxane coating solution for 30 s at room temperature (RT) and subsequently rinsed once with PBS and deionized water. For attached and attached-to-floating collagen gels, uncoated polystyrene cell culture plates were used.

The preparation of collagen gels was based on a published protocol [Wozniak et al., 2005] with modifications described below. Neutralizing solution comprising $1/10^{th}$ of the volume of collagen solution was mixed with the desired amount of dissociated HMECs in establishment or maintenance medium. Next, acidified rat tail collagen type I was added and mixed with the cell-suspension, resulting in a final collagen concentration of 1.3 mg/ml. Quickly, 200 or 400 µl of the gel mixture was transferred into a 48-well or 24-well cell culture plate on ice, respectively. The plate was placed in an incubator set to 37 °C to allow polymerization of collagen fibers. After 1 h, 300 (48-well plate) or 600 µl (24-well plate) of medium with supplements was added carefully to the edge of the culture dish. The concentration of supplements, including FCS, Forskolin and Y-27632 was calculated for the total volume of the gel with medium. To detach the collagen gels, they were encircled with a pipet tip and plates were gently shaken.

Cells in collagen gels were cultured for 8 to 20 days. To determine the number of cells per gel, collagen gels were digested with 300 U/ml collagenase I (Sigma) for 1 h at 37 ºC, dissociated by treatment with 0.15% trypsin (5 min at 37 ºC), and the cell suspension was filtered to obtain single cells. Cells were counted as described above.

Microscopy: Images of structures in collagen gels were acquired on a Leica DM IL LED microscope equipped with a HiPlan 10x/0.22 PH1 objective. Images of whole gels were taken with a Zeiss SteREO Lumar.V12 microscope with a NeoLumar S 0.8x objective (6.4 x Zoom).

3.1.6 3D culture of HMECs in Matrigel

For culture in rBM/Matrigel, the desired amount of freshly isolated and dissociated HMECs in establishment medium was resuspended in cold growth factor reduced Matrigel on ice and plated into 24-well polystyrene cell culture plates (400 µl/well). Matrigel was allowed to polymerize in an incubator at 37 °C. After 1 h, 600 µl of establishment medium was added and cultures were treated like 3D collagen gels.

3.2 Stainings

3.2.1 2D immunofluorescence

Fluorescence describes the absorption of light of a certain wavelength and subsequent emission of light of a longer wavelength by chemical compounds called fluorophores. Fluorescence microscopy makes use of this phenomenon to reveal the presence of molecules of interest with high sensitivity and spatial resolution. For this, fluorescently labeled antibodies are used, which recognize primary antigen-specific antibodies. The secondary antibodies can be detected using a regular wide field epifluorescence microscope to irradiate the specimen with excitation light and visualize the resulting emission light [Abramowitz et al., 2012, Herman et al., 2012].

For the preparation of samples for 2D immunofluorescence, all steps were performed at RT, unless stated otherwise. Tables containing all primary and secondary antibodies with their respective dilutions are presented in Chapter 2.6.1 and 2.6.2, respectively.

Cells were grown on poly-D-lysine-coated glass coverslips. Once cells had reached the desired confluency, medium was removed and cells were washed once in PBS, fixed with 4% paraformaldehyde for 15 min, and washed three times with PBS. Next, cells were permeabilized with 0.2% Triton X-100 for 2 min, washed once with PBS and were then blocked with 10% goat or donkey serum in 0.1% BSA for 1-2 h. After another washing step with PBS, the coverslips were placed on 50 µl of primary antibody solution in 0.1% BSA. After an incubation period of 1-2 h, the coverslips were washed by dipping them 5 times into PBS, and were then placed on 50 µl of secondary antibody solution in 0.1% BSA. After an incubation period of 2-3 h, the coverslips were washed by dipping them 5 times into PBS, and were then laid on 50 µl of 167 ng/ml DAPI staining solution for about 4 min. Next, coverslips were washed extensively by 10 times dipping into PBS, followed by 5 times dipping into MQ. Excess water was removed by dabbing the edges of the coverslip with a paper towel. Coverslips were mounted using a drop of Aqua-Poly/Mount mounting medium and allowed to dry over night at RT.
Images were acquired on an Axioplan 2, or on an Axio Imager.M2m imaging microscope using a 20x objective. Images were processed with Axiovision Rel 4.7/ Zen 2 pro and Gimp 2.8.2/Adobe Photoshop CS5 software.

3.2.2 3D immunofluorescence

In regular wide-field epifluorescence microscopy as used for 2D immunofluorescence described above, the entire specimen is illuminated and out-of-focus fluorescence often results in decreased resolution in the focal plane, which is a particular problem of thick specimens. Thus, for imaging of the thick structures generated in floating and attached collagen gels, confocal microscopy was used, which makes use of pinholes to focus excitation light and prevent detection of out-of-focus emission light. Thus, by only allowing detection of light from close to the focal plane, confocal images have better resolution than regular wide-field images, especially in the sample depth direction [Fellers et al., 2012].

For the preparation of samples for 3D immunofluorescence, all steps were performed at room temperature on an orbital shaker, if not indicated otherwise. Tables containing all primary and secondary antibodies with their respective dilutions are presented in Chapter 2.6.1 and 2.6.2, respectively.

Collagen gels were washed with PBS for 10 min, fixed with 4% paraformaldehyde for 15 min and washed again with PBS for 10 min. Remaining paraformaldehyde was quenched by addition of 0.15 M glycine for 10 min, upon which gels were washed again with PBS for 10 min. Cells were permeabilized with 0.2% Triton X-100 for 10 min and washed with PBS for 10 min, followed by blocking with 10% goat or donkey serum in 0.1 % BSA for 2-3 h at RT or overnight at 4 °C. After another washing step with PBS for 10 min, primary antibodies in 0.1% BSA were added and incubated at 4 °C overnight. After two washing steps with PBS for 10 min each, 167 ng/ml DAPI was added for 4 min to stain nuclei. Next, gels were washed with PBS three times for 10 min each and twice with deionized water for 5 minutes each. Collagen gels were transferred to a microscopy slide and excess water was removed using a dust-free tissue. Gels were mounted by adding 2-3 drops of Aqua-Poly/Mount mounting medium and then slowly placing a microscopy coverslip on top of the gels, without introducing any bubbles. Mounted gels were allowed to dry at RT overnight or at 4 °C over the weekend.

Images were acquired on a FLUOVIEW FV1000 inverted confocal laser scanning microscope equipped with four laser lines (405, 488, 543, and 633 nm) and UPLSAPO 60x, 40x and 20x objective lenses. FV-10-ASW 1.7 Viewer and Gimp 2.8.2/Adobe Photoshop CS5 software were used to adjust brightness across the entire image field.

3.2.3 Carmine staining

The carmine dye, a complex of aluminum and the natural dye cochineal, is commonly used to stain wholemounts of mouse MGs in order to reveal the ductal epithelial structure of the gland [Dapson, 2007]. Therefore, in this study, carmine staining was used to visualize the structures growing in collagen gels.

Carmine staining solution was prepared by boiling 1 g carmine and 2.5 g aluminum potassium sulfate in 500 ml distilled water for 20 min. After boiling, the final volume of the solution was adjusted to 500 ml by adding distilled water and the solution was strained through a filter system for sterile filtration. A crystal of thymol was added for preservation and the staining solution was stored at 4 °C. For staining of collagen gels, the gels were fixed as described above and incubated in carmine staining solution overnight at RT on an orbital shaker. Collagen gels were transferred to microscopy slides, excess water was removed with a dust-free tissue and gels were mounted as described above.

Images of single structures were acquired on a Leica DM IL LED microscope with a HiPlan 10x/0.22 PH1 objective and whole mount pictures were taken with a Zeiss SteREO Lumar.V12 microscope with a NeoLumar S 0.8x objective (10-20x zoom).

3.2.4 Immunohistochemistry and hematoxylin and eosin staining

Immunohistochemistry and hematoxylin and eosin (H&E) stainings were kindly provided by Harald S. Bartsch and Karl Sotlar (Institute of Pathology, Medical School, Ludwig Maximilian University Munich, Munich 80337, Germany).

For immunohistochemistry, collagen gels were fixed in 4% paraformaldehyde as described above and embedded in paraffin. 2 µm thick sections were cut from the paraffin block and stained with primary antibodies listed in Chapter 2.6.1. Primary antibodies were detected by species specific HRP-linked secondary antibodies (ultraView Universal DAB Detection Kit) according to the manufacturer's protocol.

For hematoxylin and eosin staining, formalin-fixed and paraffin-embedded (FFPE) breast tissues from cosmetic breast reduction surgeries from the tissue archives of the Institute of Pathology, Ludwig-Maximilians-University Munich, Munich, Germany, were cut into 2 µm thick sections and stained with H&E according to standard protocols. H&E stained sections

were examined by two pathologists to exclude samples exhibiting signs of dysplasia or malignancy. Tissue samples were anonymized in accordance with the ethics committee regulations.

3.2.5 Morphological analysis of gels, structures and cells

To quantify the amount of branching points, the longest branch was determined for each structure. From there, primary, secondary, tertiary and quaternary side branches were counted. One branching point was counted for each side branch.

To determine the area size of gels, structures and cells, images were opened in Image J and, if needed, spatially calibrated against an image with known value. Subsequently, the area size was determined using the tool for measurement of areas. Structures were counted using the ImageJ cell counter. Structures containing at least two branching points were considered branched.

3.3 Flow Cytometry

Flow cytometry allows for the analysis and sorting of single cells and was used in this study to derive subpopulations of HMECs. For analysis by flow cytometry, a single cell suspension is usually stained with fluorescently labeled antibodies and then aspirated into the FACS machine, where the cells pass multiple laser beams allowing for the determination of relative cell size, complexity/granularity and expression of cellular markers (labeled protein). For sorting, droplets containing one cell each are generated, charged with a certain electrical load after which they get separated by two installed deflection plates. The deflected droplets can then be collected.

3.3.1 Surface staining

For fluorescent staining of cells, freshly isolated HMECs were thawed, taken up in MECGM, given through a 40 µm strainer to remove any residual tissue fragments and cell aggregates and then counted. After centrifugation, cells were resuspended in FACS buffer and stained with fluorescent antibodies CD31-PB,CD45-V450, CD49f-PE, EpCAM-FITC and CD10-APC (antibodies are listed in Chapter 2.6.3) for 40 min on ice protected from light. After washing with PBS, controls were resuspended in approximately 500 µl FACS buffer per $1x10^6$ cells and samples were resuspended in 100 µl FACS buffer per $1x10^6$ cells to allow for efficient sorting. 7-AAD was added to one control and all samples, and incubated for at least 15 min to exclude dead cells from the analysis.

3.3.2 Analysis and sorting of cells

For analysis and sorting of primary HMEC populations, cell debris was excluded based on SSC-A/FSC-W followed by exclusion of doublets using both FSC-A/FSC-W and SSC-A/SSC-W gates. Live (7-AAD$^-$), Lineage negative (Lin$^-$, CD31$^-$, CD45$^-$) cells were then separated into four populations based on the expression of CD49f and EpCAM. (Stroma: CD49f$^-$/EpCAM$^+$, LM: CD49f$^-$/EpCAM$^+$, LP: CD49f$^+$/EpCAM$^+$, B: CD49f^{hi}/EpCAM$^-$). The basal (B) population was further subdivided into B− and B+ cells (B−: CD10$^-$/CD49f^{hi}/EpCAM$^-$, B+: CD10$^+$/CD49f^{hi}/EpCAM$^-$) using a FACSAria^{TM} III/IIIU. Desired populations were sorted into tubes containing basic medium, using the purity or 4-way purity mode to ensure that only drops free of contaminating cells were sorted. After the sort, cells were washed losing as few cells as possible, by directly adding PBS to the limit of the tube. Tubes were then centrifuged and the pellet was taken up in seeding medium (2D culture) or in basic medium (3D culture). The leftover cells were reanalyzed by flow cytometry to assess purity of the sort. Only experiments with less than 1% of contaminating cells were used for experiments and further analysis. FlowJo V10 was used for post-analysis.

3.4 Extreme limiting dilution analysis

In limiting dilution analysis, cells are usually seeded/transplanted in degrading dilutions up to doses in which no activity can be detected any more. By counting the cultures/transplants in which activity can be detected, the rate of cells of interest can be inferred [Hu et al., 2009].

In order to determine structure-forming units (SFU), HMECs were seeded into floating collagen gels in limiting dilution up to doses in which no branched structure/sphere formation could be detected. At least six gels per cell dose were prepared in 48-well plates, as described in Chapter 4.1.5. The generated structures were stained with carmine and images were taken on a Zeiss SteREO Lumar V12 microscope with a NeoLumar S 0.8× objective (10-20× zoom). Gels which contained at least one branched structure were counted as positive. Branched structures were defined as containing at least two branching points and being 0.057 mm^2 or more in size. Limiting dilutions were analyzed using ELDA software, a webtool described previously [Hu et al., 2009]. This webtool is especially suited for analysis of limiting dilution data from stem cell research, as it implements methods to give reliable confidence intervals in situations when all assays give positive or negative results and includes a test to compare active cell frequencies between multiple data sets [Hu et al., 2009]. Using this method, 95% confidence intervals for the frequency of active cells in a group and p-values to compare differences in active cell frequencies between groups, are given.

3.5 Molecular biology techniques

3.5.1 RNA extraction

For RNA extraction, the RNeasy Mini Kit in combination with QIAshredder columns and the RNase-free DNase Set from Qiagen were used. In case of 2D cultures, cells were grown on 6-well polystyrene plates to approximately 80% confluency. Plates were placed on ice and each well was washed with PBS and lysed with 350 µl RLT buffer containing 1% β-mercaptoethanol to prevent degradation of RNA by RNases. In case of freshly isolated cells, cells were sorted by FACS as described above and collected in MECGM. After centrifugation at ~490 × *g* for 5 min, medium was removed and the pellet was lysed in RLT buffer containing 1% β-mercaptoethanol. For homogenization, cell lysates were vortexed for 30 s, frozen at -80 °C for at least 1 h, thawed on ice and again vortexed for 30 s. Cell lysates were transferred to QIAshredder columns and centrifuged for 2 min at maximum speed (21100 × *g*) for further homogenization and removal of cellular debris. RNA was purified using the RNeasy Mini Kit from Qiagen (silica technology), including an additional DNA-digestion step using the RNase-free DNase Set from Qiagen, both of which were performed according to the manufacturer's instructions. RNA was eluted in RNAse free water and stored at -80 °C.

3.5.2 Determination of RNA concentration

RNA concentration was measured photometrically using the Nano-Drop ND-1000. Specifically, absorption of light at a wavelength of 260 nm was measured against a water reference, and RNA concentration was determined by the software based on Beer's Law.

3.5.3 Reverse transcription

1 µg total RNA was reverse transcribed using the EasyScriptPlus cDNA Synthesis Kit from Applied Biological Materials, according to the manufacturer's Oligo(dT) protocol. Synthesized cDNA was stored at -20 °C.

3.5.4 Quantitative real time polymerase chain reaction (RT-PCR)

Quantitative real-time PCR (RT-PCR) was performed using the PowerSYBR® Green PCR Master Mix from Applied Biosystems. The reaction mixture per sample had a volume of 10 µl, containing 2 µl (10 ng) cDNA, 0.25 µl (50 nM) of each forward and reverse primer, 2.5 µl DNase/RNase-free H_2O and 5 µl PowerSYBR Green PCR Master Mix containing deoxynucleotides (dNTPs), SYBR® Green I Dye and AmpliTaq Gold® DNA Polymerase (Table 3.1). Samples were run on a QuantStudio 12K Flex qPCR System with the cycling

program listed in Table 3.2. Briefly, AmpliTaq Gold® DNA Polymerase was activated and double-stranded cDNA was detected during 40 cycles of amplification. After amplification, a melting curve was generated to assess the dissociation-characteristics of the generated cDNA dimers during heating, allowing for detection of nonspecific product formation.

Relative expression of the target gene compared to the housekeeping gene PRL32 was calculated according to the ΔC_T method (Schmittgen and Livak, 2008) by subtracting the C_T value of the gene of interest from the C_T value of the housekeeping gene. The fold change of transcript levels between gene of interest and housekeeping gene was determined with the formula $2^{\Delta CT}$. We chose to show absolute values of a representative single experiment multiplied by 1000. All primers used are listed in Chapter 2.10.

Table 3.1 RT-PCR reaction mixture per sample

Component	Used Volume (Final concentration)
Forward primer	0.25 µl (50 nM)
Reverse primer	0.25 µl (50 nM)
DNase/RNase-free H_20	2.5 µl
PowerSYBR Green PCR Master Mix	5 µl
cDNA	2 µl (1 ng/µl)
Total volume	**10 µl**

Table 3.2 RT-PCR cycling program

Cycles	Step	Temperature	Duration
1	Initial activation of AmpliTaq Gold® DNA Polymerase	95 °C	10 min
40	Denaturation to yield single stranded cDNA molecules	95 °C	15 s
	Annealing of primers to cDNA	60 °C	30 s
	Extension of cDNA	72 °C	16 s
	Melting curve	70 to 95 °C	

3.5.5 Microarray

For gene expression analysis, the Affymetrix Human Gene 2.0 ST array, a single-channel whole transcriptome DNA-microarray, was used. This array contains short unlabeled DNA molecules (probes) of a known sequence. The target cDNA specifically binds to probes with complementary DNA sequence after which probe-target pairs can be detected and quantified.

3.5.5.1 Expression profiling

For expression profiling, total RNA from freshly sorted HMECs (B−, B+ and LP populations) was isolated using the RNeasy Mini Kit, in combination with QIAshredder columns and

RNase-free DNase Set (all Qiagen), as described above. Further processing of RNA samples, expression profiling and statistical transcriptome analysis were kindly performed by Martin Irmler (Institute of Experimental Genetics, Helmholtz Center Munich, Neuherberg, Germany).

In short, total RNA was amplified and reverse transcribed using the Ovation Pico WTA System V2 according to the manufacturer's protocol. This system is optimized to generate cDNA from small amounts of RNA for use in gene expression analysis applications including microarrays. Generation of the first strand of cDNA is achieved using a mix of RNA/DNA chimeric oligodT and random primers and reverse transcriptase. Thereby, amplification is initiated both at the 3'end as well as throughout the entire transcriptome of the sample, such that even compromised RNA is reverse transcribed. The resulting mRNA/cDNA hybrid molecules contain a RNA tag sequence (SPIA tag) at the 5'end of the cDNA molecule. In the second step, the mRNA is fragmented allowing DNA polymerase to synthesize a second cDNA strand, containing DNA complementary to the RNA SPIA tag. Amplification of cDNA is achieved using the chimeric DNA/RNA SPIA primers, DNA polymerase and RNase H.

After removal of the RNA portion of the SPIA primer by RNase H, a new SPIA primer can bind and DNA polymerase starts to synthesize cDNA, thereby displacing the existing strand. Importantly, every time a SPIA primer binds to the cDNA, a new substrate for RNase H is created, triggering the next round of cDNA synthesis. Thus, by constant initiation of DNA replication, this method allows for rapid accumulation of cDNA even from low amounts of RNA.

Encore Biotin Module from Nugen was used for chemical and enzymatic fragmentation and biotin-labeling of amplified cDNA. The resulting 50-100 base long cDNA products were subsequently hybridized on Affymetrix Human Gene 2.0 ST arrays. Washing, staining and scanning were done according to the Affymetrix Expression Protocol including minor modifications as suggested in the Encore Biotin Protocol.

3.5.5.2 Statistical transcriptome analysis

Expression console (v.1.3.0.187, Affymetrix) was used for quality control and to obtain annotated normalized RMA gene-level data (standard settings including median polish and sketch-quantile normalisation).

Statistical analyses were performed by utilizing the statistical programming environment R [R.D.C.T., 2008] implemented in CARMAweb [Rainer et al., 2006]. Genewise testing for

differential expression was done employing the (limma) t-test and Benjamini-Hochberg multiple testing correction (FDR <10%). To reduce the background, sets of regulated genes were filtered for average expression >10 in at least one of the three groups. Heatmaps were generated with CARMAweb.

Gene Ontology (GO) term enrichment is based on the Gene Ontology system of classification of sets of genes. In this classification system, genes are assigned to predefined bins based on their functional characteristics. GO term and pathway enrichment analyses ($p<0.01$) were done with GePS (Genomatix). This system makes use of information from public and proprietary databases to identify enriched pathways and GO terms.

Array data have been submitted to GEO (Accession Number GSE64248):
http://www.ncbi.nlm.nih.gov/geo/query/acc.cgi?token=cvwdayyudbydzwj&acc=GSE64248

3.5.5.3 Principal component analysis

Principal component analysis (PCA) was used to reduce the dimensionality of data with the intention to find patterns in a multidimensional microarray dataset. PCA is a mathematical algorithm which allows for reduction of the dimensionality of data while maintaining most of its variation. For this, principal components are identified as new variables. The first principal component is determined as the direction at which the samples have the largest variation. Next, the direction which is uncorrelated (perpendicular) to the first principal component and along which the samples again show the largest variation is determined. This direction represents the second principal component [Ringner, 2008]. Thereby, each sample was represented by only two variables (principal components) and was plotted in a two dimensional scatter plot. Principal component analysis was kindly performed by Steffen Sass (Institute of Computational Biology, Helmholtz Center Munich, Neuherberg, Germany).

3.5.6 Lentivirus production and transduction of target cells

Lentiviral vectors are a valuable tool for the delivery of transgenes into the genome of target cells. Their ability to integrate into the genome of both dividing and non-dividing cells is an advantage over other retroviruses, which only integrate into the genome of dividing cells. In this study, second generation vectors were used to produce replication defective, self-inactivating lentiviruses which are safe to work with.

3.5.6.1 Plasmids and virus production

Production of Lentivirus expressing eGFP or mCherry was kindly performed by Benjamin Hirschi (Institute of Stem Cell Research, Helmholtz Center for Health and Environmental Research Munich, Neuherberg, Germany). In short, 6 µg pRRL vector coding either for eGPF or mCherry, 2.1 µg pMD2.G envelop plasmid, and 3.9 µg psPAX2 packaging plasmid were mixed with 36 µl polyethyleneimin (PEI) transfection reagent followed by incubation for 15 min. The transfection mix was added dropwise to HEK293T high performance cells cultured at 70-80% confluency on a 10 cm cell culture dish in DMEM + 10% FCS. After incubation at 37 °C overnight, medium was removed and changed to 5 ml MECGM basic medium. Cells were kept at 37 °C and virus containing medium was collected 24 h and 48 h post transfection, filtered through a 0.45 µm PVDF filter to remove cell debris, and stored at -80 °C.

3.5.6.2 Lentiviral transduction of target cells

HMECs from donors M8, M9, M10 were thawed as described above and cultured in a 6-well polystyrene cell culture plate in 2 ml establishment/maintenance medium. At day 7 of culture, half of the medium was replaced by fresh maintenance medium before 1 ml of lentiviral GFP/Cherry suspension containing 3.3 µg/ml protamine sulfate, was slowly added to the cells. Addition of positively charged polycations like protamine sulfate enhances transduction efficiency of lentiviral vectors by reducing repulsion between negatively-charged cells and virus and mediating binding of the viral particle to the cell surface [Denning et al., 2013].
After incubation for 4 h at 37 °C, medium containing the viral particles was removed, cells were washed twice with PBS and then trypsinized with 0.3 ml 0.15 % trypsin to destroy all remaining virus and generate a single cell suspension. After all cells had detached, trypsin was neutralized by addition of 1 ml TNS, cells were filtered through a 35 µm nylon mesh and counted as described above. Next, cells exposed to lentiviruses carrying eGFP or mCherry were mixed in a 1:1 ratio and seeded into floating collagen gels at different densities (100, 500, 2000, 5000 cells per 400 µl gel) in maintenance medium. Gels containing 500-5000 and gels containing 100 cells were fixed after 17 and 18 days, respectively, and were subsequently stained with DAPI and mounted as described above.

3.6 Statistical analysis

Box-and-whisker plots to present data as median ± 25% were generated with GraphPad Prism Software using the Tukey method for plotting whiskers and outliers. All other data are

presented as mean ± standard deviation (SD). Student's t-test was used to compare two groups (two-tailed, unpaired), unless stated otherwise. *$p<0.05$ was considered significant.

A correlation coefficient (r) was calculated to measure the direction and strength of a possible linear relationship between two variables. In correlation analysis, r is always between –1 and +1: $r = –1$ describes a perfect negative linear relationship, $r = 0$ indicates that there is no linear relationship and $r = +1$ describes a perfect positive linear relationship. Thus, the closer r is to

–1/+1, the stronger the linear relationship. Here, I describe a correlation of $r \geq 0.7 / \leq –0.7$ as strong, $\geq 0.5 / \leq –0.5$ as moderate and $\geq 0.3 / \leq –0.3$ as weak [Taylor, 1990].

The correlation coefficient was determined using the "CORREL" function of Excel.

4 Results

4.1 Development of a three-dimensional culture system for the generation of breast organoids

4.1.1 Primary HMECs generate TDLU-like structures in floating collagen gels

The major aim of this study has been the development of an organotypic 3D culture model for primary HMECs, in which morphological and physiological characteristics of the human MG *in situ* are recapitulated (see 'Aims of the study'). Collagen I is the major component of the human breast ECM and provides defined properties that can be modified *in vitro* to change physical parameters or to model different microenvironments by addition of ECM components. Furthermore, it has previously been shown that primary human mammary organoids form branched structures when cultured within collagen I gels and that cells of the human breast carcinoma cell line T47D can build tubules in floating collagen I gels, implying the ability to self-organize in the described environment [Foster et al., 1983, Wozniak et al., 2005].

Therefore, I chose to use collagen I (hereafter referred to as collagen) as substrate for a 3D culture system. I seeded single primary HMECs into floating collagen gels based on the previously published protocol by Wozniak and Keely, to determine whether this would allow generation of multicellular structures that recapitulate the complex architecture of the MG *in situ* [Wozniak et al., 2005]. To do so, a single cell suspension of freshly isolated HMECs was mixed with neutralizing solution and acidic collagen type I on ice, and subsequently transferred to a siloxane coated cell culture dish. After polymerization, collagen gels were detached by encircling them with a pipet tip followed by careful shaking of the plate (Figure 4.1A).

After 10-12 days, I observed the formation of a variety of multicellular structures that could be divided into non-branched and branched structures (Figure 4.1B). The non-branched structures included tubule-like structures (sticks), and round structures (spheres and multi-spheres). The branched structures all contained multiple branching points, resembling the complex branched network of human breast epithelium. Two types of branched structures, named thin and star-like structures, had very thin ducts. In addition, the latter was characterized by a high number of ducts emerging from the center of structures, thereby failing to recapitulate the branched morphology of the epithelium of the human MG *in situ*. In contrast, the third type of branched structure showed complex branching with thick ducts and

distinct alveoli at the end of the ducts. These structures resembled TDLUs, the functional units of the human MG *in situ* and the place where most breast cancers arise (Figure 4.1C). Therefore, these structures were called TDLU-like structures.

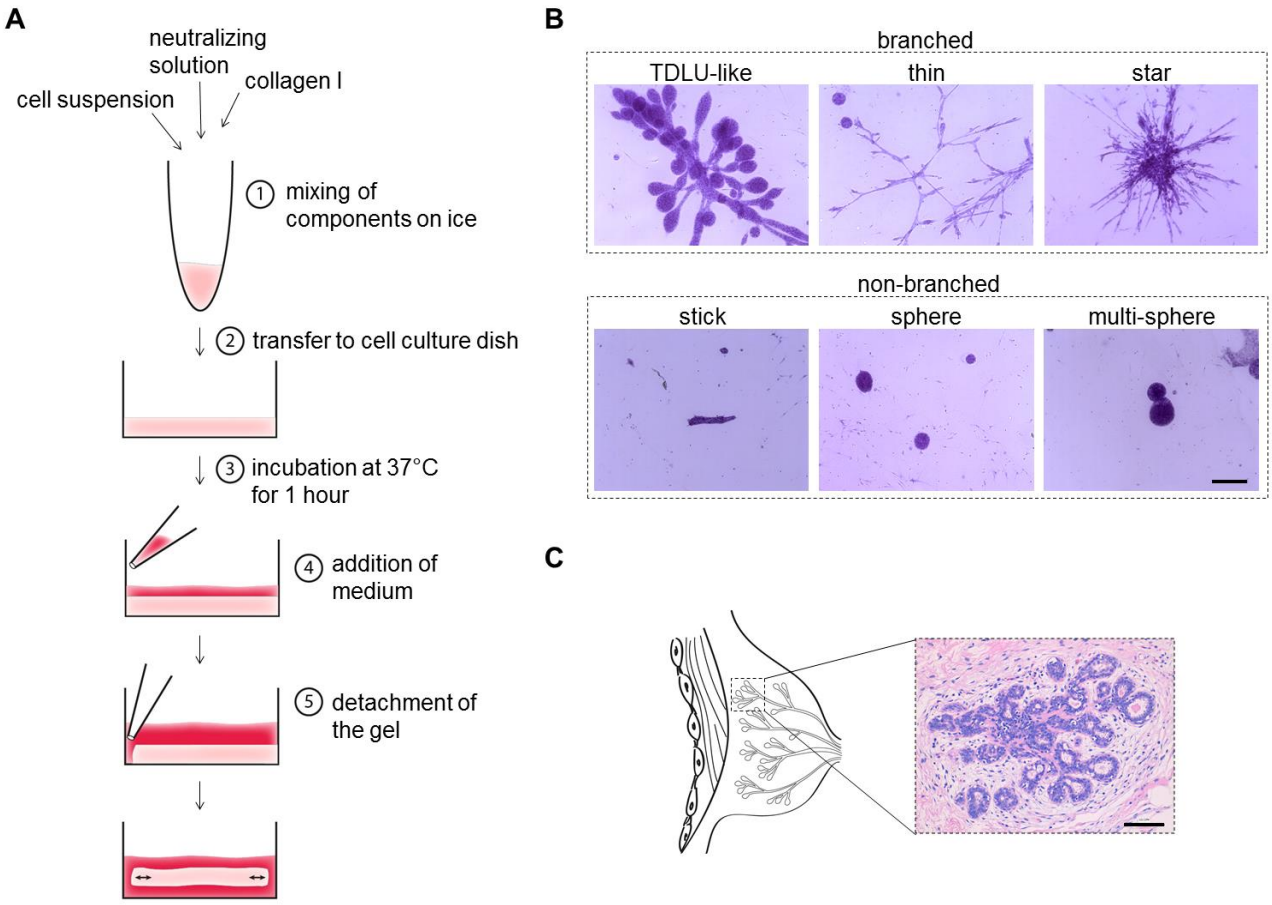

Figure 4.1 Generation of TDLU-like structures in floating collagen gels.
(A) Generation of floating collagen gels. In short, a single cell suspension of HMECs in culture medium was mixed with neutralizing solution on ice. Next, collagen I was quickly added and the mixture was transferred into siloxane coated cell culture plates. Collagen was allowed to polymerize for 1 h at 37 °C, after which cell culture medium was added carefully to the edge of the dish. Next, collagen gels were detached by encircling the gels with a pipet tip and careful shaking of the plate.
(B) Bright-field microscopy: carmine-stained representative images of different types of branched and non-branched structures in floating collagen gels (donor M8). Scale bar: 200 µm.
(C) Bright-field microscopy: Hematoxylin and Eosin-stained section of a TDLU from a healthy woman. Scale bar: 100 µm.

4.1.2 Matrigel does not support the generation of TDLU-like structures

Another hydrogel which is commonly used for 3D culture of MECs is rBM/Matrigel (see Chapter 1.3). To compare cellular behavior in Matrigel with that in floating collagen gels, freshly isolated HMECs were seeded in pure Matrigel or in a mixture of 50% collagen and 50% Matrigel. Strikingly, growth of HMECs was not supported under these conditions (data

not shown), suggesting that Matrigel does not represent a physiological extracellular environment for HMECs. In line with these observations, it has been reported that HMECs need to be established in 2D conditions before they can be cultured in Matrigel or, alternatively, require the presence of stromal cells [Dontu et al., 2003, Eirew et al., 2008]. Taken together, as culture in floating collagen better supported the growth of HMECs and allowed for the formation of structures resembling TDLUs of the human MG *in situ*, I chose to use collagen as substrate for a 3D culture system.

4.1.3 Improvement of culture conditions to promote the generation of TDLU-like structures

Seeding HMECs into floating collagen gels and quantifying the different types of structures revealed that only about 1/2,000 cells was able to give rise to a branched structure and even fewer cells, 1/10,000, gave rise to a TDLU-like structure. To promote the growth of cells giving rise to TDLU-like structures, thereby facilitating their characterization, I sought to improve culture conditions. Rho-associated kinase (ROCK) is a downstream effector of the small GTPase RhoA, an important regulator of the cytoskeleton and cellular contraction. Upon activation by RhoA, ROCK phosphorylates and activates LIM kinase, leading to inactivation of the actin-depolymerizing factor cofilin and stabilization of actin filaments. In addition, activated ROCK promotes cellular contractility by phosphorylation of myosin light chain (MLC) and inactivation of MLC phosphatase [Amano et al., 2010]. Inhibitors of ROCK were promising candidates to improve culture conditions for TDLU-like structure forming cells, as they were shown to increase colony formation of murine MECs in both 2D and 3D culture systems [Guo et al., 2012, Makarem et al., 2013]. In addition, it was recently shown that inhibition of ROCK can increase the regenerative potential of mouse MECs which are cultured in 2D and then transplanted back into a cleared fat pad [Prater et al., 2014].

Therefore, two different inhibitors of ROCK, Y-27632 and Thiazovivin, were added to the growth medium upon plating of freshly dissociated HMECs. Strikingly, treatment with 3 μM of Y-27632 increased branched-structure formation by 5-fold (Figure 4.2A) and formation of TDLU-like structures by 3-fold (Figure 4.2B). Similarly, treatment with Thiazovivin increased branched structure formation up to 7-fold (Figure 4.2A). Notably, higher concentrations of ROCK inhibitors, i.e. 10 μM Y-27632 or 1 μM Thiazovivin prevented formation of TDLU-like structures and instead promoted formation of star-like structures (Figure 4.2C). In addition, morphogenesis was completely perturbed if treatment with ROCK inhibitors was continued after 5 days of culture (Figure 4.2E). However, the fact that

prolonged treatment/high concentrations of ROCK inhibitor perturbed morphogenesis is not surprising considering that ROCK signaling regulates actin cytoskeleton dynamics and cellular contraction. Thus, a single initial treatment with 3 µm Y-27632 at initial plating, and subsequent removal of ROCK inhibitors by a complete medium change at day 5 of culture, was implemented into the standard 3D culture protocol in order to promote cell survival and structure formation as well as proper morphogenesis. Importantly, the addition of ROCK inhibitors primarily promoted the formation of branched structures which had thin ducts and few alveoli and were classified as thin and star-like structures (Figure 4.2C).

Compounds like Forskolin and Cholera Toxin cause an increase of intracellular levels of the second messenger cAMP by activation of adenylate cyclase. They are commonly used for culture of mammary epithelial cells and have been described to promote polarization and lumen formation in 3D cultures of the epithelial breast cell line MCF10A [Nedvetsky et al., 2012, Stampfer, 1982]. Thus, I added Forskolin to the cell culture medium to promote alveologenesis of branched structures. Indeed, when adding 10 µM Forskolin to freshly isolated primary HMECs in floating collagen gels, I observed a 3-fold increase in the formation of branched structures (Figure 4.2A) and a 12-fold increase in the formation of TDLU-like structures (Figure 4.2B), while the formation of non-branched structures was increased by only 1.5-fold (Figure 4.2D). Importantly, Forskolin promoted the formation of TDLU-like structures also in the presence of 1-10 µM Y-27632 or 0.1-0.3 µM Thiazovivin (Figure 4.2B), so that both ROCK inhibitors and Forskolin could be used together to specifically increase the number of TDLU-like structures formed. However, in the presence of high concentrations (1 µM) of Thiazovivin, the ability of Forskolin to promote formation of TDLU-like structures seemed to be lost, likely due to Thiazovivin overriding the effect of Forskolin (Figure 4.2B).

In summary, treatment with 3 µM Y-27632 once at initial plating of cells and subsequent removal at day 5 of culture, together with continuous treatment with 10 µM Forskolin with every medium change, optimally promoted the formation of TDLU-like structures and was therefore used as standard culture condition.

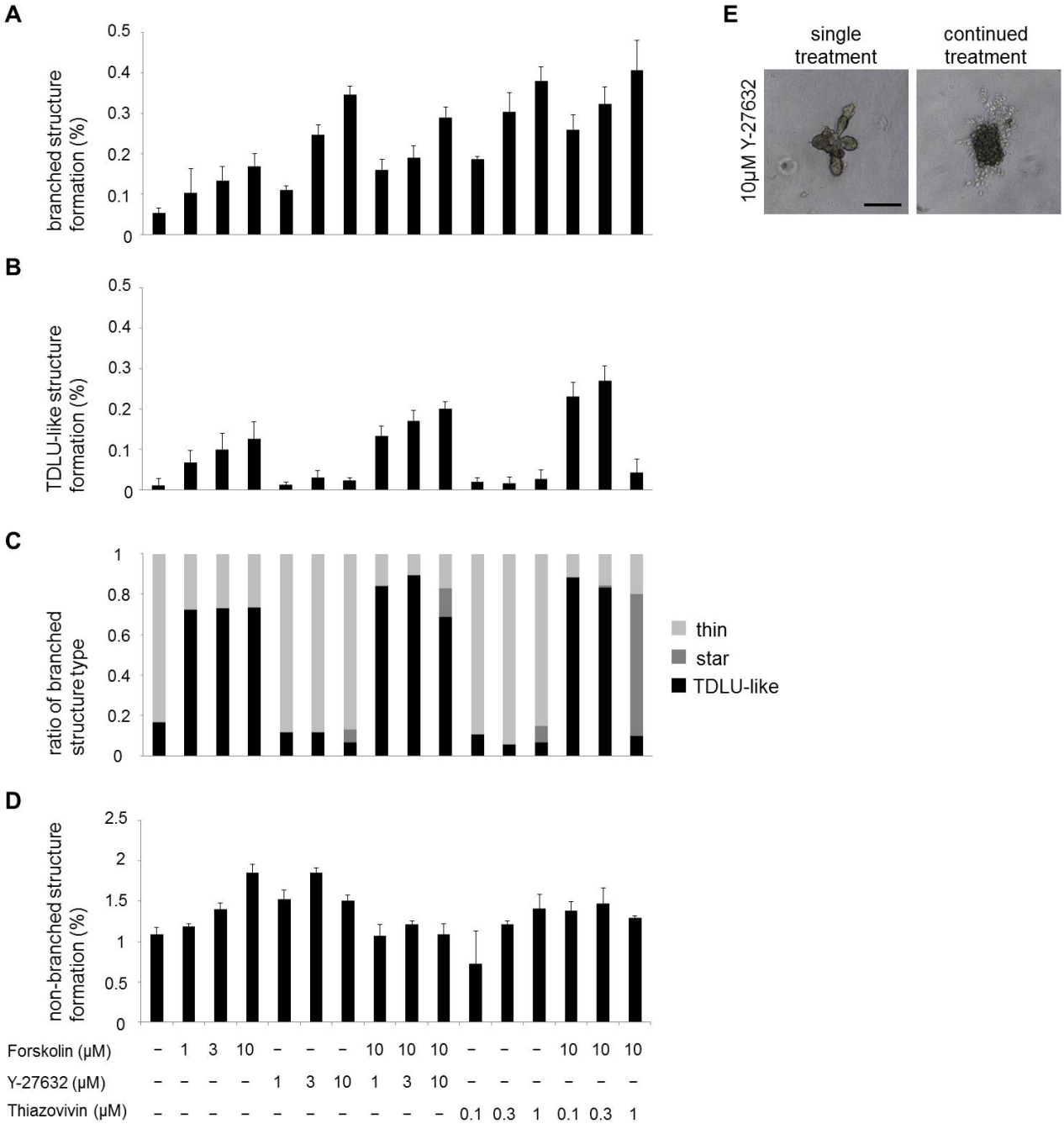

Figure 4.2 Identification of culture conditions promoting the generation of TDLU-like structures.
(A) Freshly isolated HMECs (donor M8) were cultured in the presence of different concentrations of Forskolin (continuous treatment), Y-27632 and Thiazovivin (both one-time treatment at day 0 of culture) in floating collagen gels for 14 days. 400 µl collagen gels, $1x10^4$ cells seeded per gel. n=3 gels/condition. Structure formation is given per 100 seeded cells.
(B) Effect of different culture conditions on the generation of TDLU-like structures, refer to (A). n=3 gels/condition. Structure formation is given per 100 seeded cells.
(C) Effect of different culture conditions on the ratio of thin, star and TDLU-like branched structure subtypes, refer to (A). n=3 gels/condition.
(D) Effect of culture conditions on the generation of non-branched structures, refer to (A). n=3 gels/condition. Structure formation is given per 100 seeded cells.
(E) Bright-field microscopy: representative images of basal cells (donor M5) in floating collagen gels, treated with 10 µM Y-27632 one-time at day 0 of culture or treated with every medium change. Scale bar: 200 µm.
(A,B,D) Data are shown as mean ± standard deviation (s.d.).

4.1.4 TDLU-like structures can be passaged

A hallmark of murine MaSCs/progenitors is self-renewal which can be assessed by serial transplantation into and repopulation of cleared mammary fat pads. Analogous to this, I tested whether HMECs were able to generate TDLU-like structures over multiple passages in floating collagen gels. Thus, I seeded single cell suspensions of HMECs into floating collagen gels. Once structures had formed, the collagen gels were enzymatically digested and the cells were trypsinized and filtered. The resulting single cell suspension was then re-plated into floating collagen gels. I observed that HMECs could generate branched structures for up to 2 passages (Figure 4.3A). At passage 3, branched structure formation was replaced by sphere formation indicating loss of regenerative, but maintenance of proliferative capacity. Based on these results, the culture system developed here can be used to analyze the self-renewal capacity of HMECs for up to two passages. To allow for TDLU-like structure formation for more than 3 passages, future studies should aim to further improve 3D culture conditions.

4.1.5 TDLU-like structure formation is maintained in 2D culture in the presence of Forskolin

Genetic manipulation and expansive growth are facilitated in 2D rather than 3D culture conditions. Thus, I tested whether TDLU-like structure forming cells can be maintained in 2D culture conditions. For this, freshly isolated bulk HMECs were cultured in 2D on regular polysterene culture plates for five passages.

For quantification of cells with TDLU-like structure forming ability, extreme limiting dilution analysis (ELDA) was performed [Hu et al., 2009]. For this method, limiting dilutions of 2D-cultured HMECs were seeded into floating collagen gels for passage 1, 3 and 5 (Figure 4.3B). Once structures had formed, gels containing at least one TDLU-like structure were quantified. The ELDA-software tool was used to calculate the rate of TDLU-like structure forming cells in the different conditions. ELDA revealed a branched structure forming unit (B-SFU), describing the fraction of cells able to give rise to a TDLU-like structure, of 1/290 and 1/250 for cells of passage 1 and 3, respectively. Notably, B-SFU of passage 5 cells was dramatically decreased to 1/1350 cells, indicating loss of regenerative capacity over multiple passages (Figure 4.3A). The fact that regenerative capacity was maintained longer in 2D- than in 3D-cultured HMECs suggests that a stiff rather than a compliant culture environment supports an undifferentiated cell state.

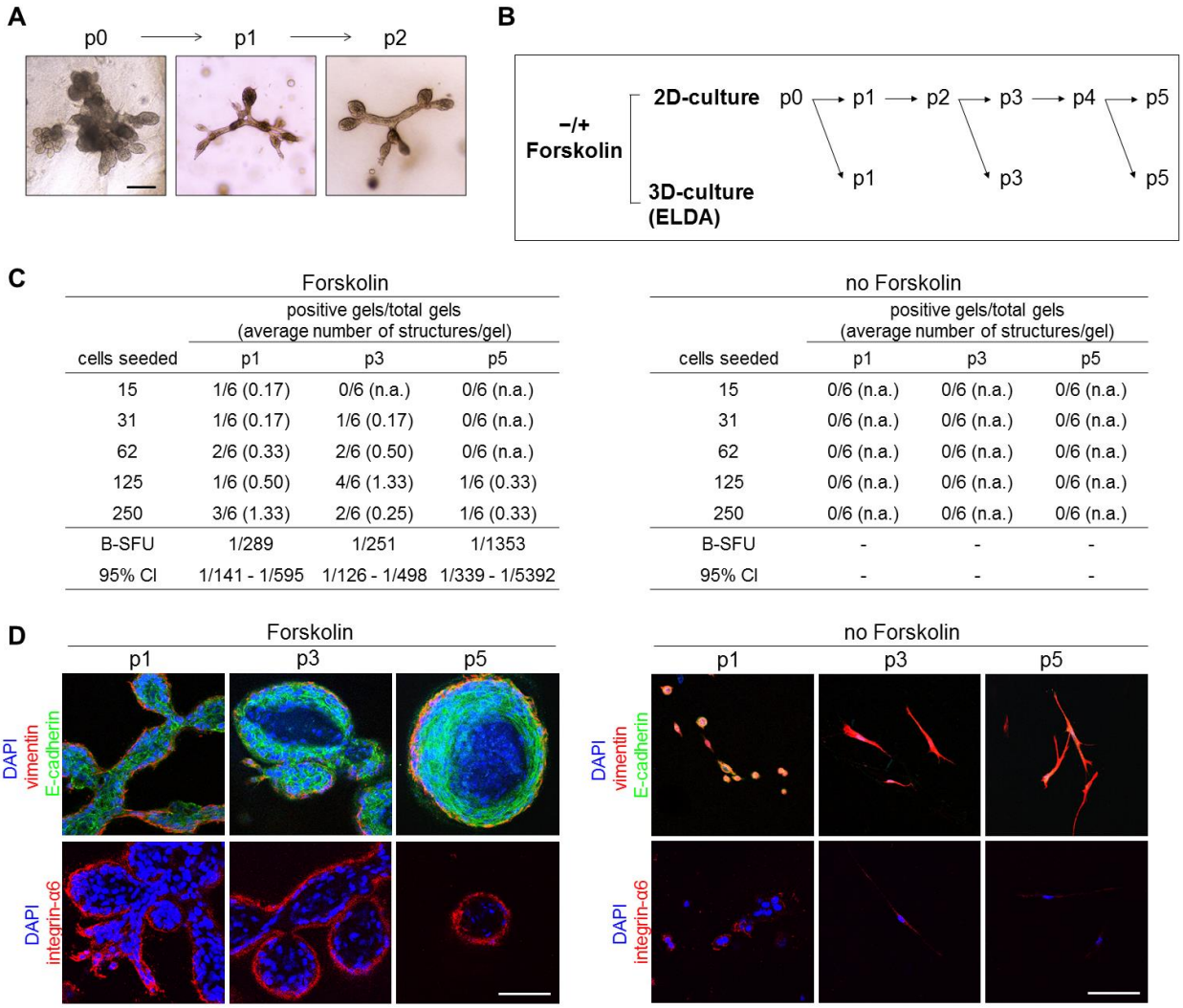

Figure 4.3 Forskolin is required for maintenance of TDLU-like structure formation *in vitro*.
(A) Bright-field microscopy: representative images of HMEC-derived branched structures (donor M8), at subsequent passages in 3D. Scale bar: 200 µm.
(B) Experimental setup: freshly isolated HMECs (donor M4) were cultured in 2D in the absence or presence of 10 µM Forskolin for five passages, and transferred to floating collagen I gels in limiting dilution at passage 1, 3 and 5. p=passage.
(C) Extreme limiting dilution analysis: determination of branched structure-forming units (B-SFU) at passage 1, 3 and 5 after 2D culture, refer to (B). Data are mean and 95% confidence intervals (CI).
(D) Confocal microscopy: representative TDLU-like structures at passage 1, 3, and 5 after 2D culture, refer to (B). Vimentin (red), E-cadherin (green), integrin-α6 (red), DAPI (blue). Scale bars: 100 µm.

Importantly, maintenance of regenerative capacity required the presence of Forskolin, as cells cultured in its absence had completely lost regenerative ability already at passage 1 (Figure 4.3C). Notably, this loss of regenerative ability coincided with epithelial to mesenchymal transition (EMT), i.e. the loss of epithelial and the acquisition of mesenchymal features.

The process of EMT is involved in critical steps of morphogenesis, fibrosis and cancer progression [Lamouille et al., 2014, Thiery et al., 2009]. Epithelial cells are characterized by apico-basal polarity and strong cell-cell adhesion. In 2D culture settings, epithelial cells

exhibit a cobblestone-like morphology and are usually contained within well-organized clusters. Markers for epithelial cells include cell-cell adhesion molecule E-cadherin and membrane-localized β-catenin, which links cadherins to the cytoskeleton [Lamouille et al., 2014, Thiery et al., 2009]. Another marker of epithelial cells is the zinc finger transcription factor Ovol2 (Ovo-like 2) which was shown to protect the epithelial cell fate of murine MECs required for normal mammary morphogenesis and regeneration *in vivo* [Watanabe et al., 2014].

During EMT, epithelial cell-cell adhesion is lost, cells acquire migratory and invasive features and exhibit front-to-back polarity. In mesenchymal cells, E-cadherin is typically replaced by N-cadherin, and the cells express intermediate filament vimentin and fibronectin, a glycoprotein of the ECM. Additional markers for EMT include Twist, Snail, Slug and Zeb1 which are pleiotropically acting transcription factors mediating the EMT program downstream of extracellular signals [Lamouille et al., 2014, Thiery et al., 2009]. Snail and Slug belong to the Snail family of zinc finger transcription factors. They can promote EMT by binding to E-box motifs found in the E-cadherin promoter region, repressing transcriptional expression of E-cadherin [Batlle et al., 2000, Cano et al., 2000]. ZEB1 is another zinc finger TF and can also repress E-cadherin transcriptional expression by binding to E-box motifs in its promoter region [Eger et al., 2005]. However, all of these transcription factors not only affect transcription of E-cadherin but have been implicated in transcriptional downregulation of other cell-cell adhesion proteins such as claudins, occludins and desmosome proteins as well as the transcriptional upregulation of mesenchymal markers like fibronectin and N-cadherin [Lamouille et al., 2014, Thiery et al., 2009].

Immunofluorescence revealed that passage 1 cells cultured in floating collagen gels in the absence of Forskolin generated loose agglomerations of round cells. These agglomerations of cells were positive for the mesenchymal marker vimentin while retaining expression of E-cadherin (Figure 4.3D, left). When cells cultured in the absence of Forskolin were transferred to floating collagen gels at later passages, they showed complete front-to-back polarization and had lost all expression of E-cadherin, indicating acquisition of a mesenchymal phenotype (Figure 4.3D, right).

The acquisition of a mesenchymal phenotype was also reflected in 2D cultures. Cells cultured in 2D in the absence of Forskolin acquired front-to-back polarization and downregulated epithelial markers E-cadherin and membranous β-catenin, while they upregulated mesenchymal markers fibronectin and Zeb1 as determined by immunofluorescent staining (Figure 4.4A). The acquisition of mesenchymal features was further reflected at the transcript

level by downregulation of epithelial marker *OVOL2* and upregulation of mesenchymal markers *ZEB1*, *CDH2* (encoding N-cadherin), *VIM*, and *FN1* (Figure 4.4B).

Thus, the switch from epithelial to mesenchymal phenotype was reflected by changed transcriptional and post-transcriptional expression of multiple markers. Interestingly, within 5 passages in the absence of Forskolin, CD49f/integrin-α6 was lost on both protein and transcript level (Figure 4.4C). As CD49f is the major receptor for the basement membrane component laminin, these findings suggest that the interaction of cells with their environment becomes defective in the absence of Forskolin which likely affects the cell's inability to generate branched structures in floating collagen gels. Together, these results suggest that culture of HMECs in the presence of Forskolin prevents 2D culture induced EMT and maintains regenerative potential.

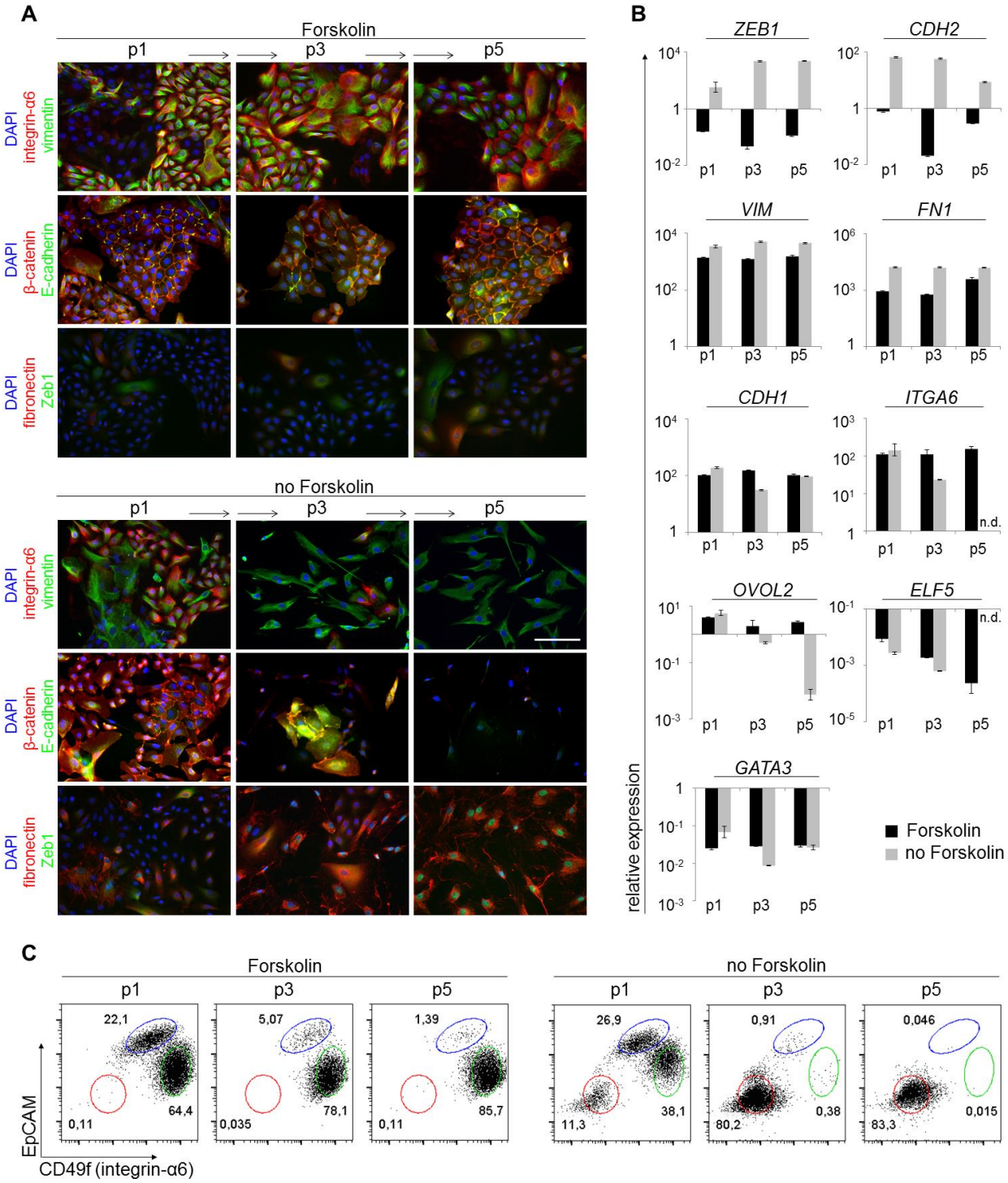

Figure 4.4 Forskolin prevents 2D culture induced EMT.
(A) 2D-Immunofluorescence: representative images of HMECs cultured in 2D, in the absence or presence of 10 µM Forskolin at passage 1, 3 and 5 (donor M4). Integrin-α6 (red), vimentin (green), β-catenin (red), E-cadherin (green), fibronectin (red), Zeb1 (green), DAPI (blue). Scale bar: 100 µm.
(B) RT-PCR: *ZEB1*, *CDH2* (N-cadherin), *VIM* (vimentin), *FN1* (fibronectin) and *CDH1* (E-cadherin), *ITGA6* (integrin-α6), *OVOL2*, *ELF5* and *GATA3* mRNA expression of HMECs cultured in 2D, as described in (A). n=3. Data are shown as mean ± standard deviation (s.d.).
(C) Flow cytometry analysis of CD49f and EpCAM expression in Lin- HMECs cultured in 2D (see Figure 4.3B).

4.1.6 Single HMECs give rise to TDLU-like structures

MaSCs/bipotent progenitors of the mouse MG are defined by the ability of a single cell to regenerate a cleared mammary fat pad in serial transplantation [Shackleton et al., 2006, Stingl et al., 2006]. Thus, if single HMECs are able to form a TDLU-like structure in floating collagen gels, the assay can be used as proxy for reconstitution of a cleared mammary fat pad. To read out the ability of single HMECs to generate a TDLU-like structure, I tested clonality of TDLU-like structures.

To test whether single HMECs can give rise to a TDLU-like structure, a fraction of HMECs was labeled with eGFP or mCherry fluorescent protein by lentiviral transduction. A mixture of eGFP-, mCherry-expressing and unlabeled cells was then seeded into floating collagen gels in increasing concentrations of 100, 500, 2000 and 5000 cells/gel. Once TDLU-like structures had formed after 10-11 days, gels were fixed with paraformaldehyde and nuclei were stained with DAPI. Confocal microscopy was used to determine the frequency of clonal structures identified by complete overlap of eGFP or mCherry with DAPI. By contrast, polyclonal structures were multicolored. Quantification of monoclonal and polyclonal structures showed that gels seeded with 100 to 500 cells contained mainly monoclonal structures with a complete overlap of eGFP/mCherry and DAPI and only few multicolored structures (Figure 4.5A,B). Of the multicolored structures, some consisted of two large monoclonal parts and apparently had merged late in their developmental process. Others contained intermingled patches of colored cells and therefore likely had merged at the beginning of structure formation. Importantly, the fraction of multicolored structures increased with high cell densities (Figure 4.5A; 2000 to 5000 cells/gel), suggesting that polyclonality is largely a result of proximity. Interestingly, the ratio of spheres to branched structures increased in gels seeded with higher numbers of cells, suggesting that high density impairs branched-structure formation (Figure 4.5C). Indeed, it has been previously reported that regeneration and bipotent capacity of murine MECs are reduced if cells are transplanted in the presence of luminal cells [Van Keymeulen et al., 2011]. In summary, these results show that single HMECs are able to give rise to TDLU-like structures if seeded at low density. Thereby, TDLU-like structure formation in floating collagen gels can be used as proxy assay for MG reconstitution.

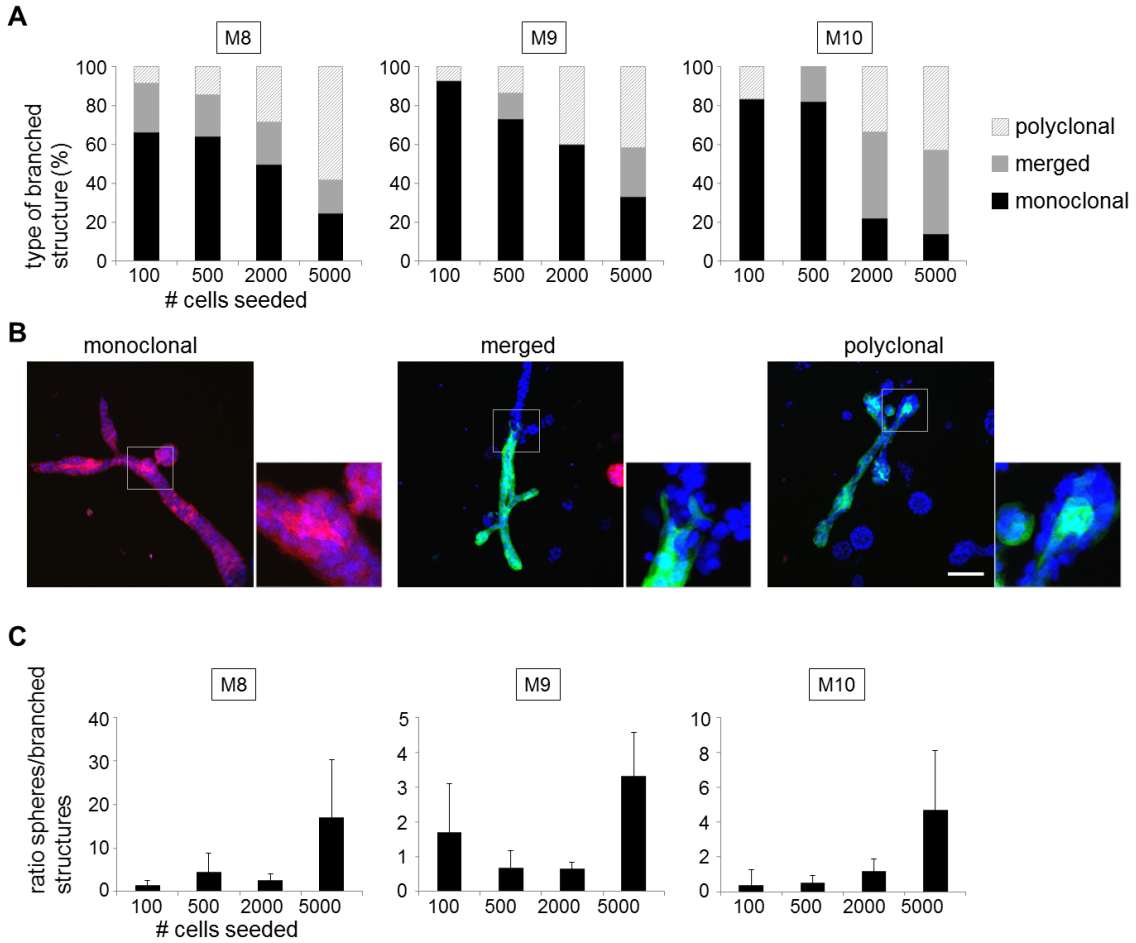

Figure 4.5 Single HMECs give rise to TDLU-like structures.
(A) Quantification of monoclonal, merged and polyclonal structures formed by eGFP, mCherry and unlabeled passage 1 cells (donors M8, M9, M10) in floating collagen I gels: 100, 500, 2000 or 5000 cells were seeded per well (24-well plate). Monoclonal: complete structure eGFP or mCherry positive. Merged: monoclonal structure merged with second structure. Polyclonal: eGFP/mCherry-positive and -negative areas. n≥9 eGFP/mCherry-positive structures/condition.
(B) Confocal microscopy: representative images of monoclonal, merged and polyclonal structures as defined in (A). Scale bar: 100 µm.
(C) Quantification of the ratio of spheres and branched structures in floating collagen gels used for analysis of clonality in (A). n=5 fields of view of at least 6 gels/condition. Data are shown as mean ± standard deviation (s.d.).

4.2 Enrichment of TDLU-like structure forming cells

4.2.1 TDLU-like structure formation varies between donors

The composition and behavior of HMECs depend on the genetic background, hormonal status and developmental stage of the individual donor from which they are derived [Tanos et al., 2012]. HMECs used in this study were obtained from a variety of donors, ranging between 17-69 years of age and parity of 0-2. Therefore, the cells were expected to exhibit heterogeneous TDLU-like structure forming ability in floating collagen gels. To assess reproducibility of TDLU-like structure formation between donors, bulk HMECs from 9 different donors were seeded into floating collagen gels. Branched structure formation, i.e. the number of branched structures formed per seeded cells, was very heterogeneous as was expected from the different ages and parity of the donors (Figure 4.6A-C). Based on the results, donors could be divided into three groups defined by high, medium and low branched structure formation. Specifically, donors M7/M3/M4 exhibited high, donors M10/M8/M9 medium and donors M2/M6/M1 low branched structure formation with an average of 0.23, 0.11 and 0.04% of cells giving rise to a branched structure, respectively. Sphere formation, i.e. the number of spheres generated per seeded cells, was also very heterogeneous between different donors. Notably, sphere formation did not reflect branched structure formation, as donors with low branched structure formation presented with high or low sphere formation and vice versa (Figure 4.6B,C).

As HMECs from donor M8 presented with moderate branched structure and sphere forming ability, they were used to determine a representative value for both parameters. For this, M8 HMECs were seeded into floating collagen gels in limiting dilution for ELDA which revealed a B-SFU of 1/1005 and sphere-structure forming unit (S-SFU) of 1/55 (Figure 4.6D). In summary, HMECs from different donors exhibit differences in TDLU-like structure and sphere formation which may be determined by multiple parameters, including genetic background, hormonal status and developmental stage. Notably, age- and parity-dependent differences in structure formation could not be detected within cells from the limited number of donors analyzed. However, the influence of the different parameters on branched structure and sphere formation will need to be assessed in more detail in future studies using a larger patient group.

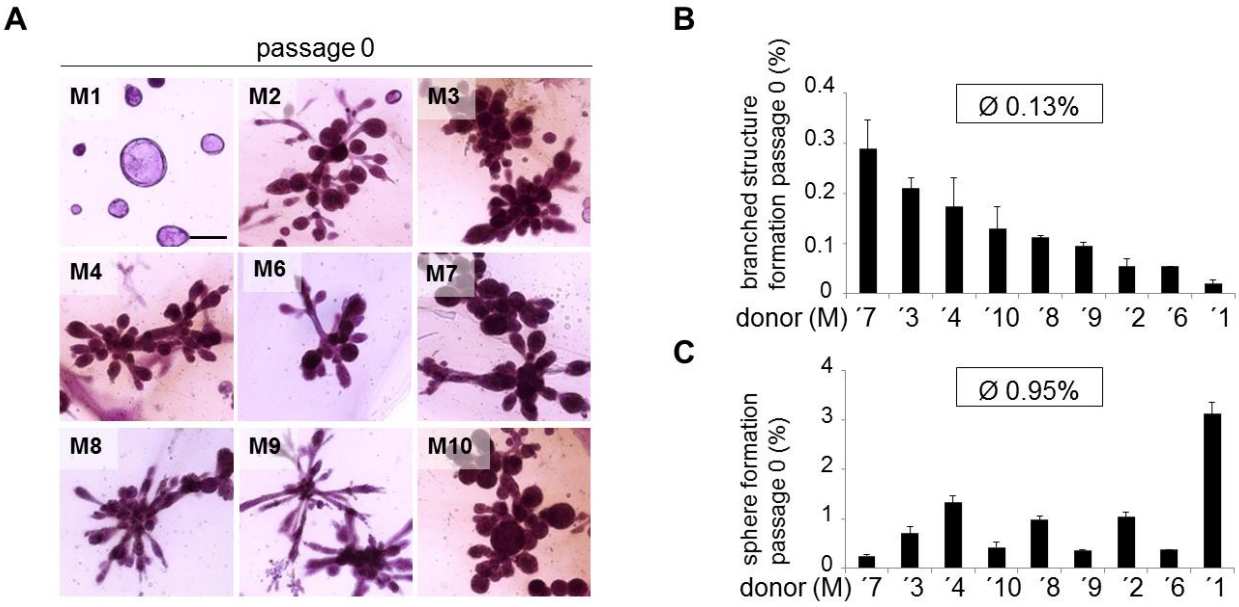

D

cells seeded	M8	positive gels/total gels
	sphere	branched
		(average number of structures/gel)
125	7/8	1/8 (0.13)
250	8/8	0/8 (n.a.)
500	8/8	4/8 (0.63)
750	8/8	4/8 (0.88)
1000	8/8	6/8 (1.50)
1500	8/8	6/8 (2.00)
SFU	1/55 (S-SFU)	1/1005 (B-SFU)
95% CI	1/26 - 1/118	1/645 - 1/1564

Figure 4.6 The frequency of TDLU-like structure-forming cells varies between donors.
(A) Bright-field microscopy: carmine-stained representative images of TDLU-like structures from freshly isolated bulk HMECs of nine donors (M1-M4, M6-M10) in floating collagen I gels. 400 µl collagen gels, $2x10^4$ cells seeded per gel. Scale bar: 200 µm.
(B) Branched-structure formation/100 seeded HMECs at day 9 of culture. n=2 gels/donor.
(C) Sphere formation/100 seeded HMECs at day 9 of culture. n=2 gels/donor.
(D) Extreme limiting dilution analysis: determination of sphere and branched structure-forming units (S-SFU and B-SFU, donor M8). Data are mean and 95% confidence intervals (CI).
(B,C) Data are shown as mean±s.d

4.2.2 TDLU-like structure formation is increased by short-term 2D culture

Genetic manipulation is facilitated by 2D rather than 3D culture, as both DNA and viruses are more easily taken up in 2D or spin transductions than in 3D cultures. However, 2D culture does not recapitulate the mechanical environment, morphology and function of the tissue *in vivo* and may thereby affect stem cell/progenitor function. In Chapter 4.1.5 it was shown that TDLU-like structure formation is maintained in 2D culture for up to two passages. Next, I wanted to test whether the differences in branched structure formation between different donors (Figure 4.6A-C) was also maintained upon 2D culture. For this, HMECs used in

Figure 4.6B,C had also been established in 2D culture. For passage 2, these HMECs were transferred into floating collagen gels (Figure 4.7A). The morphologies of TDLU-like structures generated by freshly isolated and 2D-cultured HMECs were similar, suggesting that cell-behavior was not significantly changed upon short-term establishment in 2D culture (Figure 4.6A, 4.7A). However, the differences in branched structure formation observed at passage 0 were not reflected after 2D culture (Figure 4.6B, 4.7B). Specifically, at passage 0, HMECs from donors M7/M3/M4 exhibited the highest branched structure forming capacity. In contrast, after 2D culture (passage 2), the highest branched structure forming ability was observed in HMECs from donors M10/M8/M9. These data suggest that differences in branched structure formation are not maintained in 2D culture. In addition, branched structure forming cells from different donors seem to have different abilities to expand/ be generated in 2D culture.

Notably, short-term 2D culture generally increased branched-structure and sphere formation efficiency by ~12-fold and ~4-fold, respectively (Figure 4.7B,C). This dramatic increase might be explained by the observation that at least 50% of freshly isolated HMECs are not viable, as determined by labeling with 7-AAD (Figure 4.7D). 7-AAD is a cell-death marker which labels dying cells by penetrating the cell membrane and intercalating with DNA, thereby changing its fluorescent properties. The low viability determined by 7-AAD staining likely resulted from the process of tissue dissociation, digestion and further processing (which takes up to 28 hours) and subsequent cryostorage. Thus, a high fraction of freshly isolated cells seeded into floating collagen gels does not survive, resulting in underestimation of structure forming potential. However, once established in 2D culture, a higher percentage of cells survive passage into floating collagen gels, which is then reflected in increased structure formation.

In summary, the ratio of branched structure forming cells is more than doubled upon short-term 2D culture. These data suggest that in 2D culture, branched structure forming cells either expand more efficiently than other HMECs, or that HMECs acquire branched structure forming ability *de novo*. However, the original differences in branched structure formation between donors were not reflected after 2D culture, suggesting that branched structure forming cells from different donors have different abilities to expand/ be generated in 2D culture.

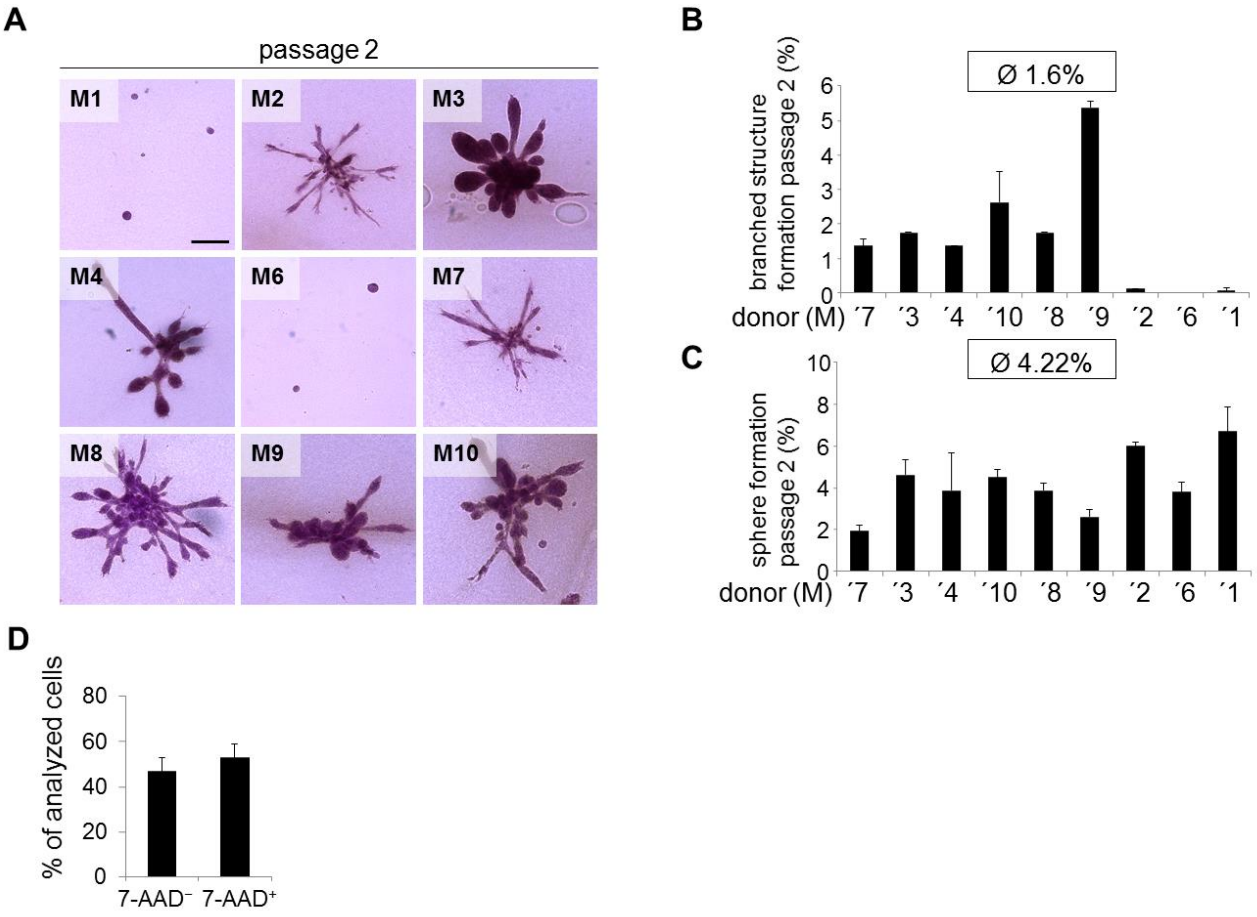

Figure 4.7 The frequency of TDLU-like structure-forming cells is increased by 2D culture.
(A) Bright-field microscopy: carmine-stained representative images of TDLU-like structures from nine donors (M1-4, M6-M10), 12 days of 2D culture prior to transfer to collagen I gels. 400 µl collagen gels, $8x10^2$ cells seeded per gel. Scale bar: 200 µm.
(B) Branched-structure formation/100 seeded HMECs, established in 2D culture (see E) at day 9 of culture. n=2 gels/donor.
(C) Sphere formation/100 seeded HMECs, established in 2D culture (see E) at day 9 of culture. n=2 gels/donor.
(D) Viability of freshly isolated HMECs determined by FACS, using 7-AAD: n=10 donors (M1-M10).
(B,C,D) Data are shown as mean±s.d

4.2.3 $CD10^+/CD49f^{hi}/EpCAM^-$ cells are enriched for TDLU-like structure formation

Reconstitution of cleared mammary fat pads *in vivo* has suggested that murine MaSCs/bipotent progenitors are enriched within the basal cell population [Shackleton et al., 2006, Stingl et al., 2006]. Studies using human mammary epithelial cells have concluded that also human MaSCs are enriched within the basal population [Eirew et al., 2008]. Thus, I set out to determine whether TDLU-like structure forming cells were predominantly contained within the basal cell population. Specifically, I determined whether the size of the basal and luminal cell population predicts TDLU-like structure and sphere formation in floating collagen gels. For this purpose, I used a previously established FACS protocol to purify basal and luminal cell populations [Eirew et al., 2008]: 7-AAD was used to exclude dead cells. To

exclude endothelial and hematopoietic cells, the markers CD31 and CD45 were used. CD31, also known as platelet endothelial cell adhesion molecule (PECAM)-1, is an adhesion molecule belonging to the immunoglobulin superfamily. It is expressed on the surface of endothelial cells, platelets, monocytes, polymorphonuclear cells and some circulating lymphocytes, predominantly naïve CD8+ T-cells [DeLisser et al., 1994]. CD45, also known as Protein tyrosine phosphatase, receptor type, C (PTPR), is a phosphatase which is involved in the cellular response to environmental processes. It is expressed on all nucleated hematopoietic cells except erythrocytes and plasma cells. CD45 is also expressed on hematopoietic stem cells and osteoclasts which are of hematopoietic origin [Hermiston et al., 2003, Shivtiel et al., 2008].

By sorting for 7-AAD$^-$/CD31$^-$/CD45$^-$ cells, the mammary cell suspension was thus cleared of the majority of dead, endothelial and hematopoietic cells. In the next step, viable (7-AAD$^-$) Lin− (CD31$^-$/CD45$^-$) cells were subdivided based on expression of CD49f and EpCAM. This yielded 4 populations: stromal cells (Stroma, CD49f$^-$/EpCAM$^-$), luminal mature cells (LM, CD49f$^-$/EpCAM$^+$), luminal progenitor cells (LP, CD49f$^+$/EpCAM$^+$), and basal cells (B, CD49f^{hi}/EpCAM$^-$) (Figure 4.8A). Stroma and LM cells did not show clonogenic activity in floating collagen gels and were therefore excluded from analysis (data not shown). For analysis, freshly isolated bulk HMECs from nine different donors were seeded into floating collagen gels and allowed to generate structures. Next, the number of sphere and TDLU-like structures formed per seeded cells was correlated with the size of the LP and basal population among viable Lin− cells from flow cytometry analysis (Figure 4.8B,C). Specifically, correlation analysis was performed as described in Chapter 3.6. Linear correlations with a correlation coefficient (r) of $r = \geq 0.7/\leq -0.7$, $r = \geq 0.5/\leq -0.5$ and $r = \geq 0.3/\leq -0.3$ were described as strong, moderate and weak, respectively. Cells of the basal population showed weak negative correlation with sphere formation ($r = -0.22$) as well as weak positive correlation with branched structure formation ($r = 0.14$). These data suggest that the basal population is depleted of sphere forming cells and likely contains rare branched structure forming cells. In contrast, the size of the LP population showed strong positive correlation with sphere formation ($r = 0.80$) and moderate negative correlation with branched structure formation ($r = -0.68$), suggesting that LP predominantly form spheres.

As discussed above, regenerative potential was ascribed to the basal population in both human and mouse. In addition, correlation analysis performed here suggested that the LP population predominantly forms spheres. Therefore, the lack of correlation between basal population size and regenerative potential was likely due to heterogeneity of the basal population.

Thus, I reasoned that additional cell surface markers may allow for enrichment of cells with TDLU-like structure forming ability within the basal population. A thorough literature search revealed the cell surface metalloendopeptidase CD10 as possible candidate to enrich for TDLU-like structure forming cells. CD10 antibody was reported to label the myoepithelium in immunohistochemical sections of normal human breast tissue [Santagata et al., 2014]. Furthermore, CD10 had previously been used as marker for basal HMECs [Bachelard-Cascales et al., 2010, Keller et al., 2012]. In addition, CD10 was shown to enrich for HMECs with the ability for form mammospheres, i.e. proliferate in anchorage independence, a trait associated with MaSCs [Bachelard-Cascales et al., 2010]. Thus, I analyzed the expression of CD10 in HMECs from nine donors by FACS. This analysis revealed two distinct populations within the CD49f^{hi}/EpCAM^{-} basal (B) cell fraction with on average ~30% of basal cells expressing CD10. CD10 was also expressed on average in 10%, 1% and 47% of the LM, LP and stromal fraction, respectively (Figure 4.8D).

Strikingly, branched structure formation moderately correlated with the size of the CD10+ basal population (r = 0.44). In contrast branched structure formation only weakly correlated with the size of CD10+ fractions of stroma, LP or LM cells (Figure 4.8E; r = −0.2, 0.15, 0.08, respectively). These data suggested that CD10 expression within the basal population can be used to enrich for cells with regenerative capacity.

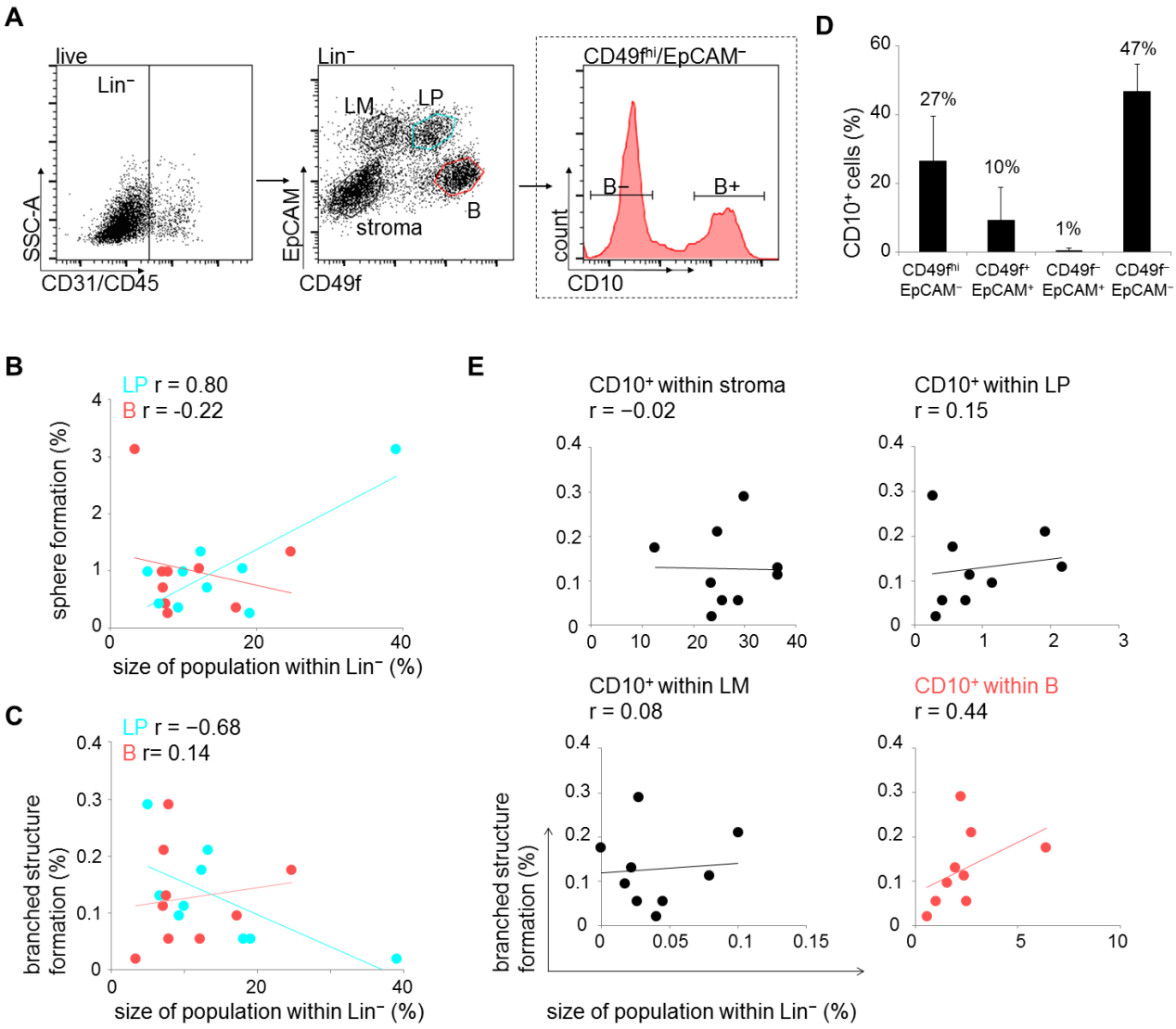

Figure 4.8 TDLU-like structure-forming potential correlates with the size of the CD10⁺/CD49f^hi/EpCAM⁻ population.

(A) FACS strategy for freshly isolated HMECs: dead cells (7-AAD− = live), hematopoietic (CD45+) and endothelial cells (CD31+) were excluded. EpCAM and CD49f were used to depict the following populations among live (7-AAD⁻) Lin− (CD45⁻/CD31⁻) cells: stroma (CD49f⁻/EpCAM⁻), luminal mature (LM, CD49f⁻/EpCAM⁺), luminal progenitors (LP, CD49f⁺/EpCAM⁺) and basal (B, CD49f^hi/EpCAM⁻). LP and basal (B) populations were isolated. The basal (B) population was further subdivided into B− (CD10⁻/CD49f^hi/EpCAM⁻) and B+ (CD10⁺/CD49f^hi/EpCAM⁻) cells.

(B) Linear correlation between sphere formation/100 freshly isolated HMECs and size of the LP population (blue dots), or size of the B population (red dots) within the Lin− population. One dot represents one donor.

(C) Linear correlation between TDLU-like structure formation/100 freshly isolated HMECs and size of the LP population (blue dots) or the basal (B) population (red dots) within the Lin− population. One dot represents one donor.

(D) Percentage of CD10+ cells within the 4 populations defined by CD49f and EpCAM described in (A) based on flow cytometry. The average of 10 donors is shown (M1-M10). Data are shown as mean ± standard deviation (s.d.).

(E) Linear correlation between branched structure formation and size of the CD10+ stromal population (CD10⁺/CD49f⁻/EpCAM⁻), the CD10+ LP population (CD10⁺/CD49f⁺/EpCAM⁺,), the CD10+ LM population (CD10⁺/CD49f⁻/EpCAM⁺) and the CD10+ basal (B) population (CD10⁺/CD49f^hi/EpCAM⁻, red dots). One dot represents one donor.

To test for this, I sorted basal cells, CD10+ basal cells (named B+), CD10− basal cells (named B−) and LP cells and seeded them into floating collagen gels in limiting dilution to quantify branched structure forming units (B-SFU).

ELDA revealed that approximately one in 413 B+ cells gave rise to a TDLU-like structure (B-SFU = 1/413). Thereby, the B+ population was dramatically enriched for B-SFU over all other populations, with 7-, 30- and 12-fold enrichment over the basal (basal all), B− and LP cells, respectively (Figure 4.9A). Within the basal CD49f^{hi}/EpCAM^{-} population, the vast majority of TDLU-like structure forming cells is thus contained within the B+ population while the B− population is almost devoid of these cells (B-SFU = 1/12386). Therefore, CD10 is a useful marker to enrich for TDLU-like structure forming cells within the basal CD49f^{hi}/EpCAM^{-} population of the human MG. Based on some published sorting protocols CD10 can be utilized instead of CD49f to enrich for basal cells [Bachelard-Cascales et al., 2010, Keller et al., 2012]. However, the results presented here reveal that CD10 must be used in combination with CD49f and EpCAM in order to deplete CD10 positive cells of luminal and stromal populations which are generally lacking regenerative potential.

A

Population	Cells seeded	Positive gels/ total gels (Average number of structures/ gel)			B-SFU (95% CI)
		M8	M9	M10	
Basal +	125	2/8 (0.25)	2/7 (0.43)	1/8 (0.25)	1/413 (1/291 - 1/585)
	250	3/8 (0.38)	4/8 (0.50)	2/8 (0.25)	
	500	5/8 (0.75)	8/8 (2.25)	6/8 (1.00)	
Basal -	1000	0/8	1/8 (0.13)	0/8	1/12386 (1/7034 - 1/21811)
	2000	2/8 (0.25)	2/8 (0.25)	0/8	
	4000	4/8 (0.50)	2/8 (0.25)	1/8 (0.13)	
Basal all	250	0/8	1/8 (0.13)	1/7 (0.14)	1/2690 (1/1562 - 1/4635)
	500	0/8	1/8 (0.25)	2/7 (0.29)	
	1000	3/8 (0.75)	2/8 (0.25)	3/7 (0.86)	
LP	500	1/8 (0.13)	0/8	0/8	1/5122 (1/3372 - 1/7778)
	1000	3/8 (0.50)	0/14	3/14 (0.63)	
	2000	9/14 (1.50)	0/14	6/14 (1.00)	

Figure 4.9 TDLU-like structure-forming potential is contained within a CD10^{+}/CD49f^{hi}/EpCAM^{-} population

(A) Extreme limiting dilution analysis: Determination of branched structure-forming units (B-SFU) of B+ (Basal +), B− (Basal−), basal (Basal all) and LP populations defined in (A) from donors M8, M9 and M10. Data are mean and 95% confidence intervals (CI).

Notably, the B-SFU determined for the B+ population is likely an underestimation of their true TDLU-like structure forming ability as FACS is toxic in 50-75% of cells [Giraddi et al., 2015]. Furthermore, the cells still need to adjust to the *in vitro* environment as they are

cultured for the first time and unknown quantities of cells are lost during handling. Therefore, the B-SFU of 1/413 cells observed in the B+ population suggests that TDLU-like structure forming cells are not rare.

Strikingly, also the LP population displayed limited TDLU-like structure formation (B-SFU = 1/5122, see Chapter 4.2.6 and 4.5.1). There are different possible explanations for this observation. First, the LP population might have been contaminated with basal cells during the sorting procedure. Second, the LP population might indeed contain rare luminal cells which have the ability to generate TDLU-like structures. Third, TDLU-like structure forming ability might have been induced by de-differentiation of LP cells after isolation from the MG. The possible scenarios will be discussed in detail in Chapter 4.2.6.

In summary, I have found that TDLU-like structure forming cells are predominantly contained within the basal cell population. Within this population, CD10 can be used to further enrich for cells with TDLU-like structure forming ability, revealing that these cells cannot be considered rare.

4.2.4 CD10^{+}/CD49f^{hi}/EpCAM^{-} cells belong to the basal lineage

ELDA revealed that B+ cells are enriched for TDLU-like structure forming cells compared to B− and LP cells. To analyze the unique features of B+ cells over B− and LP cells, gene expression profiling was performed on freshly sorted B+, B− and LP cells from six donors. Genewise testing for differential expression was done employing the (limma) t-test and Benjamini-Hochberg multiple testing correction (FDR <10%). To reduce the background, sets of regulated genes were filtered for average expression >10 in at least one of the three groups.

To compare overall gene expression patterns of the different samples, principal component analysis (PCA) was used. PCA is a mathematical algorithm which allows for reduction of the dimensionality of data while maintaining most of its variation (see Chapter 3.4.4.3). By the identification of two new variables (principal components), each sample could be represented in a two dimensional scatter plot (Figure 4.10A). Notably, PCA revealed a clearly distinct cluster for each population, irrespective of the donor. Thus, gene expression patterns are robust within the sorted subpopulations even though the size of the distinct subpopulations varies. In addition, these results reflect the robustness in structure formation within these populations (Figure 4.10A): Cells of the LP and B+ population predominantly form spheres and TDLU-like structures, respectively. Most cells of the B− population do not build multicellular structures. Based on the current literature, it was assumed that both the B+ and B− population belong to a population exclusively containing basal cells [Eirew et al., 2008].

Strikingly, however, there was a great distance between the B+ and the B− cluster on the axis of both principal components, indicating that B+ and B− cells have a very distinct gene expression pattern (Figure 4.10A). Considering that the majority of B− cells does not proliferate/form multicellular structures *in vitro*, these data put into question the basal epithelial identity of these cells.

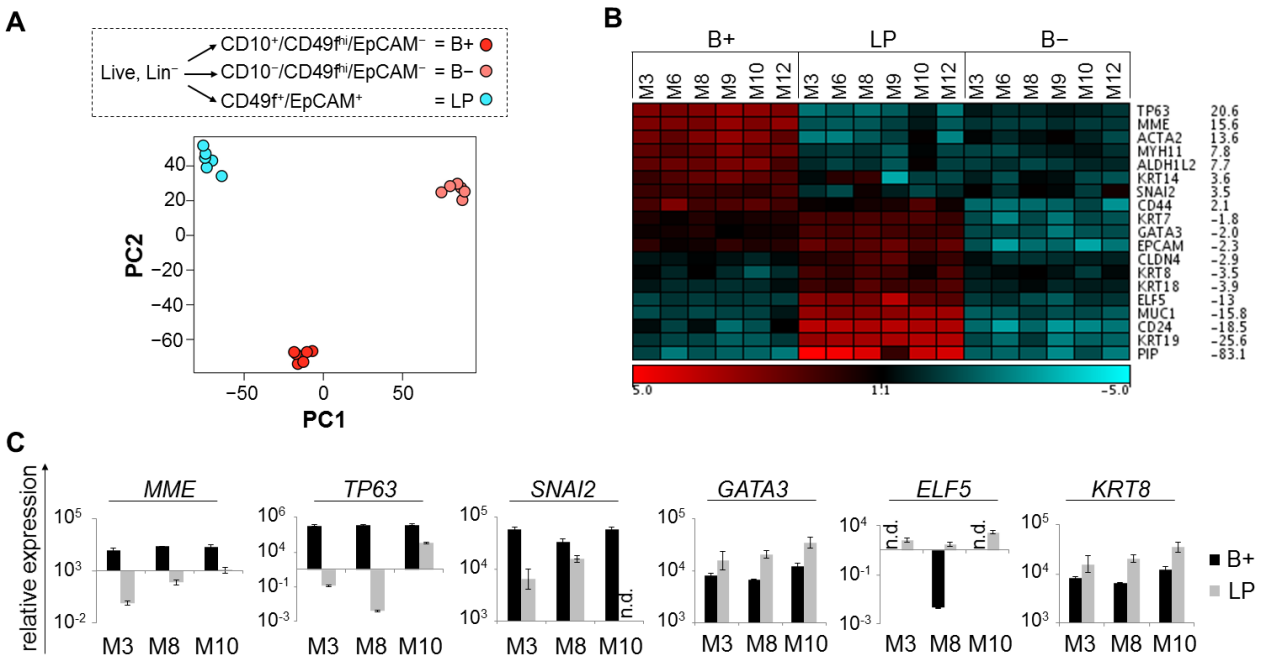

Figure 4.10 The CD10⁺/CD49f^hi/EpCAM⁻ population expresses basal markers
(A) Gene expression profiling: mRNA for microarray analysis was derived from the three subpopulations B+, B− and LP from freshly isolated HMECs of six donors (M3, M6, M8, M9, M10, M12). Unsupervised clustering of all samples was followed by principal component analysis (PCA).
(B) Heatmap: expression values of up- and downregulated luminal and basal genes in all samples. Fold-change of B+ versus LP expression levels. Red (high) and blue (low) indicates log2 expression values. Scale bar is in log2.
(C) RT-PCR: Expression of *MME/CD10*, *TP63*, *SNAI2*, *GATA3*, *ELF5* and *KRT8* mRNA in B+ and LP cells. n=3. Data are shown as mean ± standard deviation (s.d.).

To assess the lineage identity of the different subpopulations, I compared the transcript levels of genes (FDR <10%; average expression >10) characteristic for basal or luminal cell fates (Figure 4.10B). As expected, the basal-associated gene *MME*, coding for CD10, was most highly expressed in B+ cells, validating the sorting procedure. Other basal-associated genes like *TP63* and *SNAI2* were also upregulated in B+ cells [Guo et al., 2012, Lim et al., 2010, Santagata et al., 2014]. In contrast, luminal-associated genes like *GATA3*, *ELF5* and *KRT8* were more highly expressed in LP cells than in B+ cells (Figure 4.10B) [Asselin-Labat et al., 2007, Kouros-Mehr et al., 2006, Lee et al., 2011, Oakes et al., 2008, Santagata et al., 2014]. The expression level of these genes was confirmed by qPCR (Figure 4.10C).

As expected, these results confirmed that the LP and B+ populations contain cells with a luminal and basal gene expression pattern, respectively. Use of the marker combination $CD10^{+}/CD49f^{hi}/EpCAM^{-}$ and $CD49f^{+}/EpCAM^{+}$ thus seemed to enrich for basal and luminal HMECs, respectively. In contrast, the expression of both basal and luminal-associated genes was low in B− cells (Figure 4.10B,C). Use of the marker combination $CD10^{-}/CD49f^{hi}/EpCAM^{-}$ thus seems to enrich for cells with neither basal nor luminal mammary epithelial gene expression pattern. Thereby, these results put into question the epithelial identity of B− cells.

4.2.5 $CD10^{-}/CD49f^{hi}/EpCAM^{-}$ cells might represent a specialized mammary stromal population

As the B− population did not seem to belong to the basal or luminal lineage based on gene expression profiling (Figure 4.10B), a more unbiased approach was chosen to reveal the identity of cells within this population. Analysis of the 20 most highly upregulated transcripts (FDR<10%; average expression >10) in the B− over B+ population included *IGK* (encoding immunoglobulin chains), *LYVE1* and *CDH5* (encoding VE-cadherin), indicative of B cells, T cells, as well as lymph and vascular endothelial cells (Figure 4.11A). To obtain a functional profile of the genes expressed by B− cells, GO-term analysis was performed on genes differentially regulated between B− and B+ population with a FDR<10%, average expression >10 and FC>3×. GO-term analysis revealed groups of genes associated with circulatory system development, cytokine-receptor binding, antigen binding, VEGF and angiogenesis to be significantly overrepresented in the B− compared with the B+ gene expression profile (Figure 4.11B). Together, these data suggest that the B− cell population predominantly comprises stromal cells, specifically vascular- and lymphendothelial cells as well as B and T cell lymphocytes. Notably, I expected these cells to be removed during the sorting procedure by exclusion of CD31 and CD45 positive cells. In line with a stromal identity of B− cells, it has been argued that all cells located at basal positions express CD10 in immunohistochemical sections of the human MG [Santagata et al., 2014]. Notably, these results indicate that depletion of stromal cells using CD31 and CD45 as markers for exclusion of endothelial and hematopoietic cells does not result in their complete elimination. In line with this, it has been reported that certain types of endothelial cells, for instance those found in spleen and kidney capillaries, are negative for CD31 [Pusztaszeri et al., 2006]. In addition, transitional B cells as well as plasmablasts and plasma cells are known to downregulate CD45 and would therefore not be excluded in the used sorting protocol [Zikherman et al., 2012].

A

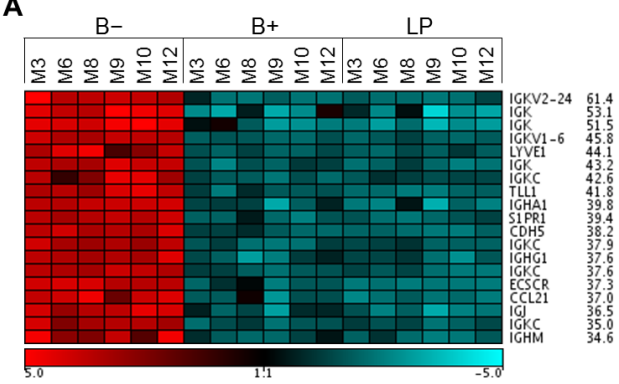

B

GO-term (GO-term ID/ pathway ID)	p-value	observed genes	top regulated genes
circulatory system development (GO:0072359)	3.84E-19	116	CDH5
cytokine receptor binding (GO:0005126)	1.98E-06	31	CCL21
antigen binding (GO:0003823)	1.05E-03	12	IGKC, IGHA1, IGHG1, IGJ
vascular endothelial growth factor (VEGF) (PW_VEGF_HOMO_SAPIENS)	8.89E-15	51	CDH5, ECSCR
angiogenesis (PW_ANGIOGENESIS_HOMO_SAPIENS)	2.69E-09	47	S1PR1, CDH5

C

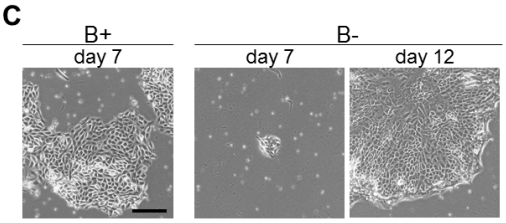

Figure 4.11 CD10 staining reveals a stromal component within the CD49f^{hi}/EpCAM^{-} population.
(A) Heatmap: expression values of the top 20 significantly (FDR<10%) upregulated genes in B− samples versus B+ samples with corresponding fold-changes. Red (high) and blue (low) indicates log2 expression values. Scale bar is in log2.
(B) GO term analyses: selected significantly enriched GO terms (P<0.01) associated with genes differentially regulated between B− and B+ populations (FDR<10%, FC>3×).
(C) Bright-field microscopy: representative images of B+ and B− cells cultured in 2D in the presence of 10 µM Forskolin at day 7/12 of culture (donor M10). Scale bar: 200 µm.

In summary, these considerations suggest that the CD49f^{hi}/EpCAM^{-} population contains a stromal component which is negative for CD31 and CD45. As a result, using CD10 as a cell surface marker does not enrich regenerative cells within a basal population, but instead leads to purification of the basal population from stromal cells. While revealing the presence of a stromal fraction within the CD49f^{hi}/EpCAM^{-} basal population, it should be noted that these results do not exclude the presence of a rare population of CD10^{-}/CD49f^{hi}/EpCAM^{-} mammary epithelial cells. At day 7 of culture in regular 2D polystyrene cell culture plates, B+ cells had already built cohesive epithelial islands, while only few adherent cells could be detected in B− cell cultures (Figure 4.11C). However, after another five days, the B− cells grew out to generate epithelial colonies morphologically similar to those generated by the B+ cell population (Figure 4.11C). It remains to be tested whether these colonies are derived from contaminating epithelial cells or whether the B− population indeed contains a small population of CD10^{-}/CD49f^{hi}/EpCAM^{-} epithelial cells. Either way, these results suggest that the B− population is mainly composed of stromal cells, including vascular and lymphatic endothelial cells as well as B and T cell lymphocytes, while a small epithelial component cannot be excluded.

4.2.6 CD49f$^+$/EpCAM$^+$ luminal progenitor cells exhibit limited TDLU-like structure-forming potential

As described above, the size of the CD49f$^+$/EpCAM$^+$ LP cell population showed strong positive correlation with sphere formation and moderate negative correlation with branched structure formation (Figure 4.8B,C). Based on these data, LP cells predominantly form spheres. In line with this, ELDA revealed that regenerative potential is enriched within the B+ population over the basal, B− and LP population (Figure 4.9). In line with this, LP cells from donor M9 did not generate any branched structures. Notably however, LP cells from donors M8 and M10 displayed limited TDLU-like structure formation with a B-SFU of 1/2134 and 1/4219, respectively (compare with Figure 4.9A). Summarizing the values from donors M8/M9/M10, ELDA revealed an overall B-SFU for LP cells of 1/5122 (Figure 4.9A). Importantly, this frequency could not be explained by contamination with B+ cells during the sorting procedure, as for all sorts, contamination with these cells was determined to be less than 1% (Figure 4.12A). Considering that ~1/413 B+ cells generates a branched structure and contamination within LP cells is ~1%, at least 40,000 LP cells (413 B+ cells*100) would have to be seeded in order to obtain one TDLU-like structure, resulting in a B-SFU of ~1/40,000. Conversely, contamination with B+ cells would have to be ~8% (413/5122*100), in order to obtain a B-SFU of 1/5122. While TDLU-like structure formation cannot be explained by contamination with B+ cells, there are two other possibilities: Either the LP population contains rare TDLU-like structure forming cells or LP cells acquire TDLU-like structure forming ability upon isolation from the MG, for example by de-differentiation. In accordance with our finding, it has been described previously that human LP cells can give rise to epithelial structures containing both luminal and basal cells when transplanted under the renal capsule or into a cleared humanized mammary fat pad [Keller et al., 2010, Shehata et al., 2012].

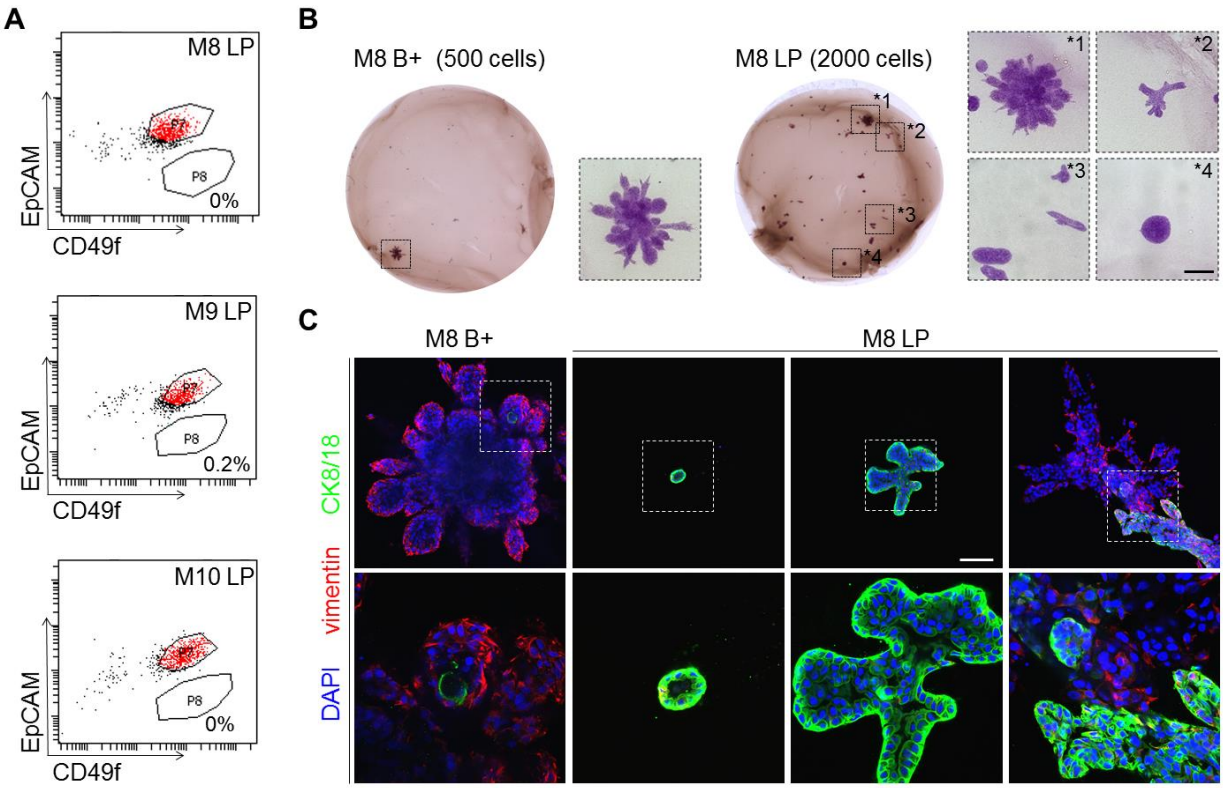

Figure 4.12 CD49f$^+$/EpCAM$^+$ luminal progenitor cells exhibit limited TDLU-like structure-forming potential
(A) Reanalysis of sorted LP cells from donors M8, M9 and M10 used for extreme limiting dilution analysis (ELDA) in Figure 4.9.
(B) Stereo and Bright-field microscopy: representative images of structures derived from LP and B+ sorted cells (donor M8) from ELDA experiment in Figure 4.9. Scale bar: 200 µm.
(C) Confocal microscopy: representative images of structures derived from LP and B+ sorted cells (donor M8). CK8/18 (green), vimentin (red), DAPI (blue). Scale bar: 100 µm.

To compare the cellular identity of TDLU-like structures generated by B+ and LP cells, confocal microscopy was performed (Figure 4.12B,C). As expected, TDLU-like structures generated by B+ cells expressed vimentin at basal positions and occasionally contained CK8/18 positive cells in luminal positions, indicating that in these positions cells were maturing towards a luminal identity.

Strikingly, both spheres and branched structures generated by LP cells showed strong expression of the luminal marker CK8/18, also at basal positions, while vimentin could not be detected (Figure 4.12C). These data suggest that LP cells are able to maintain luminal characteristics while undergoing branching morphogenesis. However, in some cases, areas of CK8/18 negative vimentin positive cells emerged that appeared disordered and invasive and were located right next to CK8/18+ areas. The close location suggested that these CD8/18−, vimentin+ cells were emerging from CD8/18+ vimentin− colonies (Figure 4.12C, right).

In summary, these results suggest that the LP cell compartment is plastic and can acquire regenerative capacity which can be morphologically similar to regeneration seen by B+ cells. However, on the cellular level, LP differ from B+ cell derived branched structures in that the generated structures continue to express luminal markers while lacking expression of vimentin. The appearance of invasive areas negative for luminal markers raise the question whether plasticity observed in LP cells is representative of normal regeneration or of illicit dedifferentiation.

4.3 B+ cell-derived TDLU-like structures contain cells with luminal features and display functionality

As described above, MaSCs/bipotent progenitors of the mouse MG are defined by the ability of a single cell to regenerate a cleared mammary fat pad in serial transplantation [Shackleton et al., 2006, Stingl et al., 2006]. In this case, regeneration includes the ability of a single mammary epithelial cell to give rise to differentiated and functional progeny: The regenerated murine mammary epithelial tree contains cells of both major mammary lineages, luminal and basal. In addition, in response to hormones released in pregnancy, the regenerated cells exhibit functional features by being able to produce milk proteins [Shackleton et al., 2006, Stingl et al., 2006]. To assess the regenerative ability of HMECs cultured in floating collagen gels analogous to the regenerative ability of murine MECs transplanted into a cleared mammary fat pad, I determined whether B+ cell-derived TDLU-like structures contain cells of the luminal lineage and display functionality.

4.3.1 B+ cell derived TDLU-like structures contain cells with luminal features

To test whether B+ cell derived TDLU-like structures generated in floating collagen gels contain cells of the luminal lineage, similar to mammary epithelial trees regenerated by murine MaSCs/bipotent progenitors, I sorted B+ and LP cells from freshly isolated HMECs and seeded them into floating collagen gels. After 20 days, collagen gels were fixed and embedded in paraffin for immunohistological detection of the basal cell marker p63 and luminal markers GATA3 and CK18. Structures generated by LP cells were negative for p63 and positive for both GATA3 and CK18 (Figure 4.13A), confirming the luminal identity of these cells and demonstrating the maintenance of luminal features during culture in floating collagen gels. Strikingly, all B+ cell derived TDLU-like structures expressed p63 at basal positions and showed GATA3 staining at luminal positions (Figure 4.13A), reflecting polarization of the human MG *in situ* and suggesting that there is a degree of luminal differentiation in B+ cell derived structures. Notably, I could not detect any expression of CK18 in B+ cell derived structures which might be explained by expression of CK18 only later in the process of luminal differentiation.

These data suggest that B+ cells cultured in floating collagen gels give rise to cells with luminal features analogous to the MaSCs/bipotent progenitors of the mouse MG. However, for mature luminal differentiation to occur, the culture period might have to be increased

and/or the culture medium might have to be optimized by addition of factors that promote terminal luminal differentiation.

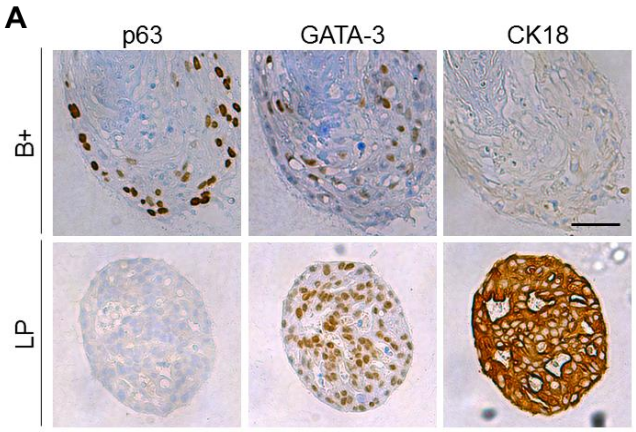

Figure 4.13 B+ cells give rise to GATA3+ cells. (A) Immunohistochemistry: expression of p63, GATA3 and CK18 in representative sections of structures derived from LP or B+ cells (donor M10), fixed at culture day 20. For LP and B+, six and five fields of view were analyzed, respectively. Scale bar: 50 µm.

4.3.2 B+ cell-derived TDLU-like structures display functionality

Contraction is a crucial function of myoepithelial/basal cells *in vivo* as it is required to promote the release of milk during lactation [Gudjonsson et al., 2005, Sopel, 2010]. Thus, to determine functionality, I aimed to assess the ability of TDLU-like structures to contract.

One of the most commonly used contraction assays is based on the ability of myofibroblasts to contract floating collagen gels. For this assay, fibroblasts are seeded into floating collagen gels and changes in gel size are determined for a certain period of time, from which a contraction index can be determined [Li et al., 2011]. Thus, the contraction assay described above was used to determine the functionality of TDLU-like structures. B+ and LP cells were seeded into floating collagen gels and were cultured for 12 days to allow for the formation of TDLU-like structures and spheres, respectively. Notably, during this initial time period of 12 days, the structures formed and increased in size but no contraction of the gels was observed. After 12 days, gels were photographed every 24 hours for two more days to determine changes in gel size (Figure 4.14A). At the end of the time course, gels containing B+ cells were contracted to half of the initial size, while gels containing LP cells did not change in size (Figure 4.14A,B).

These results show that B+ cell derived TDLU-like structures exhibit functional features by contracting floating collagen gels. The fact that contraction of gels could only be observed after an initial culture period of 12 days suggests that maturation and contractility of TDLU-like structures develop concomitantly. In addition, the lack of contraction in gels containing LP-derived spheres is not surprising, as it reflects the non-contractile function of LP cells.

To prove unequivocally that the observed changes in gel size were due to cellular contractility, I treated the cultures with factors known to increased cellular contractility. Oxytocin is a peptide hormone which is released by the posterior pituitary axon terminals upon suckling of the newborn and is required for milk-ejection from the MG. Specifically, it has been reported to induce contraction of myoepithelial mammary epithelial cells [Crowley et al., 1992, Reversi et al., 2005]. However, addition of oxytocin to TDLU-like structures did not result in increased contraction (data not shown). A reason for this might be insufficient stability of oxytocin in cell culture or requirement of additional, yet unidentified auto/paracrine factors, as has been suggested in the literature [Sopel, 2010]. TGFβ1 is a morphogen which promotes contractility of fibroblasts by inducing expression of alpha smooth muscle actin (αSMA) [Lijnen et al., 2003]. To determine whether the contraction of basal/myoepithelial cells could be further induced by addition of TGFβ1, I treated TDLU-like structures and spheres with 2.0 ng/ml recombinant TGFβ1 once at day 12 of culture. After 2 more days, this single treatment had increased the contraction of gels containing B+ cell derived TDLU-like structures by 2-fold (Figure 4.14B). In accordance with the non-contractile function of LP cells, TGFβ1 had no or only slight effects on the size of gels containing LP cell derived spheres. A slight reduction in gel size upon TGFβ1-treatment was seen in gels containing LP cells from donor M3. The small reduction in gel size might be explained by the fact that these gels contained a low number of TDLU-like structures which might have been the result of sort impurities or LP cell dedifferentiation.

It should be noted that TGFβ1 is growth inhibitory for various cell types, including HMECs [Barcellos-Hoff et al., 2000]. To exclude that growth inhibition was underlying the observed effects on gel size, the number of cells contained within a gel were counted at the end of the experiment. Importantly, cell numbers were equal between all conditions showing that gel differences in gel size were not caused by potential growth inhibitory effects of TGFβ1 (Figure 4.14C).

To confirm contraction at the single cell level, f-actin fibers and nuclei were stained with phalloidin and DAPI, respectively. Measurement of cell diameter based on the f-actin staining confirmed that cells treated with TGFβ1 were smaller than control cells (Figure 4.14D), supporting the finding that TGFβ1 promotes contraction of B+ cell derived TDLU-like structures.

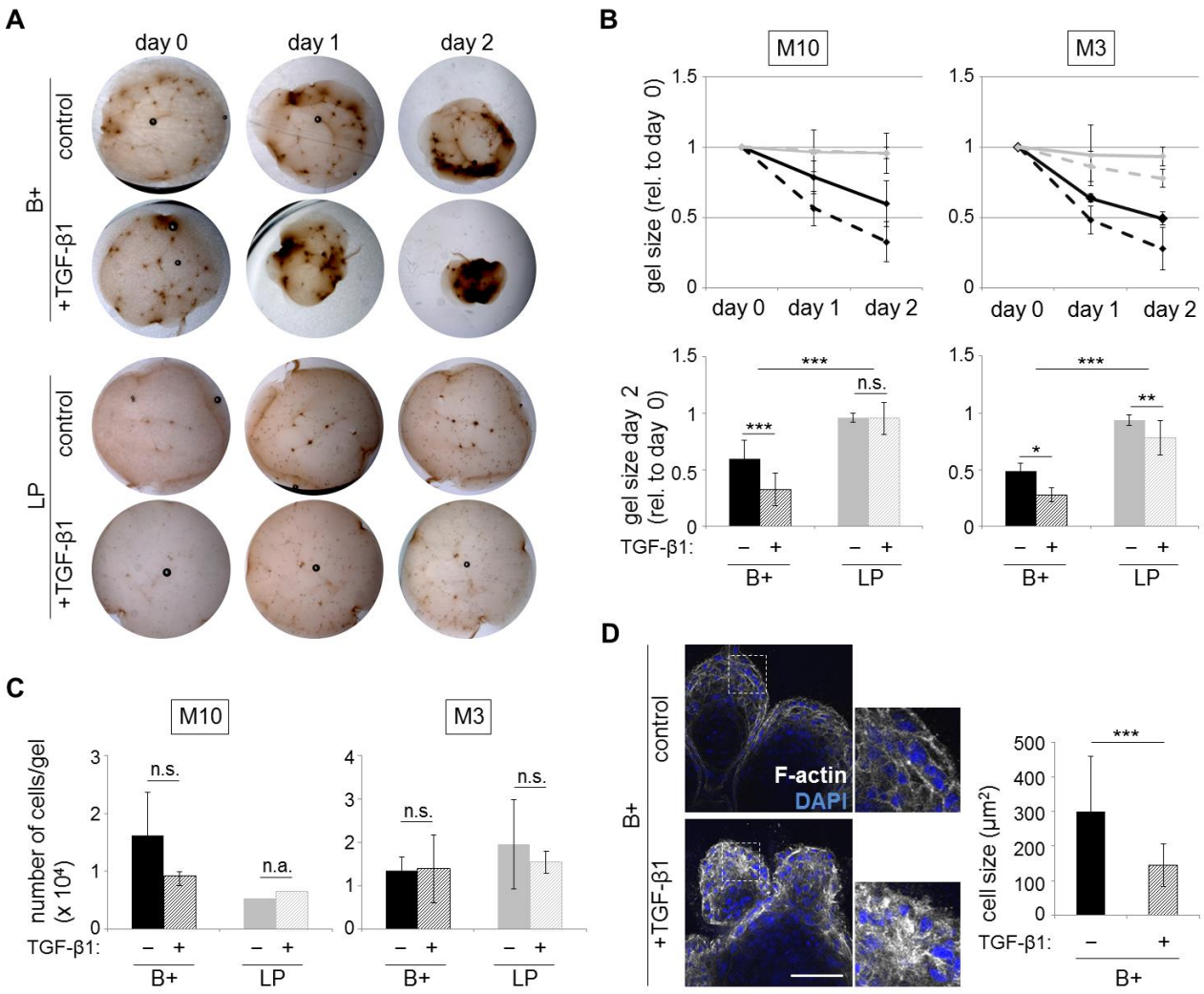

Figure 4.14 B+ cell-derived TDLU-like structures recapitulate functional aspects of the mammary gland.
(A) Bright-field microscopy: representative images of control and TGFβ1-treated gels containing B+ or LP cells from (B).
(B) Gel contraction: size of gels containing LP or B+ cells (donors M3, M10) at day 12 of culture (indicated as day 0) imaged for 2 days. 400 µl collagen gels, $3x10^3$ B+ cells or $1x10^4$ LP cells seeded per gel. Gels were treated with 2.0 ng/ml of TGFβ1 at day 0 and gel size was assessed for two more days. Gel size is plotted relative to day 0. Lower panel: bar graphs of gel size at day 2 as percentage of day 0. n=12 gels/condition.
(C) Average number of cells/gel at the end of analysis shown in (A,B). Gels containing LP cells (donor M10) were pooled and counted.
(D) Contraction of individual cells. Confocal microscopy (left): B+ cell derived structures (donor M8) were treated with TGFβ1 as in (B), and stained with Phalloidin to visualize F-actin (white) and DAPI (blue). Areas outlined are shown at higher magnification on the right. Scale bar: 100 µm. Cell size was determined for 30 cells of three different structures/condition using the ImageJ area tool.
(B,C,D) Data are shown as mean ± standard deviation (s.d.).
n.s., not significant; n.a., not applicable.

In conclusion, a functional feature of myoepithelial cells, namely contractility, can be recapitulated in floating collagen gels and further stimulated by treatment with TGFβ1. This assay might prove useful in the identification and characterization of MaSCs/bipotent progenitor cells as it was recently reported that murine MaSCs belong to the myoepithelial cell population with contractile function [Prater et al., 2014].

4.4 Matrix compliance promotes TDLU-like structure formation and luminal differentiation

4.4.1 TDLU-like structure formation depends on matrix compliance

As discussed above, B+ cells giving rise to TDLU-like structures exhibited contractile function in floating collagen gels. Thereby, the question emerged whether gel-contraction was simply a result of TDLU-like structure formation, or whether contraction was required for the generation of TDLU-like structures by providing force-feedback to the cells.

To address this question, I cultured B+ cells in floating collagen gels, representing a soft/compliant environment, in collagen gels that were left attached to the culture dish, representing a stiff/rigid environment, and in attached collagen gels that were detached once structures had formed (Figure 4.15A). While floating collagen gels promoted the formation of TDLU-like structures with prominent alveoli at their tips, structures formed in attached collagen gels lacked alveoli formation (Figure 4.15B). Instead, the tips of these structures contained elongated cells whose protrusion pointed away from the structure towards the surrounding collagen, representing an invasive phenotype (Figure 4.15B, smaller image).

Strikingly, flotation of previously attached gels caused loss of invasive morphology and formation of alveoli within 24 hours (Figure 4.15B). This result shows that HMECs respond to changes in the physical environment in a fast manner.

To further describe the different morphologies observed in floating versus attached gels, the number of primary, secondary, tertiary and quaternary side branches was determined for the different conditions (Figure 4.15C). This revealed that in addition to the complete lack of alveoli, structures formed in attached collagen gels had a 2.6 fold greater number of side branches (Figure 4.15C).

In conclusion, these results highlight the importance of force-feedback mechanisms between normal HMECs and the physical environment. A rigid/attached collagen matrix which cannot be contracted promotes the inherently invasive mechanisms of ductal elongation and side-branching while a compliant/floating collagen matrix promotes alveologenesis.

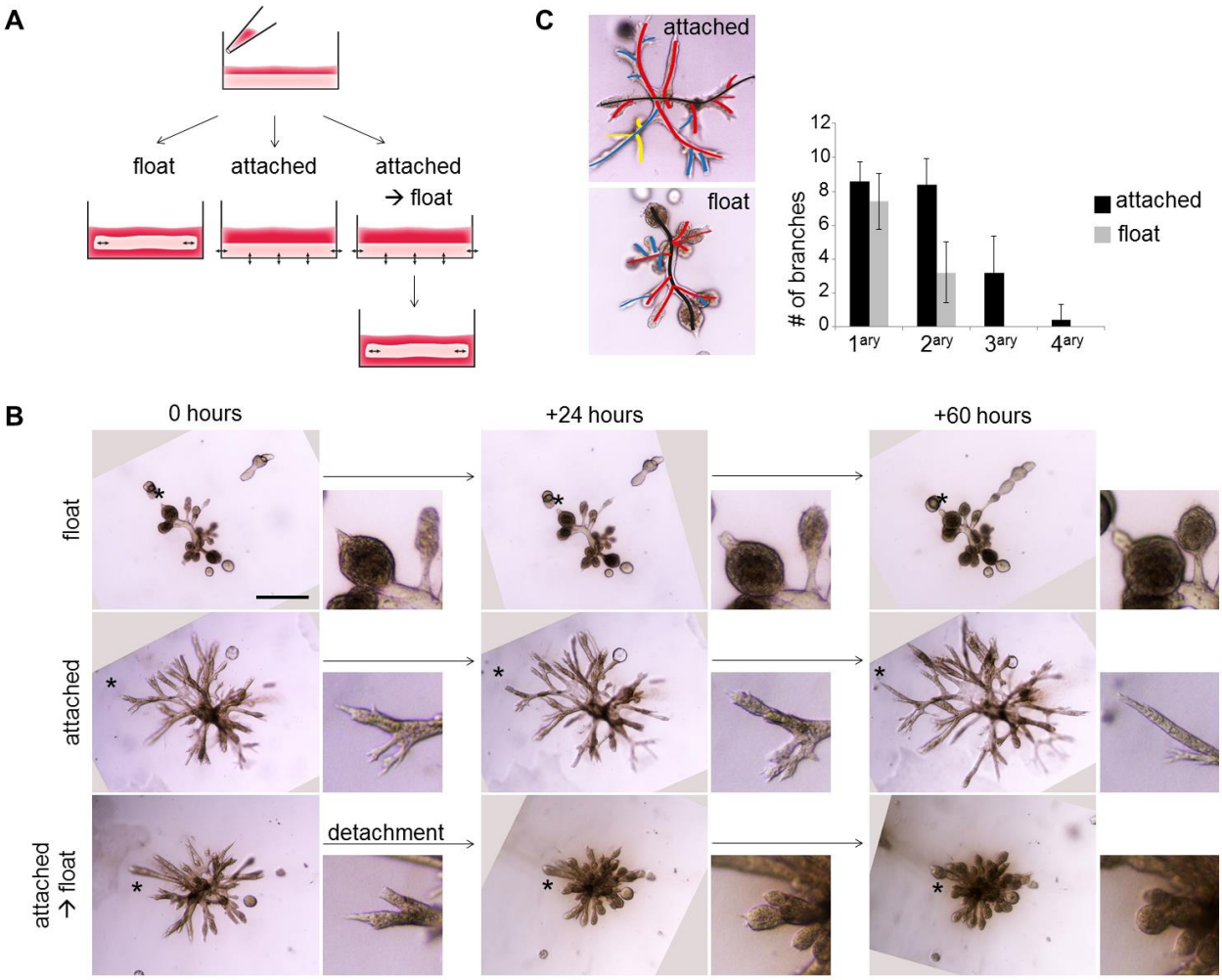

Figure 4.15 Matrix compliance in floating collagen gels is required for alveologenesis.
(A) Experimental layout: freshly isolated HMECs were seeded into collagen I gels, which were immediately detached to float (left) or left attached to the cell culture dish (middle, right). Once branched structures had formed, some attached gels were detached (right).
(B) Bright-field microscopy: representative images of HMEC-derived branched structures
(donor M8), cultured according to (A) and imaged for 60 h, starting at day 13 of culture. Smaller images: detail of area indicated by asterisk. Scale bar: 500 µm.
(C) Quantification of side branches: representative image with primary, secondary and tertiary side branches indicated by red, blue and yellow lines, respectively. The graph shows the number of side branches/structure in attached and floating collagen gels at day 13 of culture for five structures/condition (donor M8). Data are shown as mean ± standard deviation (s.d.).

4.4.2 TDLU-like structure formation depends on the cell's ability to contract in a compliant environment

As shown above, contraction of collagen gels was required for alveologenesis and TDLU-like structure formation. Next, I tested whether cellular contractility of cells was required for alveologenesis. Thus, freshly isolated HMECs were seeded into attached collagen gels and once structures had formed, gels were treated with Blebbistatin or Y-27632, every 24 hours to

prevent cellular contraction. Blebbistatin is a small molecule inhibitor which prevents contraction by directly binding to and inhibiting myosin II-ADP-Pi complex, thereby interfering with phosphate release, blocking myosin II in an active detached state [Kovács et al., 2004]. As discussed above, Y-27632 is a specific inhibitor of rho-associated protein kinase (ROCK), a kinase promoting actin-myosin contraction by phosphorylation of a variety of targets including MLC and LIM kinase [Riento et al., 2003]. After treatment with either Blebbistatin or Y-27632, the gels were detached immediately. As expected, detachment of control gels containing untreated TDLU-like structures led to a decrease in gel size to about 70% of the initial size within 4 days, suggesting that cellular contractility was functional. In contrast, gels containing TDLU-like structures treated with either Blebbistatin or Y-27632 contracted to only 90% and 80% of the initial size, respectively (Figure 4.16A). Contraction of gels treated with Y-27632 was not correlated with differences in cell proliferation/survival, as cell numbers at the end of analysis were equal between control and Y-27632 conditions (Figure 4.16B). In contrast, gels treated with Blebbistatin contained significantly less cells at the end of analysis. However, Blebbistatin-treatment inhibited detachment-induced reduction in gel size already at much earlier timepoints (24, 60 h after detachment), suggesting that this effect would also have occurred independent of proliferation/survival (Figure 4.16A). As observed before, untreated structures developed alveoli within 24-hours after detachment (Figure 4.16C). In contrast, alveologenesis was prevented in structures treated with either Blebbistatin or Y-27632. In summary, these results suggest that formation of alveoli is promoted by actin-myosin based contraction of TDLU-like structures.

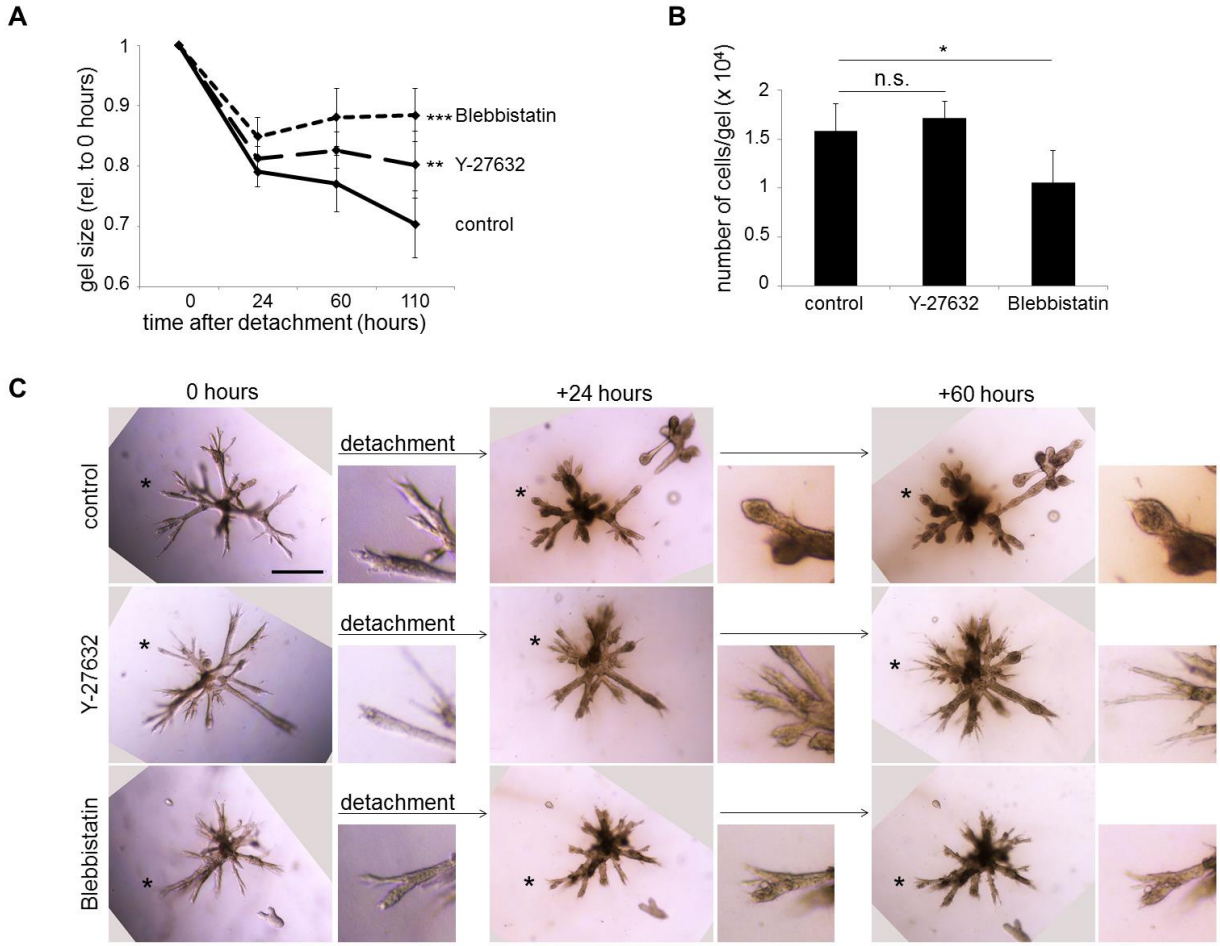

Figure 4.16 Actin-myosin based contraction in floating collagen gels is required for alveologenesis.
(A) Contraction of collagen gels: HMECs from donor M10 were grown in attached collagen gels. Once branched structures had formed, gels were detached (day 13 of culture) and treated with 10 µM Blebbistatin or 5 µM Y-27632 every 24 hours. The size of the gels was determined directly after detachment (0 hours), and after 24, 60 and 110 hours. Gel size is plotted relative to the time point of detachment (0 hours). 400 µl collagen gels, $3x10^3$ cells seeded per gel. n=16 gels/condition.
(B) Quantification of the average number of cells per gel at the end of analysis shown in (A), n=4. Data are shown as mean ± standard deviation (s.d.).
(C) Bright-field microscopy: representative images of HMEC-derived branched structures from (A) Smaller pictures are details of areas indicated with asterisk. Scale bar: 500 µm.
n.s., not significant

4.4.3 Acquisition of luminal features and correct polarization of TDLU-like structures depend on matrix compliance

As shown above, active contraction of floating collagen gels by B+ cell derived structures is required for the formation of alveoli which are the functional, milk producing units of the MG associated with luminal differentiation. To investigate whether matrix compliance promoted not only alveologenesis but also luminal differentiation at the molecular level, I cultured B+ cells in floating, attached and attached collagen gels that were detached once TDLU-like structures had formed. TDLU-like structures were analyzed by immunofluorescence and qPCR for the expression of basal/luminal and polarization markers.

In TDLU-like structures from floating and attached-to-floating collagen gels, cells of the outer layer were positive for the basal marker p63, while some cells at inner positions had acquired expression of luminal markers GATA3 and ZO-1 (Figure 4.17A,B). This finding confirms the previous observation that B+ cells give rise to cells with luminal features in floating collagen gels and that TDLU-like structures recapitulate lineage marker expression *in situ*. In addition, this finding indicates that luminal differentiation is promoted by matrix compliance.

In contrast, in structures grown in attached collagen gels, expression of p63 was not restricted to cells at basal positions and the expression of luminal marker GATA3 was observed only in rare cells in focal positions, while ZO-1 could not be detected (Figure 4.17A,B). These results suggest that culture in attached collagen gels impairs luminal differentiation.

Supporting these observations, transcript levels of luminal markers *ELF5* and ZO-1 (*TJP1*) were not detectable/lower in attached collagen gels (Figure 4.17E), while *GATA3* mRNA was expressed at similar levels in all conditions. The latter finding is in contrast to the observation that cells expressing GATA3 protein were detected at luminal positions in TDLU-like structures of floating and attached-to-floating collagen gels. These contrasting results suggest that flotation either promotes the luminal positioning of pre-existing GATA3+ cells or that it promotes the upregulation of GATA3 in only a small number of cells at luminal positions. In both cases, changes in GATA3 expression might not be detected by the assessment of overall GATA3 transcript levels.

TDLU-like structures of both floating and attached-to-floating collagen gels expressed basement membrane receptor integrin-α6 at strictly basal position (Figure 4.17C). In attached collagen gels, integrin-α6 was expressed at similar levels, but its expression occasionally extended towards more luminal positions. Expression of the basement membrane component and ligand for integrin-α6, laminin, was observed in TDLU-like structures of both floating and floating to attached gels. In contrast, expression of laminin was weak in branched structures of attached collagen gels (Figure 4.17C). These results indicate that matrix compliance promotes polarized expression of basement membrane components and their receptors.

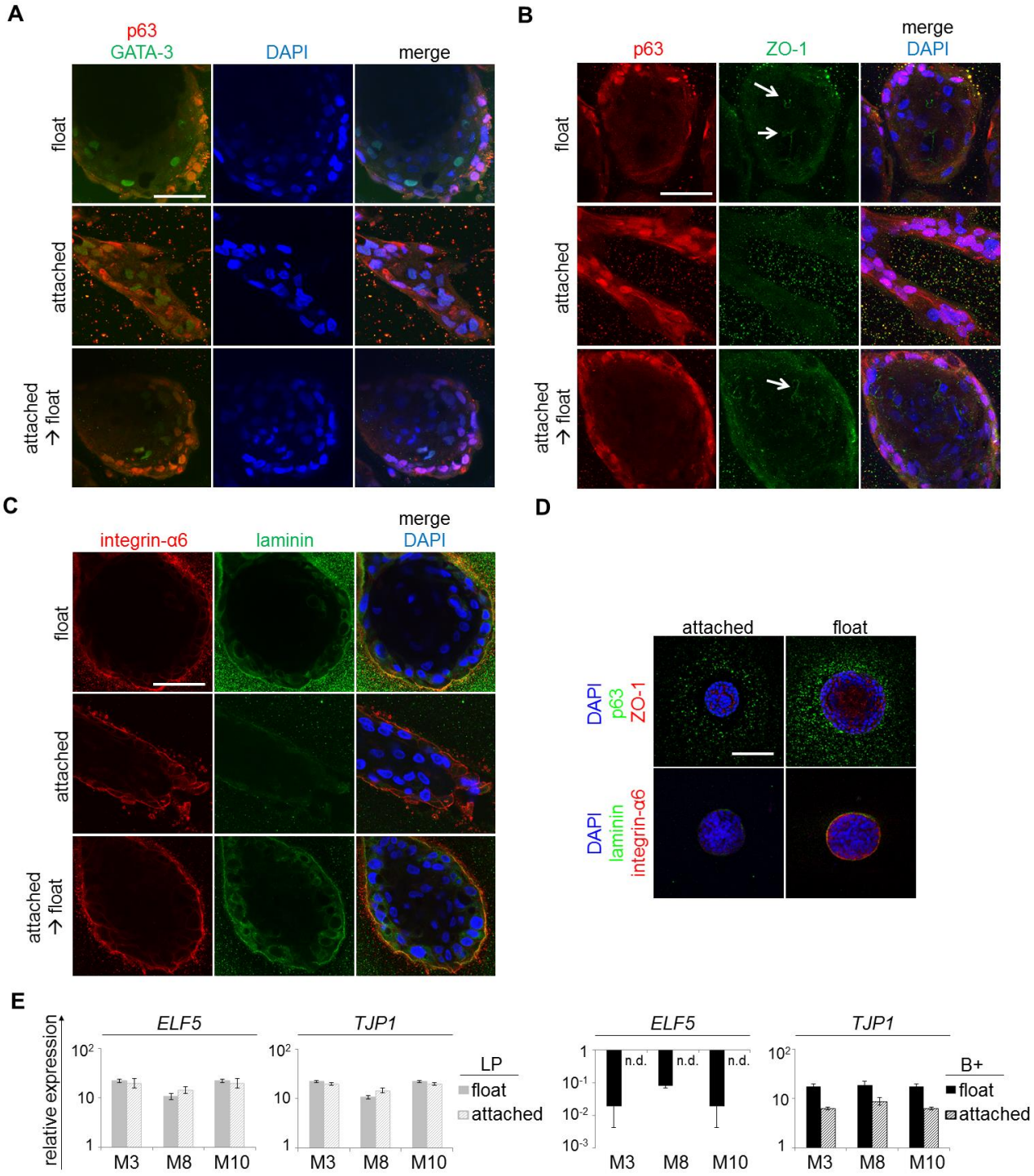

Figure 4.17 Matrix compliance in floating collagen gels is necessary for luminal differentiation of TDLU-like structures.

(A) Confocal microscopy: representative images of HMEC-derived branched structures (donor M8), cultured according to Figure 4.15A. Staining: p63 (red), GATA3 (green), and DAPI for nuclei (blue). Scale bars: 50 µm.

(B) Confocal microscopy: representative images of HMEC-derived branched structures from same origin as in (A). Staining: p63 (red), ZO-1 (green), and DAPI for nuclei (blue). Scale bars: 50 µm.

(C) Confocal microscopy: representative images of HMEC-derived branched structures from same origin as in (A). Staining: integrin-α6 (red), laminin (green) and DAPI for nuclei (blue). Scale bars: 50 µm.

(D) Confocal microscopy: representative images of HMEC-derived spheres (donor M8), cultured in floating and attached collagen gels, at day 14 of culture. p63 (green), ZO-1 (red), integrin-α6 (red), laminin (green), DAPI (blue). Scale bar: 100 µm.

(E) RT-PCR: *ELF5* and *TJP1* (ZO-1) mRNA expression in B+ and LP cell derived structures from donors M3, M8 and M10, cultured in attached and floating collagen gels. n=3. Data are shown as mean ± standard deviation (s.d.). n.d., not detectable

In LP derived spheres, high rigidity of attached collagen gels did not have any effect on the morphology and expression of luminal markers at the protein and mRNA level (Figure 4.17D,E). Considering that these cells are non-contractile and based on our observation that LP cell derived structures did not contract floating collagen gels, these results indicate that differentiation of LP cells is independent of the physical environment.

In summary, compliant/floating collagen gels promote correct polarization and acquisition of luminal features of B+ cell derived TDLU-like structures while differentiation of LP cell derived structures seem to be independent of matrix compliance.

4.5 Forskolin promotes TDLU-like structure formation by B+ and LP cells

4.5.1 Forskolin promotes TDLU-like structure formation by B+ and LP cells

Forskolin increased the number of TDLU-like structures generated by bulk primary HMECs, and was therefore used as standard supplement in the culture of HMECs (Figure 4.2B,C). Sorting of freshly isolated HMECs revealed that TDLU-like structure forming ability was predominantly contained within the B+ population (B-SFU = 1/413; Figure 4.9A). However, also LP cells exhibited limited TDLU-like structure forming potential (B-SFU = 1/5112; Figure 4.9A). Next, I addressed whether the addition of Forskolin increased B-SFU of LP and B+ cells in an equal manner, or whether its effect was more pronounced in one subpopulation. Thus, I seeded freshly isolated B+ and LP cells from 3 donors into floating collagen gels in limiting dilution in the presence or absence of Forskolin. After a culture period of 15 days, gels containing at least one TDLU-like structure were quantified. ELDA revealed that Forskolin significantly increased B-SFU of both LP and B+ cells (Figure 4.18A). Specifically, Forskolin treatment increased B-SFU of B+ and LP cells by ~1.7-fold and ~6.1-fold, respectively. However, B-SFU of B+ cells was generally much higher than B-SFU of LP cells both in the absence (~91.9-fold) or presence (~25.4-fold) of Forskolin (Figure 4.18A).

By comparing B-SFU in the absence versus presence of Forskolin, it can be calculated how many cells acquired B-SFU upon Forskolin treatment:

In LP cells, Forskolin treatment raised B-SFU 6.1-fold from 1/40992 to 1/6777 cells. Put differently, B-SFU was raised from 1/40992 to 6.1/40992 cells. This means that 5.1 among 40992 (= 1/8038) cells had newly acquired TDLU-like structure forming ability in the presence of Forskolin.

In B+ cells, Forskolin treatment raised B-SFU 1.7-fold from 1/446 to 1/267 cells. Put differently, B-SFU was raised from 1/446 to 1.7/446 cells. This means that 0.7 among 446 (= 1/637) cells had acquired TDLU-like structure forming ability in the presence of Forskolin.

Thereby, the total number of cells which newly acquired TDLU-like structure forming ability upon treatment with Forskolin was greater in the B+ than in the LP population.

Importantly, the Forskolin induced increase in B-SFU of the LP population could not be explained by contamination with B+ cells during the sorting procedure. In this experiment, contamination of the LP population with cells from the B+ population was less than 0.5% among all samples (data not shown). Considering that ~1/637 B+ cells acquired branched structure forming ability upon Forskolin treatment and assuming a contamination with B+ cells of 1%, 63,700 cells of the LP population (637 B+ cells*100) would contain one B+ cell

which would respond to Forskolin by acquiring TDLU-like structure forming ability. However, it was determined that 1/8038 cells of the LP population acquired B-SFU upon treatment with Forskolin, indicating that cells with LP identity acquire TDLU-like structure forming potential upon Forskolin treatment.

In summary, these data indicate that Forskolin treatment increases B-SFU of both B+ and LP cells. However, in absolute values, the effect of Forskolin on B-SFU is more pronounced in B+ cells than in LP cells. Based on this, the use of Forskolin as standard culture additive leads to an increased number of branched structures primarily from cells of the B+ population, which endogenously exhibits the highest B-SFU, rather than causing potentially aberrant de-differentiation of a LP cell population. Future studies will address which cells among both the B+ and LP population are particularly sensitive to treatment with Forskolin and assess the mechanism behind acquisition of B-SFU. Considering that acquisition of B-SFU in LP cells might reflect aberrant de-differentiation (see Chapter 4.2.6), it will be of particular interest to assess the mechanisms behind acquisition of B-SFU in these cells.

A

LP cells	Cells seeded	Positive gels/ total gels (Average number of structures/ gel)			B-SFU (95% CI)
		M8	M9	M10	
DMSO	500	0/8	0/8	0/8	1/40992 (1/10294 - 1/163229)
	1000	0/8	0/8	0/8	
	2000	1/8	0/8	1/8	
Forskolin	500	1/8	0/8	1/8	1/6777 (1/3843 - 1/12667)
	1000	2/8	1/8	2/8	
	2000	3/8	1/8	0/8	

B+ cells	Cells seeded	Positive gels/ total gels (Average number of structures/ gel)			B-SFU (95% CI)
		M8	M9	M10	
DMSO	125	0/8	6/8	0/8	1/446 (1/311 - 1/637)
	250	0/8	7/8	3/8	
	500	6/8)	7/8	3/8	
Forskolin	125	0/8	7/8	5/8	1/267 (1/194 - 1/368)
	250	0/8	7/8	7/8	
	500	3/8	8/8	8/8	

Figure 4.18 Forskolin promotes TDLU-like structure formation by LP and B+ cells.
(A) Extreme limiting dilution analysis: Determination of branched structure-forming units by FACS sorted LP cells (top) and B+ cells (bottom), cultured in the presence or absence of 10 µM Forskolin (B-SFU, donors M8, M9, M10). Data are mean and 95% confidence intervals (CI).

5 Discussion

The identification and characterization of human stem-/progenitor cells and the analysis of cellular plasticity have long been hampered by the limited applicability of murine in vivo assays and the failure of currently used 2D and 3D in vitro assays to recapitulate the histological architecture and functionality of the human MG. Three-dimensional organotypic assays aim to mimic the normal tissue environment and thereby allow (single) adult stem-/progenitor cells to generate organoids containing all cell types and exhibiting functionality of the specific tissue [Clevers, 2016].

Here, I have developed a novel organotypic culture system in which single primary HMECs cultured in floating collagen I gels generate structures which resemble TDLUs, the functional units of the human MG in situ. The TDLU-like structures contain both cells with basal and luminal marker expression and display functionality by contracting. Using this culture model, regenerative capacity, cell fate and plasticity of HMECs can be modeled in vitro. In addition, this model provides a tool for assessing the interplay between the molecular environment and MG architecture, function and differentiation in the setting of normal tissue development and homeostasis and to identify and characterize aberrant behavior.

The three major achievements of this study are:

1.) Development of a novel organotypic culture system in which primary HMECs generate TDLU-like structures.

2.) Description of lineage marker expression, polarization and functionality of TDLU-like structures and the dependence of these parameters on the mechanical environment.

3.) Development of a protocol for the enrichment of TDLU-like structure forming cells which were found to belong to the basal lineage.

5.1 A novel three-dimensional culture system for the generation of breast organoids

Cell lines are commonly used to study MG biology. However, immortalization and prolonged culture introduce genotypic and phenotypic changes and usually lead to the selection of a subpopulation of cells which is not representative of the original tissue [Birgersdotter et al., 2005, Petersen et al., 1992]. In order to provide a biologically more relevant system, the organotypic culture system used in this study relies on normal, freshly isolated primary HMECs isolated from reduction mammoplasties. These cells more accurately reflect the cellular behavior *in vivo* as they are isolated from tissue samples directly before use and not subjected to immortalization. Thereby, they represent the cellular composition of the donor-tissue and do not contain genetic or phenotypic aberrations which are introduced by *in vitro* immortalization. As such, they are a valuable tool to study cellular phenotypes and functions relevant *in vivo*.

In the MG, cells grow in a 3D context where they are connected to each other as well as to the surrounding basement membrane and ECM. In humans, the stroma surrounding mammary epithelial ducts and their associated basement membrane consists of connective tissue proteins, most abundantly collagen I [Howard et al., 2000]. Collagen I lends structural support to the epithelial structure and provides binding moieties for the cells thereby affecting how biochemical signals are interpreted [Birgersdotter et al., 2005, Taddei et al., 2003].

These considerations suggest that collagen I serves as a biologically relevant 3D environment *in vitro*. By taking into account previous studies showing that cells of the breast carcinoma cell line T47D generate tubular structures in freely floating collagen gels [Wozniak et al., 2005], I thus chose floating gels of collagen I as biologically relevant substrate for culturing HMEC *in vitro*.

Indeed, culture of HMECs within floating collagen I gels led to the formation of TDLU-like structures which resemble the functional units of the human breast *in situ* [Anderson et al., 1998]. Matrigel, a basement membrane protein mix produced by a mouse sarcoma cell line, is another substrate commonly used for 3D-culture of mammary epithelial cells. However, it is derived from mouse sarcoma cells and its exact composition is not defined and varies from lot to lot [Benton et al., 2014]. Here, formation of TDLU-like structures was not supported in Matrigel, or a mixture of collagen I and Matrigel, suggesting that it represents a biologically less relevant substrate for HMECs than collagen I. It should be noted that in contrast to these data other research groups have reported successful cultivation of basal HMECs in Matrigel.

However, this inconsistency can be explained by different culture setups. Specifically, other researchers included pre-culture of single cell suspensions or have used tissue fragments or different culture media, the latter of which might have led to selection of a certain subpopulation of cells able to grow in Matrigel [Dontu et al., 2003, Villadsen et al., 2007]. In addition, HMEC feeder layers have been used, which are a source of signaling molecules and ECM proteins. Thereby, the molecular environment of the cells growing in Matrigel is changed which might have led to improved survival and growth [Villadsen et al., 2007]. In summary, floating collagen I gels rather than Matrigel allow for 3D-morphogenesis of HMECs *in vitro* and provide a growth environment resembling the tissue context of HMECs *in vivo*. Thereby, the organotypic culture system presented here will be a valuable tool to study cellular phenotypes and functions relevant *in vivo*.

5.2 Critical parameters of TDLU-like structure formation

The generation of TDLU-like structures described above depended on three critical parameters which will be discussed below: intracellular cAMP levels, physical forces of the ECM and cellular contractility.

5.2.1 Intracellular cAMP levels

cAMP is a second messenger which plays an important role in the cellular response to hormones and neurotransmitters. The intracellular levels of cAMP are regulated by two groups of enzymes: Adenylate cyclases catalyze the conversion of ATP to cAMP, while cyclic nucleotide phosphodiesterases (PDEs) degrade the phosphodiester bonds in cAMP, hydrolyzing cAMP to AMP [Rehmann et al., 2007, Sassone-Corsi, 2012]. Forskolin directly binds to adenylate cyclase by hydrophobic interactions, causing its continuous activation and increased cAMP production [Tang et al., 1998].

Here, continuous treatment with Forskolin was found to promote TDLU-like structure formation in floating collagen gels. This effect might rely on the stimulation of pathways involved in steroid hormone signaling, which is the major driver of MG development after puberty, stimulating ductal elongation, side branching and alveologenesis *in vivo* [Brisken et al., 2010]. Indeed, both estrogen and progesterone signaling were found to increase intracellular cAMP levels in mammary epithelial cells: Daily injection of either estrogen or progesterone was shown to increase cAMP levels in ovariectomized mice, in which the ovaries, the major source of estrogen and progesterone had been removed surgically

[Sheffield et al., 1987]. Also in the breast cancer cell line MCF-7, estrogen was shown to stimulate adenylate cyclase and cAMP-regulated gene expression [Aronica et al., 1994, Zivadinovic et al., 2005]. On the functional level, activation of cAMP signaling by implantation of pellets containing Forskolin or other cAMP raising agents was shown to stimulate end bud development and restore duct diameter in ovariectomized mice with underdeveloped and regressed ductal epithelial tree [Silberstein et al., 1984]. These data suggest that agents raising cAMP levels can be used to replace parts of steroid hormone signaling. Thereby, treatment with Forskolin might be useful to promote growth and differentiation of HMECs *in vitro*. This would be a great achievement, as hormone receptor expression gets lost upon *in vitro* culture of primary HMECs.

So far, efforts preventing the loss of steroid hormone receptor expression include culture of crude tissue fragments containing stromal components, which allows for HR maintenance for a short period in culture but does not allow for analysis of independent cells [Tanos et al., 2013]. In addition, culture of primary HMECs in the presence of small molecule inhibitors of TGF-β signaling was reported to maintain ER expressing cells with functional estrogen signaling in 2D culture [Fridriksdottir et al., 2015]. However, these findings could not be reproduced in our hands (data not shown).

Future studies should assess more closely downstream effects of cAMP signaling and the overlap with steroid hormone signaling. In addition, hormone receptor(s) responsible for cAMP signaling in mammary epithelial cells *in vivo* should be identified. For this the development of *in vitro* culture conditions supporting the maintenance of functional steroid hormone signaling in primary HMECs will be of great help.

Treatment with Forskolin not only increased TDLU-like structure formation but also increased the number of times TDLU-like structures could be passaged in floating collagen gels. In addition, Forskolin treatment was necessary for the maintenance of an epithelial phenotype of HMECs cultured in 2D or 3D conditions. Furthermore, in branched structures were more compact and cells expressing the luminal marker Gata3+ appeared earlier in the center of structures in presence of Forskolin, suggesting that Forskolin promotes self-organization. Compounds raising intracellular cAMP levels have long been known to sustain growth and increase proliferation of primary human and murine MECs cultured in various *in vitro* assays [Stampfer, 1982]. Therefore, some part of these effects, including increased TDLU-like structure formation, could be explained by increased proliferation. However, other effects like maintenance of epithelial cell fate, improved self-organization and compaction of TDLU-like structures seem to be independent on proliferation. Indeed, increased cAMP levels

have been associated with a variety of effects: For instance, increased cAMP levels were shown to induce mesenchymal to epithelial transition in mesenchymal derivatives of immortalized HMECs by activation of PKA [Pattabiraman et al., 2016]. In addition, increased levels of cAMP were shown to promote lumen formation in 3D rBM cultures of the human mammary epithelial cell line MCF10A by accelerating the re-distribution of integrin-α6 to the periphery, causing polarization of outer cells and promoting apoptosis of inner cells [Nedvetsky et al., 2012].

Future studies should dissect the downstream signaling pathways responsible for the different observed effects more closely. In eukaryotes, three main classes of cAMP effectors have been identified: protein kinase A (PKA), exchange factor directly activated by cAMP (EPAC) and cyclic nucleotide-gated ion channels (CNGC) [Rehmann et al., 2007]. More recently, additional cAMP effectors have been discovered, including popeye domain containing (Popdc) proteins which are involved in various physiological processes including cell-cell adhesion and epithelial function [Schindler et al., 2016]. It is likely that the different effects observed here are mediated via different cAMP effectors. Therefore, selective cAMP analogs and inhibitors as well as PKA and EPAC inhibitors will be used to see whether they can mimic or prevent the described effects of Forskolin treatment.

As mentioned above, steroid hormones might be the physiological stimuli upstream of increased cAMP signaling. The classical estrogen receptors (ER) and progesterone receptors (PR) act as intracellular transcription factors. Upon binding to ligand, they translocate to the nucleus, where they bind to specific sequences of DNA either directly or indirectly via other transcription factors. In the cytosol, ER and PR are subject to extensive cross-talk with other signaling pathways: For instance, activated ER and PR can induce the membrane proximal Src-kinase leading to downstream signaling via epidermal growth factor receptor (EGFR), mitogen-activated protein kinase (MAPK) and phosphatidylinositol-3-kinase [Tanos et al., 2012]. In addition, other signaling pathways impinge on HRs and affect their transcriptional activity, coactivator interaction and nuclear localization [Tanos et al., 2012]. For example, PKA was shown to activate ERα-mediated transcription via cAMP [Fujimoto et al., 1994]. Furthermore, cAMP can be induced downstream of the membranous estrogen receptor GPR30 and membrane localized progestin receptors (mPRs) [Prossnitz et al., 2008]. GPR30 is a transmembrane G-protein coupled receptor (GPCR). Once activated by binding of estrogen, GPER can activate adenylate cyclase via stimulatory G-proteins [Prossnitz et al., 2014]. Indeed, GPER was shown to be required for estrogen-mediated generation of cAMP [Filardo et al., 2002]. mPRs are members of the progestin and adiponextin Q receptor family which are

similar to GPCRs in that they are 7-transmembrane proteins and activate G-proteins and their downstream target adenylate cyclase [Dressing et al., 2011]. GPER and mPRs are therefore strong candidates in the search for hormone receptors upstream of the cAMP effects observed here. Future studies should therefore assess whether GPER and mPR signaling can cause increased TDLU-like structure formation similar to Forskolin. For this, GPER-selective agonists like G-1 and antagonists like G36, as well as mPR specific agonist can be used [Bologa et al., 2006, Dennis et al., 2011, Kelder et al., 2010].

5.2.2 Physical forces of the extracellular matrix and cellular contractility

Besides Forskolin, matrix compliance and cellular contractility were found to be crucial parameters for TDLU-like structure formation and cellular differentiation. Specifically, the development of alveoli-like buds and differentiation towards the luminal lineage were only observed in floating/compliant collagen gels but not in attached/rigid collagen gels. In addition, the use of small molecule inhibitors Y-27632 and Blebbistatin revealed that within floating/compliant gels both processes depended on actin-myosin based contraction.

Consistent with these findings, it has previously been reported that matrix rigidity affects the growth, morphogenesis and differentiation of mammary epithelial cells *in vitro*: Matrices with high stiffness as a result of collagen concentration, crosslinking, matrix attachment or interpenetrating polymer networks were shown to disrupt normal morphogenesis and favor the generation of multicellular structures with a malignant/invasive phenotype [Chaudhuri et al., 2014, Levental et al., 2009, Paszek et al., 2005, Provenzano et al., 2009, Wozniak et al., 2003].

In addition, maintenance of luminal lactational differentiation of mammary epithelial cells from pregnant/pre-lactating mice was maintained only on compliant/floating but not on rigid/attached collagen gels [Emerman et al., 1977, Streuli et al., 1990].

Indeed, I observed that rigid/attached collagen gels caused persistent elongation and increased formation of side branches of basal-cell derived branched structures. In contrast, the formation of spheres by luminal progenitor cells was not affected by increased rigidity in attached collagen gels. In accordance with these data, the process of increased elongation and formation of side branches has been related to a basal epithelial program in invasive breast cancer using collagen gels as experimental tool [Cheung et al., 2013].

High matrix stiffness is observed in breast tumors and has been linked to tumor progression and invasion [Levental et al., 2009, Paszek et al., 2005, Provenzano et al., 2009]. Notably, the compression modulus of breast tumor tissue is comparable to the compression modulus of

stiff collagen gels with a concentration of 4 mg/ml [Paszek et al., 2005]. The fact that I observe persistent elongation and increased formation of side branches in attached/rigid collagen gels suggest that the responsiveness of breast cancer cells to the physical environment is conserved in normal mammary epithelial cells and plays a role in normal MG development/morphogenesis. Indeed, it has been reported that normal tissue behavior depends on tensional homeostasis of exogenous forces generated by the cells themselves and endogenous forces from the outside which are transmitted via the cytoskeleton [Paszek et al., 2010]. Focal Adhesions, clusters of integrins which physically connect the cell to the ECM are the principal mediators of tensional homeostasis, balancing endogenous and exogenous forces to generate a favorable environment for cell function [Provenzano et al., 2009]. In MaSCs, endogenous forces might be particularly important, since these cells display contractility [Prater et al., 2014]. As described above, here I have shown that endogenous contractility regulates invasion into collagen gels and is required for generation of alveoli and luminal differentiation in floating collagen gels.

Notably, generation of alveoli by HMECs in floating collagen gels was further increased by the addition of Forskolin. As discussed above, Forskolin is known to promote the distribution of integrin-α6 to the periphery, thereby accelerating the polarization of MCF10A cells cultured in 3D rBM cultures [Nedvetsky et al., 2012]. Importantly, staining of laminin, the receptor for integrin-α6, was only detected in structures grown in floating but not attached collagen gels. Increased generation of alveoli in floating collagen gels treated with Forskolin might thus be caused by increased adhesion to laminin via integrin-α6. Thereby, the effects of flotation, cellular contraction and Forskolin might be based on anchorage of HMECs to the basement membrane, as the basis to establish basal polarity supporting the formation of alveoli.

Future studies will aim at a deeper understanding of the role of matrix rigidity, cellular contractility and cAMP signaling on morphogenesis and differentiation of HMECs and their relevance in normal development as well as pathological processes. It should be noted that with the current conditions, luminal differentiation in B+ cell derived TDLU-like structures was not complete, as ZO-1 and K18 staining were only rarely observed and the structures were not responsive to hormones (data not shown). Thus, a first step should consist of further improvement of culture conditions to support terminal differentiation of luminal cells.

In vivo, the MG only terminally differentiates during pregnancy and lactation [Howard et al., 2000, Russo et al., 2004], suggesting that culture conditions should aim to mimic the signaling environment during this developmental step.

It is known that the hormones progesterone and prolactin are involved in luminal differentiation and milk production [Brisken et al., 1999, Brisken et al., 2010, Gallego et al., 2001]. Downstream of progesterone and prolactin signaling, increased expression of cyclinD1 regulates proliferation of PR+ cells [Beleut et al., 2010, Hennighausen et al., 2005]. In addition, both hormones were shown to induce transcription of Receptor activator of nuclear factor kappa-B ligand (RANKL) has been implicated in increased expression of Elf5 in luminal progenitor cells, proliferation of the Elf5 expressing population as well as lobuloalveolar differentiation and production of milk protein [Lee et al., 2013]. Importantly, Elf5 seems to be a master regulator of terminal luminal differentiation, alveolar morphogenesis and milk production as knock-out of Elf5 prevents development of the secretory alveolar epithelium during pregnancy while overexpression of Elf5 in virgin mice led to precocious alveolar differentiation and milk secretion [Oakes et al., 2008].

In addition to these hormone regulated signaling pathways, signals from basal cells might be required for terminal luminal differentiation. Specifically, it was shown that expression of Nrg1 as direct transcriptional target of p63 in K14+ basal cells, led to activation of Erbb4 receptor and downstream STAT5A signaling in luminal cells, which was required for luminal proliferation and differentiation during pregnancy [Forster et al., 2014]. Notably, both prolactin and Neuregulin/Nrg1 signaling cause activation and nuclear translocation of STAT5, suggesting the importance of this pathway in luminal differentiation [Forster et al., 2014, Hennighausen et al., 2005]. Therefore, these signaling pathways must be considered in efforts to generate culture conditions supporting terminal luminal differentiation.

5.3 Identification, quantification and enrichment of regenerative HMECs

Identification and characterization of human and murine MaSCs/progenitors is a major focus of MG research. It is the basis to understand cellular hierarchies and analyze normal and aberrant differentiation processes.

5.3.1 Identification and quantification of regenerative HMECs

Adult/somatic stem cells are defined by the ability to self-renew and to differentiate into specialized progeny. In the mouse, the stem cell character of MECs can be tested by transplanting these cells into the fat pad of recipient mice cleared of endogenous epithelium [Shackleton et al., 2006, Stingl et al., 2006]. There, the ability to give rise to differentiated progeny is reflected by the regeneration of a mammary epithelial tree containing cells of both major mammary lineages, luminal and basal. Serial transplantations allow assessment of the

self-renewal ability of the detected MaSCs. Importantly, by transplanting the cells in limiting dilution up to doses in which no regeneration of the mammary fat pad is observed, the rate of cells with stem cell characteristics can be inferred [Hu et al., 2009].

Here, I have developed a tool to detect HMECs with regenerative capacity by their ability to generate TDLU-like structures containing cells with basal and luminal characteristics in floating collagen gels. For quantification of these regenerative cells, I have performed extreme limiting dilution analysis (ELDA) as described by Hu et al. [Hu et al., 2009]. Specifically, limiting dilutions of HMECs were seeded into floating collagen gels up to doses in which no TDLU-like structure formation was observed, and gels containing at least one TDLU-like structure were quantified. Subsequently, the ELDA-software tool was used for mathematical analysis of the percentage of TDLU-like structure containing cultures at each dilution and estimation for regenerative cell frequency in the original population.

In summary, the developed assay provides a tool for the quantification of human MECs with regenerative capacity which is analogous to the transplantation assay used for quantification of murine MaSCs. In contrast to transplantation assays, in which two mammary fat pads per mouse can be injected with cell suspension, the 48-well format of *in vitro* floating collagen gels allows for an increased number of replicates.

5.3.2 Enrichment of regenerative HMECs

The identification and characterization of MaSCs/progenitors is a major focus of MG research and cells with regenerative capacity seem to be contained within the basal lineage in both human and mouse (see Chapter 1.2.4). In line with the current literature, ELDA in floating collagen gels revealed that TDLU-like structure formation is enriched in the basal CD49f^{hi}/EpCAM^{-} basal population over the LP CD49f^{+}/EpCAM^{+} population.

Here, I looked for additional markers to further enrich for TDLU-like structure forming cells. CD10 is a metalloendopeptidase which cleaves and inactivates a variety of peptide hormones, including oxytocin, a hormone released by the pituitary gland upon breastfeeding and which mediates myoepithelial cell contraction to support milk release [Maguer‐Satta et al., 2011]. CD10 has been shown to enrich for HMECs which build mammospheres, i.e. proliferate when cultured in anchorage independence and give rise to colonies expressing both luminal and basal markers in 2D culture, both traits associated with MaSCs [Bachelard‐Cascales et al., 2010].

Using CD10 as additional marker, I could show that regenerative cells were enriched within the $CD10^{+}/CD49f^{hi}/EpCAM^{-}$ (B+) population over the $CD49f^{hi}/EpCAM^{-}$ basal population by approximately 7-fold, while TDLU-like structure formation was almost depleted in the $CD10^{-}/CD49f^{hi}/EpCAM^{-}$ (B−) population. CD10 is thus a useful marker to enrich for TDLU-like structure forming cells.

Importantly, gene expression analysis confirmed the basal epithelial identity of the B+ population. However, the genes most highly expressed in the B− population were associated with stromal cells, specifically CD31− and CD45− endothelial and hematopoietic cells. These results indicate that sorting for CD10+ basal cells did not enrich for TDLU-like structure forming cells within a basal population, but rather purification of the basal population by exclusion of stromal cells. Therefore, CD10 does not serve as a marker for MaSCs but for basal cells. This statement is supported by an exhaustive immunohistochemical analysis of cell fate markers in the human MG, which has revealed that all cells at basal positions express CD10 [Santagata et al., 2014].

These data raise the question about the identity of the B− population. In vivo, high resolution imaging showed that in the postnatal MG, MECs are in close contract with lymphendothelium and blood vessels and that they are regulated together during branching morphogenesis and breast cancer progression [Alitalo et al., 2012, Betterman et al., 2012]. Strikingly, B− cells express CD49f (integrin-α6) which is the receptor for the basement membrane component laminin, as described above. Thereby, the B− population identified here might represent the lymph and vascular endothelial population which is in direct proximity of HMECs, linked to the basement membrane via their laminin receptors opposite to mammary epithelial cells. Given the role of the stromal population during MG morphogenesis and breast cancer progression, future studies will work on the characterization of the B− population using the in vitro assay described here. Specifically, by addition of this population to the assay, its influence on HMECs with different genetic backgrounds can be tested.

5.4 Regeneration in the human and murine mammary gland- MaSCs or unipotent progenitors?

Based on transplantation studies, the mammary repopulating unit (MRU) for murine basal MECs ($CD24^{med}/CD49f^{hi}$ or $CD29^{hi}/CD24^{+}$) is approximately 1/60, implying that one in 60 cells has regenerative capacity [Shackleton et al., 2006, Stingl et al., 2006]. Using human cells, Eirew et al. have determined that approximately 1/1000 – 1/10000 basal HMECs ($CD49f^{+}/EpCAM^{lo}$) show regenerative capacity upon transplantation under the kidney capsule of immune compromised mice [Eirew et al., 2008]. In addition, here I have shown that the B-SFU of $CD49f^{hi}/EpCAM^{-}$ HMECs cultured in floating collagen gels is 1/2690 and can be increased to 1/413 cells by using the marker CD10.

According to these data, the B-SFU of HMECs is slightly lower than the MRU of murine MECs determined by transplantation. Some of these differences might result from tissue processing and culture: naturally, due to the high amount of tissue, processing of primary human tissue is a time consuming process, taking approximately 48 hours, after which cells are usually cryopreserved. In contrast, processing of the much lower volume of murine tissue usually takes no more than 3 hours, after which cells can be sorted and transplanted back into a murine fat pad. The survival of murine MECs is further supported by the physiological tissue environment in which the cells are transplanted. In general, the determined MRU and B-SFU of murine and human basal MECs are likely underestimations, as FACS is known to be toxic in 50-75% of cells and unknown quantities of cells are lost during handling [Giraddi et al., 2015].

Based on these considerations, a high number of both human and mouse basal MECs contains regenerative capacity. Importantly, the number of MRU can change depending on transplant and culture conditions. For instance, it was shown that the MRU of murine MECs can be increased if Matrigel is transplanted together with the cells [Shehata et al., 2012, Vaillant et al., 2011]. Furthermore, the number of murine MaSCs/progenitors was shown to increase upon culture in the presence of ROCKi or soluble factors produced by fibroblasts [Makarem et al., 2013, Prater et al., 2014]. These data show that not only a high number of both human and mouse basal MECs contains regenerative capacity but that the number of regenerative cells can vary depending on conditions during *in vitro* culture and transplantation. These findings completely contradict the concept of a rare and fixed MaSC.

Indeed, according to recent data, post embryonic development and homeostasis of the murine MG could be independent of the existence of stem cells/bipotent progenitors. As discussed in Chapter 1.2.4, various lineage tracing studies, the latest using thorough statistical analysis of multicolor lineage tracing and lineage tracing at saturation, have convincingly stated that unipotent rather than bipotent stem cells/progenitors mediate pubertal development, adult tissue homeostasis as well as pregnancy and lactation in the murine MG [Van Amerongen et al., 2012, Van Keymeulen et al., 2011, Wuidart et al., 2016]. Contradictory results have been reported from two other lineage tracing studies. However, in the first study, a high fraction (30%) of the mammary epithelium was labeled, which complicates the clear demarcation of clonal patches and could have affected their quantification [Rios et al., 2014]. In the second study, it was argued that protein C receptor (PROCR) marks a population of multipotent mammary cells. However, the PROCR+ cells showed very little clonal output, as most of the clones generated in the course of a 6-week tracing period during pubertal MG development contained only one basal and one luminal cell [Wang et al., 2015]. This limited clonal output is in conflict with PROCR+ cells being able to initiate the complete postnatal outgrowth of the murine mammary epithelium and suggests that PROCR cannot be used as marker for MaSCs.

Thus, while there are multiple conflicting studies, data suggesting that postnatal MG development is mediated by unipotent stem cells/progenitors are convincing. However, future studies are needed to settle the debate on the existence or absence of multipotent MaSCs.

The concept that an epithelial tissue is maintained by unipotent progenitors rather than multipotent stem cells/progenitors is not restricted to the MG. Like the MG, sweat and prostate glands contain an inner luminal and outer basal/myoepithelial layer of cells. Lineage tracing studies in these organs have led to the conclusion that all three glands originate from multipotent embryonic stem/progenitor cells which get replaced by unipotent luminal and basal progenitors in the adult tissue [Lu et al., 2012, Wuidart et al., 2016]. If the murine MG (and possibly the human MG) is indeed maintained by unipotent progenitors similar to the above named tissues, the question emerges as to why MECs exhibit regenerative capacity upon transplantation and *in vitro* culture. Two possible answers to this question are that regenerative capacity might be generated *de novo*, or that myoepithelial cells contain regenerative capacity which is revealed only under certain circumstances. Possible triggers for *de novo* generation or revelation of regenerative capacity include transplantation, *in vitro* culture, wounding, a changing microenvironment and genetic aberration during cancer development and progression. As mentioned above, first experimental data support the

possibility of *de novo* generation/revelation of regenerative capacity: After *in vitro* culture in the presence of a ROCK inhibitor, MRUs of colonies of single cell derived basal MECs was increased to 65%, suggesting that the majority or even entire myoepithelial/basal cell population contains MRU potential [Prater et al., 2014]. In addition, Matrigel culture in the presence of fibroblast-derived factors was shown to increase MRU formation by murine MECs [Makarem et al., 2013]. The acquisition/revelation of stem cell features has also been observed in other organs: Recent studies on epidermis, intestinal epithelium, lung and MG have indicated that the fate and differentiation potential of epithelial cells can change during tissue repair after injury and that committed epithelial lineage cells of various organs, including the gut, lung, stomach, liver and pancreas, can acquire stemness [Donati et al., 2015]. For instance, Dll1+ cells in the gut are short-lived cells derived from Lgr5+ progenitors committed to the secretory lineage. After tissue injury by gamma-irradiation, these committed cells revert back to intestinal stem cells and take part in tissue regeneration. This conversion of Dll1+ committed cells to Lgr5+ ISCs can also be observed when Dll1+ cells are cultured *in vitro* [Blanpain et al., 2014]. Furthermore, recent studies have shown that unipotent epidermal progenitors can de- or re-differentiate to become multipotent: During normal tissue homeostasis, Lrig1+ epidermal stem cells contribute only to specific areas of the pilosebaceous unit, but give rise to all epidermal compartments in skin reconstitution assays [Donati et al., 2015, Jensen et al., 2009, Page et al., 2013].

Thus, a very urgent question which needs to be addressed by the MaSC field is whether the concept of a rare mammary stem/progenitor cell is still valid. Alternatively, one could think of a much more plastic system relying on a population of myoepithelial cells which can acquire/reveal regenerative capacity only under certain circumstances. If the latter proved true, it would explain why the decade-long efforts of identifying a MaSC marker have not been successful thus far: Up to date, it is not possible to isolate a pure population of MaSCs, i.e. cells with regenerative capacity in transplantation assays. Instead, these cells can only be enriched within a population of basal cells, e.g. using the marker combination of CD49f and EpCAM [Shackleton et al., 2006, Stingl et al., 2006]. As most data arguing against the presence of adult multipotent MaSCs are derived from lineage tracing studies using mouse models (see Chapter 1.2.4), future studies should also aim at transferring the gained insight to the human system. The assay developed here will be a valuable tool for doing so. A first step at addressing the existence/absence of a human MaSC population could be single cell gene expression analyses. Specifically, single cell RNA sequencing of the B+ population exposed here could reveal the existence or absence of B+ subpopulations with increased or decreased

TDLU-like structure forming ability. Obviously, similar studies could be performed for murine cells. If evidence for the absence of a rare and fixed mammary stem cell population accumulates, current efforts focusing on the identification of novel stem cells markers should be brought down in favor of studies aiming at finding the triggers for the revelation/acquisition of stem cell features. The organotypic culture system presented here could be adjusted for developing an environment triggering the acquisition of stem cell traits, the read-out being TDLU-like structure formation. For instance, the culture system could be used to mimic a wounding or cancer setting by addition of inflammatory factors like interleukins, growth hormones, cancer associated fibroblasts or cancer cells themselves.

5.5 Regenerative capacity of LP cells: aberrant de-differentiation?

The vast majority of TDLU-like structure forming cells belonged to the basal population, however, LP cells were found to exhibit limited TDLU-like structure forming capacity (B-SFU: 1/5122). Regenerative capacity of LP cells has been described before: When transplanted under the renal capsule or into a humanized fat pad of immune compromised mice, human LP cells can give rise to structures containing both luminal and basal cells [Keller et al., 2012, Shehata et al., 2012].

Strikingly, TDLU-like structure formation of LP cells was approximately 6-fold higher in the presence of Forskolin than in its absence and some of the structures exhibited signs of aberrant (de-)differentiation.

Notably, the frequency of TDLU-like structure formation determined in this study varied dramatically between LP cells from different donors. One possible explanation for this might be different hormone levels which depend on inter-individual differences, phase of the menstrual cycle and potential use of hormone replacement therapy [Brisken et al., 2010, Tanos et al., 2012]. Indeed, high levels of progesterone and estrogen have been associated with expansion of the basal and luminal cell population and increased regenerative capacity. In the mouse, high levels of estrogen and progesterone occurring during pregnancy or dioestrus, were shown to cause expansion of the luminal ($CD49f^{lo}$/CD24+ or $CD29^{lo}/CD24^{+}$) and basal MaSC ($CD49f^{hi}/CD24^{+}$ or $29^{hi}/CD24^{+}$) population [Asselin-Labat et al., 2010, Joshi et al., 2010]. The increased MaSC population also exhibited increased regenerative capacity in transplantation assays [Asselin-Labat et al., 2010]. Molecularly, Progesterone was suggested to act on ER+/PR+ luminal cells causing them to secrete Wnt4 and RANKL,

inducing proliferation of MaSCs in a paracrine fashion [Asselin-Labat et al., 2010, Joshi et al., 2010].

Similarly, the size of the human LP ($CD49f^+/EpCAM^+$) population increases during the luteal phase of the menstrual cycle, when progesterone levels are high. In addition, the number of ki67+ cells is increased in the progesterone-high phase and the frequency of *in vitro* colony formation by LP cells is increased, suggesting that proliferation and differentiation are affected [Joshi et al., 2015]. These data show a potential link between increased hormone levels and regenerative capacity of LP cells, as has been observed for the basal MaSC population in transplantation assays.

High levels of estrogen and progesterone have also been associated with the development of breast cancer. The levels of estrogen and progesterone rise and fall with every menstrual cycle and a high number of menstrual cycles and thus a high number of times a woman is exposed to high levels of estrogen and progesterone is correlated with an increased breast cancer risk [Apter et al., 1989, Bernstein, 2002, Kelsey et al., 1993, Trichopoulos et al., 1972]. Similarly, increased hormone levels due to estrogen plus progestin based hormone replacement therapy significantly increase breast cancer risk [Chlebowski et al., 2015]. Thus, the link between high levels of estrogen and progesterone and both de-differentiation/regenerative capacity and tumor development indicate a potential relation between these two effects.

Indeed, breast cancer has been associated with illicit dedifferentiation of LP cells: For example, MG tissue of BRCA1 mutation carriers contains an expanded LP population. This population is likely at the origin of breast tumors which are usually classified as TNBC and exhibit a basal-like gene expression profile, thus changing their gene expression profile from luminal-like to basal-like [Lim et al., 2009, Molyneux et al., 2010]. Further evidence for illicit de-differentiation comes from two studies showing that expression of $PIK3CA^{H1047R}$ in K8+ luminal cells in the mouse induced reprogramming into a basal-like cell fate and increased regenerative capacity upon transplantation [Koren et al., 2015, Van Keymeulen et al., 2015]. Thus changes in the genetic background can cause de-differentiation of luminal mammary epithelial cells resulting in the generation of tumors with basal features.

How can the positive link between exposure to estrogen/progesterone, increased LP populations, their aberrant de-differentiation and the risk of developing breast cancer be explained? Part of the answer could be that the cyclical expansion of the LP population increases the possibility of mutagenic hits, leading to aberrant de-differentiation and tumor development. However, here I have observed that within less than 14 days, Forskolin treatment increased TDLU-like structure formation by LP cells, indicating their de-

differentiation. During this short time-period, spontaneous acquisition of mutagenic hits in a relevant number of cells is highly unlikely. Thereby, these data suggest that de-differentiation of LP cells can occur independent of mutagenic hits and can be easily induced, for instance by a changing signaling environment.

Therefore, the triggers for de-differentiation of LP cells should be investigated in more detail. Along these lines, it should be addressed whether the Forskolin-induced increase in TDLU-like structure formation by LP cells results from signaling pathways that also act downstream of estrogen and progesterone signaling. As mentioned above, GPR30 is a G-protein coupled estrogen receptor which, upon activation, stimulates adenylate cyclase to produce cAMP, the same secondary messenger as induced by Forskolin [Filardo et al., 2002]. In addition, cAMP can be induced downstream of mPRs [Prossnitz et al., 2008]. Furthermore, it should be investigated whether de-differentiation of LP cells facilitates their transformation.

Importantly, the assay presented here not only allows for analysis of regenerative potential of LP cells by quantification of TDLU-like structures, but also provides a platform for the analysis of morphological abnormalities. For instance, it was shown that LP cell derived branched structures exhibited a broad range of morphologies from simple structures with only few branches to typical TDLU-like structures and complex branched structures with invasive phenotype. While most LP-derived structures were strongly positive for markers of luminal cells like CD8/18, in a few cases, I observed CK8/18-negative, vimentin-positive areas that appeared disordered and invasive which might reflect illicit-dedifferentiation. Furthermore, the study of regenerative capacity and morphological changes can be combined with further *in vitro* analysis, like lineage marker expression, functionality and gene expression. Thereby, the effects of genetic modulation, treatment with signaling molecules and changes in extracellular matrix on the behavior of LP cells can be analyzed in detail. Ultimately, these studies will lead to a better understanding of the development of LP-derived breast cancer.

6 References

Abramowitz, M., Davidson, M.W. (2012) Introduction to Fluorescence. Available from: http://www.olympusmicro.com/primer/lightandcolor/fluorointroduction.html.

ACS (2014). Available from: http://www.cancer.org/. Accessed on: 17.08.2016.

Alitalo, A., Detmar, M. Interaction of tumor cells and lymphatic vessels in cancer progression. Oncogene. 31 (2012) 4499-4508.

Althuis, M.D., Dozier, J.M., Anderson, W.F., Devesa, S.S., Brinton, L.A. Global trends in breast cancer incidence and mortality 1973-1997. International journal of epidemiology. 34 (2005) 405-412.

Amano, M., Nakayama, M., Kaibuchi, K. Rho-kinase/ROCK: a key regulator of the cytoskeleton and cell polarity. Cytoskeleton. 67 (2010) 545-554.

Anderson, E., Clarke, R.B., Howell, A. Estrogen responsiveness and control of normal human breast proliferation. J Mammary Gland Biol Neoplasia. 3 (1998) 23-35.

Apter, D., Reinilä, M., Vihko, R. Some endocrine characteristics of early menarche, a risk factor for breast cancer, are preserved into adulthood. International Journal of Cancer. 44 (1989) 783-787.

Aronica, S.M., Kraus, W.L., Katzenellenbogen, B.S. Estrogen action via the cAMP signaling pathway: stimulation of adenylate cyclase and cAMP-regulated gene transcription. Proceedings of the National Academy of Sciences. 91 (1994) 8517-8521.

Ashe, H.L., Briscoe, J. The interpretation of morphogen gradients. Development. 133 (2006) 385-394.

Asselin-Labat, M.-L., Vaillant, F., Sheridan, J.M., Pal, B., Wu, D., Simpson, E.R., Yasuda, H., Smyth, G.K., Martin, T.J., Lindeman, G.J. Control of mammary stem cell function by steroid hormone signalling. Nature. 465 (2010) 798-802.

Asselin-Labat, M.L., Sutherland, K.D., Barker, H., Thomas, R., Shackleton, M., Forrest, N.C., Hartley, L., Robb, L., Grosveld, F.G., van der Wees, J., Lindeman, G.J., Visvader, J.E. Gata-3 is an essential regulator of mammary-gland morphogenesis and luminal-cell differentiation. Nat Cell Biol. 9 (2007) 201-209.

Bachelard-Cascales, E., Chapellier, M., Delay, E., Pochon, G., Voeltzel, T., Puisieux, A., Caron de Fromentel, C., Maguer-Satta, V. The CD10 enzyme is a key player to identify and regulate human mammary stem cells. Stem Cells. 28 (2010) 1081-1088.

Barcellos-Hoff, M.H., Ewan, K.B. Transforming growth factor-beta and breast cancer: Mammary gland development. Breast cancer research : BCR. 2 (2000) 92-99.

Batlle, E., Sancho, E., Franci, C., Dominguez, D., Monfar, M., Baulida, J., Garcia De Herreros, A. The transcription factor snail is a repressor of E-cadherin gene expression in epithelial tumour cells. Nat Cell Biol. 2 (2000) 84-89.

Beleut, M., Rajaram, R.D., Caikovski, M., Ayyanan, A., Germano, D., Choi, Y., Schneider, P., Brisken, C. Two distinct mechanisms underlie progesterone-induced proliferation in the mammary gland. Proceedings of the National Academy of Sciences of the United States of America. 107 (2010) 2989-2994.

Benton, G., Arnaoutova, I., George, J., Kleinman, H.K., Koblinski, J. Matrigel: From discovery and ECM mimicry to assays and models for cancer research. Advanced drug delivery reviews. 79 (2014) 3-18.

Bernstein, L. Epidemiology of endocrine-related risk factors for breast cancer. J Mammary Gland Biol Neoplasia. 7 (2002) 3-15.

Betterman, K.L., Paquet-Fifield, S., Asselin-Labat, M.-L., Visvader, J.E., Butler, L.M., Stacker, S.A., Achen, M.G., Harvey, N.L. Remodeling of the lymphatic vasculature during mouse mammary gland morphogenesis is mediated via epithelial-derived lymphangiogenic stimuli. The American journal of pathology. 181 (2012) 2225-2238.

Birgersdotter, A., Sandberg, R., Ernberg, I. Gene expression perturbation in vitro—a growing case for three-dimensional (3D) culture systems. Seminars in cancer biology, 2005. Elsevier, 405-412.

Blanpain, C., Fuchs, E. Plasticity of epithelial stem cells in tissue regeneration. Science. 344 (2014) 1242281.

Bologa, C.G., Revankar, C.M., Young, S.M., Edwards, B.S., Arterburn, J.B., Kiselyov, A.S., Parker, M.A., Tkachenko, S.E., Savchuck, N.P., Sklar, L.A., Oprea, T.I., Prossnitz, E.R. Virtual and biomolecular screening converge on a selective agonist for GPR30. Nature chemical biology. 2 (2006) 207-212.

Brisken, C., Kaur, S., Chavarria, T.E., Binart, N., Sutherland, R.L., Weinberg, R.A., Kelly, P.A., Ormandy, C.J. Prolactin controls mammary gland development via direct and indirect mechanisms. Developmental biology. 210 (1999) 96-106.

Brisken, C., O'Malley, B. Hormone action in the mammary gland. Cold Spring Harbor perspectives in biology. 2 (2010) a003178.

Brisken, C., Park, S., Vass, T., Lydon, J.P., O'Malley, B.W., Weinberg, R.A. A paracrine role for the epithelial progesterone receptor in mammary gland development. Proceedings of the National Academy of Sciences. 95 (1998) 5076-5081.

Cancer Genome Atlas Network Comprehensive molecular portraits of human breast tumours. Nature. 490 (2012) 61-70.

Cano, A., Perez-Moreno, M.A., Rodrigo, I., Locascio, A., Blanco, M.J., del Barrio, M.G., Portillo, F., Nieto, M.A. The transcription factor snail controls epithelial-mesenchymal transitions by repressing E-cadherin expression. Nat Cell Biol. 2 (2000) 76-83.

Carey, L.A., Perou, C.M., Livasy, C.A., Dressler, L.G., Cowan, D., Conway, K., Karaca, G., Troester, M.A., Tse, C.K., Edmiston, S., Deming, S.L., Geradts, J., Cheang, M.C., Nielsen, T.O., Moorman, P.G., Earp, H.S., Millikan, R.C. Race, breast cancer subtypes, and survival in the Carolina Breast Cancer Study. Jama. 295 (2006) 2492-2502.

Chaudhuri, O., Koshy, S.T., Branco da Cunha, C., Shin, J.W., Verbeke, C.S., Allison, K.H., Mooney, D.J. Extracellular matrix stiffness and composition jointly regulate the induction of malignant phenotypes in mammary epithelium. Nature materials. 13 (2014) 970-978.

Cheung, K.J., Gabrielson, E., Werb, Z., Ewald, A.J. Collective invasion in breast cancer requires a conserved basal epithelial program. Cell. 155 (2013) 1639-1651.

Chlebowski, R.T., Rohan, T.E., Manson, J.E., Aragaki, A.K., Kaunitz, A., Stefanick, M.L., Simon, M.S., Johnson, K.C., Wactawski-Wende, J., O'Sullivan, M.J., Adams-Campbell, L.L., Nassir, R., Lessin, L.S., Prentice, R.L. Breast Cancer After Use of Estrogen Plus Progestin and Estrogen Alone: Analyses of Data From 2 Women's Health Initiative Randomized Clinical Trials. JAMA oncology. 1 (2015) 296-305.

Clevers, H. Modeling development and disease with organoids. Cell. 165 (2016) 1586-1597.

Crowley, W.R., Armstrong, W.E. Neurochemical regulation of oxytocin secretion in lactation. Endocrine reviews. 13 (1992) 33-65.

Daniel, C., Young, L., Medina, D., DeOme, K. The influence of mammogenic hormones on serially transplanted mouse mammary gland. Experimental gerontology. 6 (1971) 95-101.

Daniel, C.W., De Ome, K.B., Young, J., Blair, P.B., Faulkin, L.J. The in vivo life span of normal and preneoplastic mouse mammary glands: a serial transplantation study. Proceedings of the National Academy of Sciences. 61 (1968) 53-60.

Dapson, R.W. The history, chemistry and modes of action of carmine and related dyes. Biotechnic & histochemistry : official publication of the Biological Stain Commission. 82 (2007) 173-187.

DeLisser, H.M., Newman, P.J., Albelda, S.M. Molecular and functional aspects of PECAM-1/CD31. Immunology today. 15 (1994) 490-495.

Denning, W., Das, S., Guo, S., Xu, J., Kappes, J.C., Hel, Z. Optimization of the transductional efficiency of lentiviral vectors: Effect of sera and polycations. Molecular biotechnology. 53 (2013) 308-314.

Dennis, M.K., Field, A.S., Burai, R., Ramesh, C., Petrie, W.K., Bologa, C.G., Oprea, T.I., Yamaguchi, Y., Hayashi, S., Sklar, L.A., Hathaway, H.J., Arterburn, J.B., Prossnitz, E.R. Identification of a GPER/GPR30 antagonist with improved estrogen receptor counterselectivity. The Journal of steroid biochemistry and molecular biology. 127 (2011) 358-366.

Dent, R., Trudeau, M., Pritchard, K.I., Hanna, W.M., Kahn, H.K., Sawka, C.A., Lickley, L.A., Rawlinson, E., Sun, P., Narod, S.A. Triple-negative breast cancer: clinical features and patterns of recurrence. Clinical cancer research : an official journal of the American Association for Cancer Research. 13 (2007) 4429-4434.

Deome, K.B., Faulkin, L.J., Jr., Bern, H.A., Blair, P.B. Development of mammary tumors from hyperplastic alveolar nodules transplanted into gland-free mammary fat pads of female C3H mice. Cancer research. 19 (1959) 515-520.

Donati, G., Watt, F.M. Stem cell heterogeneity and plasticity in epithelia. Cell stem cell. 16 (2015) 465-476.

Dontu, G., Abdallah, W.M., Foley, J.M., Jackson, K.W., Clarke, M.F., Kawamura, M.J., Wicha, M.S. In vitro propagation and transcriptional profiling of human mammary stem/progenitor cells. Genes & development. 17 (2003) 1253-1270.

Dressing, G.E., Goldberg, J.E., Charles, N.J., Schwertfeger, K.L., Lange, C.A. Membrane progesterone receptor expression in mammalian tissues: a review of regulation and physiological implications. Steroids. 76 (2011) 11-17.

Eger, A., Aigner, K., Sonderegger, S., Dampier, B., Oehler, S., Schreiber, M., Berx, G., Cano, A., Beug, H., Foisner, R. DeltaEF1 is a transcriptional repressor of E-cadherin and regulates epithelial plasticity in breast cancer cells. Oncogene. 24 (2005) 2375-2385.

Eirew, P., Stingl, J., Raouf, A., Turashvili, G., Aparicio, S., Emerman, J.T., Eaves, C.J. A method for quantifying normal human mammary epithelial stem cells with in vivo regenerative ability. Nature medicine. 14 (2008) 1384-1389.

Emerman, J.T., Pitelka, D.R. Maintenance and induction of morphological differentiation in dissociated mammary epithelium on floating collagen membranes. In vitro. 13 (1977) 316-328.

Ewald, A.J., Brenot, A., Duong, M., Chan, B.S., Werb, Z. Collective epithelial migration and cell rearrangements drive mammary branching morphogenesis. Dev Cell. 14 (2008) 570-581.

Fellers, T.J., Davidson, M.W. (2012) Introduction to Confocal Microscopy. Available from: http://www.olympusmicro.com/primer/techniques/confocal/confocalintro.html. Accessed on: 12.10.2016.

Ferlay, J., Soerjomataram, I., Ervik, M., Dikshit, R., Eser, S., Mathers, C., Rebelo, M., Parkin, D.M., Forman, D., Bray, F. (2013) GLOBOCAN 2012 v1.10, Cancer Indidence and Mortality Worldwide: IARC CancerBase No. 11. Available from: http://globocan.iarc.fr. Accessed on: 17.08.2016.

Filardo, E.J., Quinn, J.A., Frackelton Jr, A.R., Bland, K.I. Estrogen action via the G protein-coupled receptor, GPR30: stimulation of adenylyl cyclase and cAMP-mediated attenuation of the epidermal growth factor receptor-to-MAPK signaling axis. Molecular endocrinology. 16 (2002) 70-84.

Forster, N., Saladi, S.V., van Bragt, M., Sfondouris, M.E., Jones, F.E., Li, Z., Ellisen, L.W. Basal cell signaling by p63 controls luminal progenitor function and lactation via NRG1. Dev Cell. 28 (2014) 147-160.

Foster, C.S., Smith, C.A., Dinsdale, E.A., Monaghan, P., Neville, A.M. Human mammary gland morphogenesis in vitro: the growth and differentiation of normal breast epithelium in collagen gel cultures defined by electron microscopy, monoclonal antibodies, and autoradiography. Developmental biology. 96 (1983) 197-216.

Foulkes, W.D., Smith, I.E., Reis-Filho, J.S. Triple-negative breast cancer. The New England journal of medicine. 363 (2010) 1938-1948.

Fridriksdottir, A.J., Kim, J., Villadsen, R., Klitgaard, M.C., Hopkinson, B.M., Petersen, O.W., Rønnov-Jessen, L. Propagation of oestrogen receptor-positive and oestrogen-responsive normal human breast cells in culture. Nature communications. 6 (2015)

Fujimoto, N., Katzenellenbogen, B.S. Alteration in the agonist/antagonist balance of antiestrogens by activation of protein kinase A signaling pathways in breast cancer cells: antiestrogen selectivity and promoter dependence. Molecular endocrinology (Baltimore, Md.). 8 (1994) 296-304.

Gallego, M.I., Binart, N., Robinson, G.W., Okagaki, R., Coschigano, K.T., Perry, J., Kopchick, J.J., Oka, T., Kelly, P.A., Hennighausen, L. Prolactin, growth hormone, and epidermal growth factor activate Stat5 in different compartments of mammary tissue and exert different and overlapping developmental effects. Dev Biol. 229 (2001) 163-175.

Giraddi, R.R., Shehata, M., Gallardo, M., Blasco, M.A., Simons, B.D., Stingl, J. Stem and progenitor cell division kinetics during postnatal mouse mammary gland development. Nature communications. 6 (2015)

Gudjonsson, T., Adriance, M.C., Sternlicht, M.D., Petersen, O.W., Bissell, M.J. Myoepithelial cells: their origin and function in breast morphogenesis and neoplasia. J Mammary Gland Biol Neoplasia. 10 (2005) 261-272.

Gudjonsson, T., Villadsen, R., Nielsen, H.L., Rønnov-Jessen, L., Bissell, M.J., Petersen, O.W. Isolation, immortalization, and characterization of a human breast epithelial cell line with stem cell properties. Genes & development. 16 (2002) 693-706.

Guo, W., Keckesova, Z., Donaher, J.L., Shibue, T., Tischler, V., Reinhardt, F., Itzkovitz, S., Noske, A., Zürrer-Härdi, U., Bell, G. Slug and Sox9 cooperatively determine the mammary stem cell state. Cell. 148 (2012) 1015-1028.

Gusterson, B.A., Ross, D.T., Heath, V.J., Stein, T. Basal cytokeratins and their relationship to the cellular origin and functional classification of breast cancer. Breast Cancer Research. 7 (2005) 1.

Haaksma, C.J., Schwartz, R.J., Tomasek, J.J. Myoepithelial cell contraction and milk ejection are impaired in mammary glands of mice lacking smooth muscle alpha-actin. Biology of reproduction. 85 (2011) 13-21.

Hennighausen, L., Robinson, G.W. Information networks in the mammary gland. Nature reviews. Molecular cell biology. 6 (2005) 715-725.

Herman, B., Centonze Frohlich, V.E., Lakowicz, J.R., Murphy, D.B., Spring, K.R., Davidson, M.W. (2012) Basic Concepts in Fluorescence. Available from: http://www.olympusmicro.com/primer/techniques/fluorescence/fluorescenceintro.html. Accessed on: 12.10.2016.

Hermiston, M.L., Xu, Z., Weiss, A. CD45: a critical regulator of signaling thresholds in immune cells. Annual review of immunology. 21 (2003) 107-137.

Herschkowitz, J.I., Simin, K., Weigman, V.J., Mikaelian, I., Usary, J., Hu, Z., Rasmussen, K.E., Jones, L.P., Assefnia, S., Chandrasekharan, S. Identification of conserved gene

expression features between murine mammary carcinoma models and human breast tumors. Genome biology. 8 (2007) 1.

Hoshino, K. Morphogenesis and growth potentiality of mammary glands in mice. I. Transplantability and growth potentiality of mammary tissue of virgin mice. Journal of the National Cancer Institute. 29 (1962) 835-851.

Howard, B.A., Gusterson, B.A. Human breast development. Journal of mammary gland biology and neoplasia. 5 (2000) 119-137.

Hu, Y., Smyth, G.K. ELDA: extreme limiting dilution analysis for comparing depleted and enriched populations in stem cell and other assays. Journal of immunological methods. 347 (2009) 70-78.

Jensen, K.B., Collins, C.A., Nascimento, E., Tan, D.W., Frye, M., Itami, S., Watt, F.M. Lrig1 expression defines a distinct multipotent stem cell population in mammalian epidermis. Cell stem cell. 4 (2009) 427-439.

Joshi, P.A., Jackson, H.W., Beristain, A.G., Di Grappa, M.A., Mote, P.A., Clarke, C.L., Stingl, J., Waterhouse, P.D., Khokha, R. Progesterone induces adult mammary stem cell expansion. Nature. 465 (2010) 803-807.

Joshi, P.A., Waterhouse, P.D., Kannan, N., Narala, S., Fang, H., Di Grappa, M.A., Jackson, H.W., Penninger, J.M., Eaves, C., Khokha, R. RANK Signaling Amplifies WNT-Responsive Mammary Progenitors through R-SPONDIN1. Stem cell reports. 5 (2015) 31-44.

Kelder, J., Azevedo, R., Pang, Y., de Vlieg, J., Dong, J., Thomas, P. Comparison between steroid binding to membrane progesterone receptor alpha (mPRalpha) and to nuclear progesterone receptor: correlation with physicochemical properties assessed by comparative molecular field analysis and identification of mPRalpha-specific agonists. Steroids. 75 (2010) 314-322.

Keller, P.J., Arendt, L.M., Kuperwasser, C. Stem cell maintenance of the mammary gland: it takes two. Cell stem cell. 9 (2011) 496-497.

Keller, P.J., Arendt, L.M., Skibinski, A., Logvinenko, T., Klebba, I., Dong, S., Smith, A.E., Prat, A., Perou, C.M., Gilmore, H. Defining the cellular precursors to human breast cancer. Proceedings of the National Academy of Sciences. 109 (2012) 2772-2777.

Keller, P.J., Lin, A.F., Arendt, L.M., Klebba, I., Jones, A.D., Rudnick, J.A., DiMeo, T.A., Gilmore, H., Jefferson, D.M., Graham, R.A. Mapping the cellular and molecular heterogeneity of normal and malignant breast tissues and cultured cell lines. Breast cancer research. 12 (2010) 1.

Kelsey, J.L., Gammon, M.D., John, E.M. Reproductive factors and breast cancer. Epidemiologic reviews. 15 (1993) 36-47.

Kordon, E.C., Smith, G.H. An entire functional mammary gland may comprise the progeny from a single cell. Development. 125 (1998) 1921-1930.

Koren, S., Reavie, L., do Couto, J.P., De Silva, D., Stadler, M.B., Roloff, T., Britschgi, A., Eichlisberger, T., Kohler, H., Aina, O. PIK3CAH1047R induces multipotency and multi-lineage mammary tumours. Nature. (2015)

Kouros-Mehr, H., Slorach, E.M., Sternlicht, M.D., Werb, Z. GATA-3 maintains the differentiation of the luminal cell fate in the mammary gland. Cell. 127 (2006) 1041-1055.

Kovács, M., Tóth, J., Hetényi, C., Málnási-Csizmadia, A., Sellers, J.R. Mechanism of blebbistatin inhibition of myosin II. Journal of Biological Chemistry. 279 (2004) 35557-35563.

Kuperwasser, C., Chavarria, T., Wu, M., Magrane, G., Gray, J.W., Carey, L., Richardson, A., Weinberg, R.A. Reconstruction of functionally normal and malignant human breast tissues in mice. Proceedings of the National Academy of Sciences of the United States of America. 101 (2004) 4966-4971.

Lamouille, S., Xu, J., Derynck, R. Molecular mechanisms of epithelial-mesenchymal transition. Nature reviews. Molecular cell biology. 15 (2014) 178-196.

Lee, H.J., Gallego-Ortega, D., Ledger, A., Schramek, D., Joshi, P., Szwarc, M.M., Cho, C., Lydon, J.P., Khokha, R., Penninger, J.M., Ormandy, C.J. Progesterone drives mammary secretory differentiation via RankL-mediated induction of Elf5 in luminal progenitor cells. Development. 140 (2013) 1397-1401.

Lee, H.J., Hinshelwood, R.A., Bouras, T., Gallego-Ortega, D., Valdes-Mora, F., Blazek, K., Visvader, J.E., Clark, S.J., Ormandy, C.J. Lineage specific methylation of the Elf5 promoter in mammary epithelial cells. Stem Cells. 29 (2011) 1611-1619.

Levental, K.R., Yu, H., Kass, L., Lakins, J.N., Egeblad, M., Erler, J.T., Fong, S.F., Csiszar, K., Giaccia, A., Weninger, W. Matrix crosslinking forces tumor progression by enhancing integrin signaling. Cell. 139 (2009) 891-906.

Li, B., Wang, J.H.-C. Fibroblasts and myofibroblasts in wound healing: force generation and measurement. Journal of tissue viability. 20 (2011) 108-120.

Lijnen, P., Petrov, V., Fagard, R. Transforming growth factor-β1-mediated collagen gel contraction by cardiac fibroblasts. Journal of Renin-Angiotensin-Aldosterone System. 4 (2003) 113-118.

Lim, E., Vaillant, F., Wu, D., Forrest, N.C., Pal, B., Hart, A.H., Asselin-Labat, M.L., Gyorki, D.E., Ward, T., Partanen, A., Feleppa, F., Huschtscha, L.I., Thorne, H.J., Fox, S.B., Yan, M., French, J.D., Brown, M.A., Smyth, G.K., Visvader, J.E., Lindeman, G.J. Aberrant luminal progenitors as the candidate target population for basal tumor development in BRCA1 mutation carriers. Nature medicine. 15 (2009) 907-913.

Lim, E., Wu, D., Pal, B., Bouras, T., Asselin-Labat, M.L., Vaillant, F., Yagita, H., Lindeman, G.J., Smyth, G.K., Visvader, J.E. Transcriptome analyses of mouse and human mammary cell subpopulations reveal multiple conserved genes and pathways. Breast cancer research : BCR. 12 (2010) R21.

Lu, C.P., Polak, L., Rocha, A.S., Pasolli, H.A., Chen, S.-C., Sharma, N., Blanpain, C., Fuchs, E. Identification of stem cell populations in sweat glands and ducts reveals roles in homeostasis and wound repair. Cell. 150 (2012) 136-150.

Maguer-Satta, V., Besançon, R., Bachelard-Cascales, E. Concise review: neutral endopeptidase (CD10): a multifaceted environment actor in stem cells, physiological mechanisms, and cancer. Stem Cells. 29 (2011) 389-396.

Makarem, M., Kannan, N., Nguyen, L.V., Knapp, D.J., Balani, S., Prater, M.D., Stingl, J., Raouf, A., Nemirovsky, O., Eirew, P. Developmental changes in the in vitro activated regenerative activity of primitive mammary epithelial cells. PLoS Biol. 11 (2013) e1001630.

Mallepell, S., Krust, A., Chambon, P., Brisken, C. Paracrine signaling through the epithelial estrogen receptor α is required for proliferation and morphogenesis in the mammary gland. Proceedings of the National Academy of Sciences of the United States of America. 103 (2006) 2196-2201.

McManaman, J.L., Neville, M.C. Mammary physiology and milk secretion. Adv Drug Deliv Rev. 55 (2003) 629-641.

Mikaelian, I., Hovick, M., Silva, K.A., Burzenski, L.M., Shultz, L.D., Ackert-Bicknell, C.L., Cox, G.A., Sundberg, J.P. Expression of terminal differentiation proteins defines stages of mouse mammary gland development. Veterinary pathology. 43 (2006) 36-49.

Molyneux, G., Geyer, F.C., Magnay, F.A., McCarthy, A., Kendrick, H., Natrajan, R., Mackay, A., Grigoriadis, A., Tutt, A., Ashworth, A., Reis-Filho, J.S., Smalley, M.J. BRCA1 basal-like breast cancers originate from luminal epithelial progenitors and not from basal stem cells. Cell stem cell. 7 (2010) 403-417.

Muschler, J., Streuli, C.H. Cell–matrix interactions in mammary gland development and breast cancer. Cold Spring Harbor perspectives in biology. 2 (2010) a003202.

Nedvetsky, P.I., Kwon, S.-H., Debnath, J., Mostov, K.E. Cyclic AMP regulates formation of mammary epithelial acini in vitro. Molecular biology of the cell. 23 (2012) 2973-2981.

Oakes, S.R., Naylor, M.J., Asselin-Labat, M.L., Blazek, K.D., Gardiner-Garden, M., Hilton, H.N., Kazlauskas, M., Pritchard, M.A., Chodosh, L.A., Pfeffer, P.L., Lindeman, G.J., Visvader, J.E., Ormandy, C.J. The Ets transcription factor Elf5 specifies mammary alveolar cell fate. Genes & development. 22 (2008) 581-586.

Page, M.E., Lombard, P., Ng, F., Göttgens, B., Jensen, K.B. The epidermis comprises autonomous compartments maintained by distinct stem cell populations. Cell stem cell. 13 (2013) 471-482.

Parmar, H., Cunha, G.R. Epithelial-stromal interactions in the mouse and human mammary gland in vivo. Endocrine-related cancer. 11 (2004) 437-458.

Paszek, M., Weaver, V. Biophysics. Enforcing order on signaling. Science. 327 (2010) 1335-1336.

Paszek, M.J., Zahir, N., Johnson, K.R., Lakins, J.N., Rozenberg, G.I., Gefen, A., Reinhart-King, C.A., Margulies, S.S., Dembo, M., Boettiger, D. Tensional homeostasis and the malignant phenotype. Cancer cell. 8 (2005) 241-254.

Pattabiraman, D.R., Bierie, B., Kober, K.I., Thiru, P., Krall, J.A., Zill, C., Reinhardt, F., Tam, W.L., Weinberg, R.A. Activation of PKA leads to mesenchymal-to-epithelial transition and loss of tumor-initiating ability. Science. 351 (2016) aad3680.

Perou, C.M., Sorlie, T., Eisen, M.B., van de Rijn, M., Jeffrey, S.S., Rees, C.A., Pollack, J.R., Ross, D.T., Johnsen, H., Akslen, L.A., Fluge, O., Pergamenschikov, A., Williams, C., Zhu, S.X., Lonning, P.E., Borresen-Dale, A.L., Brown, P.O., Botstein, D. Molecular portraits of human breast tumours. Nature. 406 (2000) 747-752.

Petersen, O.W., Rønnov-Jessen, L., Howlett, A.R., Bissell, M.J. Interaction with basement membrane serves to rapidly distinguish growth and differentiation pattern of normal and malignant human breast epithelial cells. Proceedings of the National Academy of Sciences. 89 (1992) 9064-9068.

Plaks, V., Boldajipour, B., Linnemann, J.R., Nguyen, N.H., Kersten, K., Wolf, Y., Casbon, A.-J., Kong, N., van den Bijgaart, R.J., Sheppard, D. Adaptive immune regulation of mammary postnatal organogenesis. Developmental cell. 34 (2015) 493-504.

Plaks, V., Brenot, A., Lawson, D.A., Linnemann, J.R., Van Kappel, E.C., Wong, K.C., de Sauvage, F., Klein, O.D., Werb, Z. Lgr5-expressing cells are sufficient and necessary for postnatal mammary gland organogenesis. Cell reports. 3 (2013) 70-78.

Podo, F., Buydens, L.M., Degani, H., Hilhorst, R., Klipp, E., Gribbestad, I.S., Van Huffel, S., van Laarhoven, H.W., Luts, J., Monleon, D., Postma, G.J., Schneiderhan-Marra, N., Santoro, F., Wouters, H., Russnes, H.G., Sorlie, T., Tagliabue, E., Borresen-Dale, A.L. Triple-negative breast cancer: present challenges and new perspectives. Molecular oncology. 4 (2010) 209-229.

Prat, A., Karginova, O., Parker, J.S., Fan, C., He, X., Bixby, L., Harrell, J.C., Roman, E., Adamo, B., Troester, M., Perou, C.M. Characterization of cell lines derived from breast cancers and normal mammary tissues for the study of the intrinsic molecular subtypes. Breast cancer research and treatment. 142 (2013) 237-255.

Prat, A., Perou, C.M. Deconstructing the molecular portraits of breast cancer. Molecular oncology. 5 (2011) 5-23.

Prater, M.D., Petit, V., Russell, I.A., Giraddi, R.R., Shehata, M., Menon, S., Schulte, R., Kalajzic, I., Rath, N., Olson, M.F. Mammary stem cells have myoepithelial cell properties. Nature cell biology. 16 (2014) 942-950.

Prossnitz, E.R., Arterburn, J.B., Smith, H.O., Oprea, T.I., Sklar, L.A., Hathaway, H.J. Estrogen signaling through the transmembrane G protein-coupled receptor GPR30. Annual review of physiology. 70 (2008) 165-190.

Prossnitz, E.R., Barton, M. Estrogen biology: new insights into GPER function and clinical opportunities. Molecular and cellular endocrinology. 389 (2014) 71-83.

Provenzano, P.P., Inman, D.R., Eliceiri, K.W., Keely, P.J. Matrix density-induced mechanoregulation of breast cell phenotype, signaling and gene expression through a FAK–ERK linkage. Oncogene. 28 (2009) 4326-4343.

Pusztaszeri, M.P., Seelentag, W., Bosman, F.T. Immunohistochemical expression of endothelial markers CD31, CD34, von Willebrand factor, and Fli-1 in normal human tissues. Journal of Histochemistry & Cytochemistry. 54 (2006) 385-395.

R.D.C.T. (2008) R: A Language and Environment for Statistical Computing. Available from: http://www.R-project.org/.

Rainer, J., Sanchez-Cabo, F., Stocker, G., Sturn, A., Trajanoski, Z. CARMAweb: comprehensive R-and bioconductor-based web service for microarray data analysis. Nucleic acids research. 34 (2006) W498-W503.

Rehmann, H., Wittinghofer, A., Bos, J.L. Capturing cyclic nucleotides in action: snapshots from crystallographic studies. Nature reviews. Molecular cell biology. 8 (2007) 63-73.

Reversi, A., Cassoni, P., Chini, B. Oxytocin receptor signaling in myoepithelial and cancer cells. J Mammary Gland Biol Neoplasia. 10 (2005) 221-229.

Riento, K., Ridley, A.J. Rocks: multifunctional kinases in cell behaviour. Nature reviews Molecular cell biology. 4 (2003) 446-456.

Ringner, M. What is principal component analysis? Nat Biotechnol. 26 (2008) 303-304.

Rios, A.C., Fu, N.Y., Lindeman, G.J., Visvader, J.E. In situ identification of bipotent stem cells in the mammary gland. Nature. 506 (2014) 322-327.

RKI. Krebs in Deutschland 2011/2012. 10. Ausgabe. Robert Koch-Institut (Hrsg) und die Gesellschaft der epidemiologischen Krebsregister in Deutschland e.V. (Hrsg). Berlin, 2015. 74-77.

Russo, J., Russo, I.H. Development of the human breast. Maturitas. 49 (2004) 2-15.

Sainsbury, J., Anderson, T., Morgan, D. ABC of breast diseases: breast cancer. British Medical Journal. 321 (2000) 745.

Santagata, S., Thakkar, A., Ergonul, A., Wang, B., Woo, T., Hu, R., Harrell, J.C., McNamara, G., Schwede, M., Culhane, A.C. Taxonomy of breast cancer based on normal cell phenotype predicts outcome. The Journal of clinical investigation. 124 (2014) 859-870.

Sassone-Corsi, P. The cyclic AMP pathway. Cold Spring Harb Perspect Biol. 4 (2012)
Schindler, R.F., Brand, T. The Popeye domain containing protein family--A novel class of cAMP effectors with important functions in multiple tissues. Progress in biophysics and molecular biology. 120 (2016) 28-36.

Shackleton, M., Vaillant, F., Simpson, K.J., Stingl, J., Smyth, G.K., Asselin-Labat, M.-L., Wu, L., Lindeman, G.J., Visvader, J.E. Generation of a functional mammary gland from a single stem cell. Nature. 439 (2006) 84-88.

Sheffield, L.G., Ayslworth, C.F., Welsch, C.W. Cyclic nucleotides and protein phosphorylation in mouse mammary glands: effects of estrogen and progesterone administered in vivo. Experimental Biology and Medicine. 185 (1987) 283-290.

Shehata, M., Teschendorff, A., Sharp, G., Novcic, N., Russell, I.A., Avril, S., Prater, M., Eirew, P., Caldas, C., Watson, C.J. Phenotypic and functional characterisation of the luminal cell hierarchy of the mammary gland. Breast Cancer Research. 14 (2012) 1.

Shieh, Y., Eklund, M., Sawaya, G.F., Black, W.C., Kramer, B.S., Esserman, L.J. Population-based screening for cancer: hope and hype. Nature reviews. Clinical oncology. (2016)

Shivtiel, S., Kollet, O., Lapid, K., Schajnovitz, A., Goichberg, P., Kalinkovich, A., Shezen, E., Tesio, M., Netzer, N., Petit, I., Sharir, A., Lapidot, T. CD45 regulates retention, motility, and numbers of hematopoietic progenitors, and affects osteoclast remodeling of metaphyseal trabecules. J Exp Med. 205 (2008) 2381-2395.

Silberstein, G.B., Strickland, P., Trumpbour, V., Coleman, S., Daniel, C.W. In vivo, cAMP stimulates growth and morphogenesis of mouse mammary ducts. Proceedings of the National Academy of Sciences. 81 (1984) 4950-4954.

Smith, G.H., Medina, D. A morphologically distinct candidate for an epithelial stem cell in mouse mammary gland. Journal of cell science. 90 (1988) 173-183.

Sopel, M. The myoepithelial cell: its role in normal mammary glands and breast cancer. Folia morphologica. 69 (2010) 1-14.

Sorlie, T., Perou, C.M., Tibshirani, R., Aas, T., Geisler, S., Johnsen, H., Hastie, T., Eisen, M.B., van de Rijn, M., Jeffrey, S.S., Thorsen, T., Quist, H., Matese, J.C., Brown, P.O., Botstein, D., Lonning, P.E., Borresen-Dale, A.L. Gene expression patterns of breast carcinomas distinguish tumor subclasses with clinical implications. Proceedings of the National Academy of Sciences of the United States of America. 98 (2001) 10869-10874.

Stampfer, M.R. Cholera toxin stimulation of human mammary epithelial cells in culture. In vitro. 18 (1982) 531-537.

Sternlicht, M.D. Key stages in mammary gland development: the cues that regulate ductal branching morphogenesis. Breast cancer research : BCR. 8 (2006) 201.

Stingl, J., Eaves, C.J., Zandieh, I., Emerman, J.T. Characterization of bipotent mammary epithelial progenitor cells in normal adult human breast tissue. Breast cancer research and treatment. 67 (2001) 93-109.

Stingl, J., Eirew, P., Ricketson, I., Shackleton, M., Vaillant, F., Choi, D., Li, H.I., Eaves, C.J. Purification and unique properties of mammary epithelial stem cells. Nature. 439 (2006) 993-997.

Stingl, J., Emerman, J.T., Eaves, C.J. Enzymatic dissociation and culture of normal human mammary tissue to detect progenitor activity. Basic Cell Culture Protocols. (2005) 249-263.

Streuli, C.H., Bissell, M.J. Expression of extracellular matrix components is regulated by substratum. The Journal of cell biology. 110 (1990) 1405-1415.

Taddei, I., Faraldo, M.M., Teuliere, J., Deugnier, M.A., Thiery, J.P., Glukhova, M.A. Integrins in mammary gland development and differentiation of mammary epithelium. J Mammary Gland Biol Neoplasia. 8 (2003) 383-394.

Tang, W.J., Hurley, J.H. Catalytic mechanism and regulation of mammalian adenylyl cyclases. Molecular pharmacology. 54 (1998) 231-240.

Tanos, T., Rojo, L.J., Echeverria, P., Brisken, C. ER and PR signaling nodes during mammary gland development. Breast Cancer Research. 14 (2012) 1.

Tanos, T., Sflomos, G., Echeverria, P.C., Ayyanan, A., Gutierrez, M., Delaloye, J.F., Raffoul, W., Fiche, M., Dougall, W., Schneider, P., Yalcin-Ozuysal, O., Brisken, C. Progesterone/RANKL is a major regulatory axis in the human breast. Science translational medicine. 5 (2013) 182ra155.

Taylor, R. Interpretation of the Correlation Coefficient: A Basic Review. Journal of Diagnostic Medical Sonography. 6 (1990) 35-39.

Thiery, J.P., Acloque, H., Huang, R.Y., Nieto, M.A. Epithelial-mesenchymal transitions in development and disease. Cell. 139 (2009) 871-890.

Tibbitt, M.W., Anseth, K.S. Hydrogels as extracellular matrix mimics for 3D cell culture. Biotechnology and bioengineering. 103 (2009) 655-663.

Trichopoulos, D., MacMahon, B., Cole, P. Menopause and breast cancer risk. J Natl Cancer Inst. 48 (1972) 605-613.

Vaillant, F., Lindeman, G.J., Visvader, J.E. Jekyll or Hyde: does Matrigel provide a more or less physiological environment in mammary repopulating assays? Breast cancer research : BCR. 13 (2011) 108.

Van Amerongen, R., Bowman, A.N., Nusse, R. Developmental stage and time dictate the fate of Wnt/β-catenin-responsive stem cells in the mammary gland. Cell stem cell. 11 (2012) 387-400.

Van Keymeulen, A., Lee, M.Y., Ousset, M., Brohée, S., Rorive, S., Giraddi, R.R., Wuidart, A., Bouvencourt, G., Dubois, C., Salmon, I. Reactivation of multipotency by oncogenic PIK3CA induces breast tumour heterogeneity. Nature. 525 (2015) 119-123.

Van Keymeulen, A., Rocha, A.S., Ousset, M., Beck, B., Bouvencourt, G., Rock, J., Sharma, N., Dekoninck, S., Blanpain, C. Distinct stem cells contribute to mammary gland development and maintenance. Nature. 479 (2011) 189-193.

Villadsen, R., Fridriksdottir, A.J., Rønnov-Jessen, L., Gudjonsson, T., Rank, F., LaBarge, M.A., Bissell, M.J., Petersen, O.W. Evidence for a stem cell hierarchy in the adult human breast. The Journal of cell biology. 177 (2007) 87-101.

Wang, D., Cai, C., Dong, X., Yu, Q.C., Zhang, X.-O., Yang, L., Zeng, Y.A. Identification of multipotent mammary stem cells by protein C receptor expression. Nature. 517 (2015) 81-84.

Watanabe, K., Villarreal-Ponce, A., Sun, P., Salmans, M.L., Fallahi, M., Andersen, B., Dai, X. Mammary morphogenesis and regeneration require the inhibition of EMT at terminal end buds by Ovol2 transcriptional repressor. Dev Cell. 29 (2014) 59-74.

Weymouth, N., Shi, Z., Rockey, D.C. Smooth muscle alpha actin is specifically required for the maintenance of lactation. Dev Biol. 363 (2012) 1-14.

Wozniak, M.A., Desai, R., Solski, P.A., Der, C.J., Keely, P.J. ROCK-generated contractility regulates breast epithelial cell differentiation in response to the physical properties of a three-dimensional collagen matrix. The Journal of cell biology. 163 (2003) 583-595.

Wozniak, M.A., Keely, P.J. Use of three-dimensional collagen gels to study mechanotransduction in T47D breast epithelial cells. Biol Proced Online. 7 (2005) 144-161.

Wuidart, A., Ousset, M., Rulands, S., Simons, B.D., Van Keymeulen, A., Blanpain, C. Quantitative lineage tracing strategies to resolve multipotency in tissue-specific stem cells. Genes & development. 30 (2016) 1261-1277.

Yalcin-Ozuysal, Ö., Fiche, M., Guitierrez, M., Wagner, K.-U., Raffoul, W., Brisken, C. Antagonistic roles of Notch and p63 in controlling mammary epithelial cell fates. Cell Death & Differentiation. 17 (2010) 1600-1612.

Young, L., Medina, D., DeOme, K., Daniel, C. The influence of host and tissue age on life span and growth rate of serially transplanted mouse mammary gland. Experimental gerontology. 6 (1971) 49-56.

Zhang, S., Gelain, F., Zhao, X. Designer self-assembling peptide nanofiber scaffolds for 3D tissue cell cultures. Seminars in cancer biology, 2005. Elsevier, 413-420.

Zikherman, J., Doan, K., Parameswaran, R., Raschke, W., Weiss, A. Quantitative differences in CD45 expression unmask functions for CD45 in B-cell development, tolerance, and survival. Proceedings of the National Academy of Sciences. 109 (2012) E3-E12.

Zivadinovic, D., Gametchu, B., Watson, C.S. Membrane estrogen receptor-alpha levels in MCF-7 breast cancer cells predict cAMP and proliferation responses. Breast cancer research : BCR. 7 (2005) R101-112.

Acknowledgements

The work as a PhD student resulting in this dissertation was essential for my scientific and personal development and allowed me to acquire many important skills that prepared me for my future career. Importantly, this work would not have been possible without the precious help of many people, the most important ones I want to thank in this paragraph.

First of all, I want to thank Magdalena Götz for giving me the opportunity to complete my PhD thesis in the institute of stem cell research. I also want to thank Magdalena for her close scientific support and advice on my project not only during progress reports and thesis committees but also in between official meetings.

My special thanks also go to Christina Scheel, who gave me the opportunity to work in her mammary stem cells group and closely supported me during my first steps as a PhD student. Thank you Christina for your scientific and non-scientific advice, numerous constructive discussions and everything you have taught me during my time as a PhD student.

I am also grateful to all the other members and former members of the Scheel Group, Johanna Schmidt, Diana Dragoi, Uwe Kloos, Lisa Meixner, Haruko Miura, Anja Krattenmacher, Elena Panzilius and Laura Eichelberger for the good working atmosphere. I am especially grateful to Haruko Miura and Lisa Meixner who supported my project as master's students. You really helped pushing forward this project and it was always fun working with you.

Thanks also to the members of my thesis committee, Magdalena Götz, Melanie Königshoff and Christina Scheel for the fruitful discussions and advice on the future course of my thesis.

Thanks also to all the members of the institute of stem cell research. Especially Filippo Calzolari, for his excitement and scientific input, Sven Falk for help with confocal microscopy, Christian Krendl for help with FACS and Angelika, Andrea and Emily for their help with everything else.

I am also grateful to Martin Irmler for his fast processing of microarray samples, to Harald Bartsch and Carl Sotlar for providing Immunohistochemistry and H&E stainings and Christian Gabka for providing us with primary breast tissue from reduction mammoplasties, the foundation for this work.

Last but not least, I want to thank my family and friends for their love, support and motivation!

Eidesstattliche Versicherung

Linnemann, Jelena
Name, Vorname

Ich erkläre hiermit an Eides statt,
dass ich die vorliegende Dissertation mit dem Thema

An organotypic assay for the quantification and characterization of regenerative primary human mammary epithelial cells

selbständig verfasst, mich außer der angegebenen keiner weiteren Hilfsmittel bedient und alle Erkenntnisse, die aus dem Schrifttum ganz oder annähernd übernommen sind, als solche kenntlich gemacht und nach ihrer Herkunft unter Bezeichnung der Fundstelle einzeln nachgewiesen habe.

Ich erkläre des Weiteren, dass die hier vorgelegte Dissertation nicht in gleicher oder in ähnlicher Form bei einer anderen Stelle zur Erlangung eines akademischen Grades eingereicht wurde.

München, 02.02.2018

Ort, Datum

Unterschrift Doktorand